Draft version November 6, 2018
Preprint typeset using LaTeX style AASTeX6 v. 1.0

CHARACTERISTICS OF LATE PHASE >100 MEV GAMMA RAY EMISSION IN SOLAR ERUPTIVE EVENTS

G. H. Share[1,2], R. J. Murphy[3], S. M. White[4], A. K. Tolbert[5,6], B. R. Dennis[5], R. A. Schwartz[5,6], D.F. Smart[7], and M. A. Shea[7]

[1]Astronomy Department, University of Maryland, College Park, MD 20740, USA
[2]National Observatory of Athens, Athens, Greece
[3]Space Science Division, Naval Research Laboratory, Washington DC 20375, USA
[4]Kirtland AFB, Albuquerque, NM 87117, USA
[5]NASA Goddard Spaceflight Center, Greenbelt, MD 20771, USA
[6]Physics Department, American University, Washington, DC 20016, USA
[7]SSSRC, Nashua, NH, 03062, USA

ABSTRACT

We characterize and catalog 30 solar eruptive events (SEEs) observed by *Fermi* LAT having late phase >100 MeV γ-ray emission (LPGRE), identified 30 years ago in what were called Long Duration Gamma Ray Flares. We show that LPGRE is temporally and spectrally distinct from impulsive phase emission in these events. The spectra are consistent with decay of pions produced by >300 MeV protons and are not consistent with primary electron bremsstrahlung. Impulsive >100 keV X-ray emission was observed in all 27 LPGRE events where observations were made. All but two of the LPGRE events were accompanied by a fast and broad coronal mass ejection (CME). LPGRE start times range from CME onset to two hours later. Their durations range from ∼0.1–20 hours and appear to be correlated with durations of >100 MeV solar energetic particle (SEP) proton events. The power-law spectral indices of the>300 MeV protons producing LPGRE range from ∼2.5–6.5 and vary during some events. Combined γ-ray line and LAT measurements indicate that LPGRE proton spectra are steeper above 300 MeV than they are below 300 MeV. The number of LPGRE protons >500 MeV is typically about 10× the number in the impulsive phase of the SEE and ranges in 9 events from ∼0.01–0.5× the number in the accompanying SEP event, with large systematic uncertainty. What appears to be late phase electron bremsstrahlung with energies up to ∼10 MeV was observed in one LPGRE event. We discuss how current models of LPGRE may explain these characteristics.

Keywords: Acceleration of particles — Sun: flares — Sun: particle emission — Sun: X-rays, gamma rays

1. INTRODUCTION

With the advent of the space age it became possible to observe solar X and γ rays above Earth's absorbing atmosphere. Dolan & Fazio (1965) provided the framework for future observations and theoretical studies in their pioneering paper describing the various components of the spectrum expected to be produced by the interactions of high-energy flare-accelerated electrons and protons in the chromosphere and photosphere. Electron bremsstrahlung is the dominant component for non-thermal emission below about 1 MeV. Nuclear line radiation from interactions of proton and alpha-particles with nuclei in the ambient solar atmosphere becomes important above a few hundred keV. In their seminal work, Ramaty et al. (1979) list the various nuclear de-excitation lines and their production cross sections. Dolan & Fazio (1965) also emphasized the importance of the 0.511 MeV positron-electron annihilation line and the 2.223 MeV neutron capture line in the γ-ray spectra. For energies >50 MeV, they concluded that radiation from the decay of neutral pions would dominate the spectrum. The pions are mostly produced by protons interacting with solar hydrogen at energies above the ∼300 MeV threshold. They also expected that positrons, produced as a result of neutral and charged pion decays, would annihilate with ambient electrons to contribute to the characteristic 511-keV line.

Based on early solar radio observations, Wild et al. (1963) and de Jager (1969) suggested that there are two phases of particle acceleration associated with solar flares. The first is the flash phase and the second occurs at a later time. *OSO*

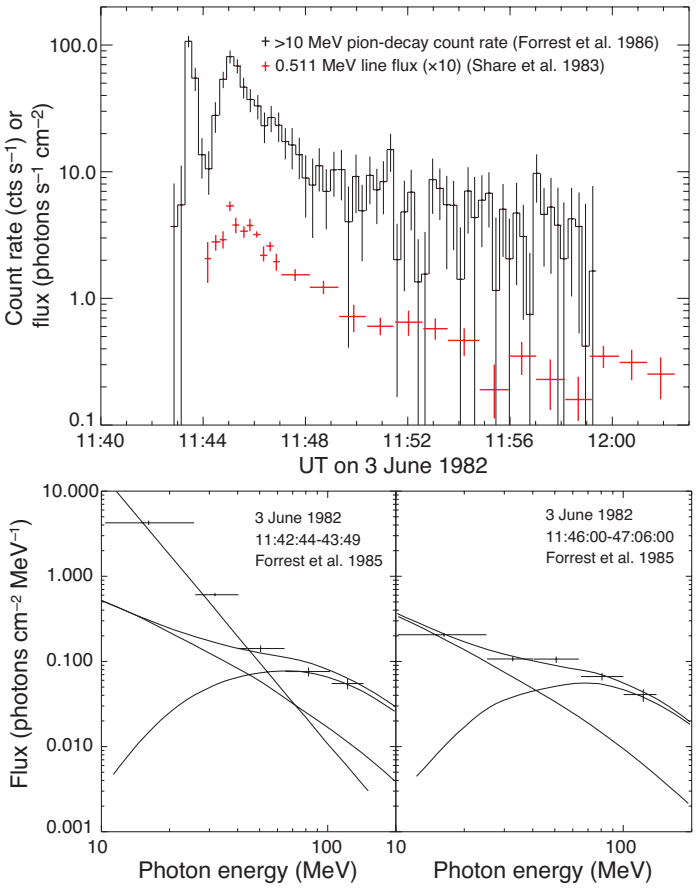

Figure 1. Observations of high-energy emission from the 1982 June 3 flare made by the *SMM* GRS. Top Panel: Time history of the pion-decay γ-ray count rate revealing two clear phases of emission (Forrest et al. 1986). Shown in red, and scaled arbitrarily, is the count rate observed in the 511 keV annihilation line (Share et al. 1983). γ-ray spectra observed during the impulsive phase (lower left panel) and during the second phase (right panel) (Forrest et al. 1985). The data points with errors show the observations. The curves show the different components of the spectrum, including: bremsstrahlung from primary impulsive-phase electrons (steep power-law spectrum), bremsstrahlung from charged pion-decay (flat power-law spectrum), and neutral pion-decay (broad peak).

5 first observed these two phases in hard X-rays from a behind-the-limb flare on 1969 March 30 (Frost & Dennis 1971). The X-ray time history had two distinct peaks. The first was impulsive and lasted only two minutes while the second began just afterward, reached a maximum in three minutes, and lasted about thirty minutes. The photon spectrum of this delayed phase emission was significantly harder than that of the impulsive phase. Because the footpoints of the flare were occulted, the hard X-rays would have had to come from electrons radiating high in the corona and/or from electrons transported by large magnetic loops and interacting in footpoints on the visible disk.

Pion-decay γ-ray emission was first detected by the Gamma Ray Spectrometer (GRS) on the *Solar Maximum Mission* (*SMM*) satellite from the solar eruptive event associated with the 1982 June 3 X8.0 *GOES*-class flare (Forrest et al. 1986). The time history of the >10 MeV γ-ray flux plotted in the top panel of Figure 1 looks remarkably similar to that observed by Frost & Dennis (1971) in hard X-rays in 1969 and it also revealed two distinct phases of emission. The late phase emission was also significantly harder than that of the impulsive phase. The impulsive phase lasted about one minute and was dominated by bremsstrahlung from flare-accelerated electrons, but it also contained what appears to be pion-decay emission. This can be be seen in the left bottom panel of Figure 1 taken from Forrest et al. (1985) in which the spectrum is broken up into three components: bremsstrahlung from flare-accelerated electrons, bremsstrahlung from charged pion-decay, and the broad peak near 70 MeV from neutral pion decay. The late phase emission began within a minute after the peak of the impulsive phase and lasted at least 15 minutes. As can be seen in the bottom right panel of Figure 1, this phase appears to be dominated by both charged and neutral pion-decay emission. Its temporal history plotted in the top panel is similar to the time history, plotted in red, that was observed for the 511 keV positron-annihilation line from decay of positively charged pions (Share et al. 1983). No spectroscopic measurements of the 511 keV line and other nuclear lines were possible during the intense impulsive

phase due to saturation effects. Neutrons from this event were also observed by GRS and by neutron monitors on Earth (Chupp et al. 1987). Murphy et al. (1987) analyzed the 1982 June 3 flare as part of their comprehensive study of high-energy processes in solar flares, which provided a quantitative understanding of the γ-ray spectrum from the decay of charged and neutral pions, the yield of 511 keV photons from positron annihilation, and their relationship to nuclear-line emission. Using the neutron data cited above and nuclear-deexcitation line data provided by Prince et al. (1983), Murphy et al. (1987) showed that the two emission phases were produced by distinctly different accelerated particle populations. The short impulsive phase emission is consistent with production by a steep ion spectrum and the late phase γ-ray emission is consistent with production by a harder ion spectrum.

In addition to the 1982 June 3 solar event, Ryan (2000) and Chupp & Ryan (2009) list twelve γ-ray events observed by several instruments and lasting from a fraction of an hour to up to eight hours. All of them were associated with *GOES* X-class flares. We summarize the characteristics of these events in Appendix A. Eleven of the thirteen events clearly exhibited late phase emission, distinct from the impulsive phase. The launch of the *Fermi* Large Area Telescope (LAT) in 2008 provided the opportunity to study a larger sample of solar eruptive events having late phase emission. Here, we refer to this emission as Late Phase Gamma-Ray Emission (LPGRE). This late phase emission was identified 30 years ago as part of what has been called a Long Duration Gamma Ray Flare. In an earlier version of this paper, we used the phrase Sustained Gamma Ray Emission (SGRE) to refer to the late phase emission.

1.1. *Early Fermi Observations of Late Phase Gamma-Ray Emission*

The *Fermi* Large Area Telescope (LAT) (Atwood et al. 2009) has a five-times larger peak effective area and four-times larger field of view than the EGRET detector (Hartman et al. 1992) on the *Compton Gamma Ray Observatory (CGRO)*. This provides an order of magnitude improvement in sensitivity to solar events over previous high-energy observations. LAT first detected >100 MeV γ-ray emission on 2010 June 12 (Ackermann et al. 2012c,b) during the impulsive *GOES*-class M2 solar flare that was associated with a 500 km s^{-1} CME and a barely detectable solar energetic particle (SEP) event. That paper primarily focused on the Gamma-ray Burst Monitor (GBM) (Meegan et al. 2009) observations of bremsstrahlung and nuclear γ-rays and the LAT >30 MeV observations during the minute-long impulsive flare. The high-energy γ-ray emission was delayed from the impulsive hard X-ray emission, but only by about 10 seconds, reflecting the time it takes to accelerate particles to tens of MeV. Ackermann et al. (2012c) found no evidence for any late phase >100 MeV emission in the hours following the flare.

After that first *Fermi* impulsive flare observation, the LAT Team reported detection of three events with late phase γ-ray emission. The first observation (Allafort et al. 2011a,b) was made just after the impulsive phase of the *GOES* M3.7 flare on 2011 March 07 that was detected by GBM at energies up to 1 MeV. The second event (Tanaka et al. 2011) followed a *GOES* M2.5 flare on 2011 June 7 detected in its impulsive phase by both *RHESSI (Reuven Ramaty High Energy Solar Spectroscopic Imager)* and GBM up to 800 keV. The third event (Tanaka et al. 2012) followed impulsive phase emission up to 300 keV detected by GBM from the *GOES* M8.7 flare on 2012 January 23. Common to all three events was an impulsive flare with >100 keV hard X-ray emission, a >1000 km s^{-1} CME, and an accompanying SEP event. In an attempt to understand the conditions that are necessary for producing LPGRE, we identify a sample of 95 solar events occurring between 2008 and 2012 having at least one of these characteristics. The relationship between LPGRE occurrence and the properties of this sample is discussed in Appendix B and relevant results are presented in the body of the paper.

In this paper we catalog 30 solar eruptive events with late phase γ-ray emission observed by LAT from 2008 until the end of 2016. We discuss our temporal and spectroscopic studies of the events and relate the measurements to the associated solar flares, radio emissions, coronal mass ejections, and solar energetic particle events. In §2, we discuss how LAT is used as a solar observatory, and in §2.1 we describe our method for analyzing LAT data. This method is different than that used by Ackermann et al. (2014) and Ajello et al. (2014) but provides comparable measurements of γ-ray fluxes and spectra. A major advantage is that the *Fermi* data can be accessed and studied using standard solar data analysis software. In §3 we list the 30 events with LPGRE and provide an example of our analysis for one of the events, including details of the observations and time histories of the emission. Similar studies of each of the other 29 events are presented in Appendix C. In §4 we describe our methods for analyzing LAT >100 MeV spectra from both the impulsive and late phases of the solar eruption, thus providing information about the protons producing these emissions. We also discuss *RHESSI* and GBM spectroscopic studies that provide further information on the proton spectra at energies below 300 MeV. In §5 we detail what we have learned about the overall characteristics of the late-phase emission and its relationship to the impulsive-phase emission and to the accompanying coronal mass ejection and solar energetic particle event. We summarize the principal characteristics of LPGRE in §6.1 and discuss their implications in § 6.2. The paper includes five appendices that: 1) summarizes pre-Fermi observations of LPGRE, 2)

describes a four-year study of the relationship between LPGRE event flares, CMEs, and SEPs, 3) details the temporal and spectral details of the 30 events, 4) presents our estimate of the number of >500 MeV SEP protons, and 5) details of the accompanying radio bursts. This allows us to focus on the scientific results in the body of the paper.

2. *FERMI*/LAT AS A SOLAR OBSERVATORY

LAT is an electron-positron pair-conversion telescope (Atwood et al. 2009) that is sensitive to γ rays from ~20 MeV to ~300 GeV. It is made up of 16 identical towers, each comprised of a tracker with alternating layers of Silicon Strip Detectors (SSD) and tungsten converter foils, and a calorimeter with logs of CsI arranged in a 'hodoscopic' configuration so that the energy deposition can be imaged in three dimensions. The towers are surrounded by a multi-tile plastic scintillator Anti-Coincidence Detector (ACD). Detector events not accompanied by an energy loss equivalent to 45% of a minimum ionizing singly-charged particle traversing an ACD tile are telemetered to the ground for further analysis. These events are further processed to produce what is known as Source class data that are used for celestial γ-ray studies and for studying LPGRE after intense solar hard X-ray emission abates (Ackermann et al. 2014). For our analysis, we used both what the LAT team call 'Pass7' and 'Pass8' selections of these data, depending on when the event was processed. More detailed information on the *Fermi*/LAT instrument, operation, and data related to solar flare observations can be found in Ackermann et al. (2012c, 2014) and Ajello et al. (2014). During intense solar flares, when there are large energy losses in the ACD from pileup of tens of keV X rays, Source class data are not available because their quality is compromised. To allow analysis of high-energy γ-rays during flares, the LAT team developed two special classes of data: LAT Low Energy (LLE) data (Ackermann et al. 2012c) and Pass8 Solar Flare Transient Class data (Pesce-Rollins et al. 2015a).

In the standard *Fermi* sky-survey mode, the spacecraft points away from the Earth and rocks ±50° from the zenith on alternating 95-minute orbits. Therefore, the Sun can typically be observed only for ~20-40 minutes every one or two orbits for an average duty cycle of 15-20%. Depending on statistics, data can be accumulated over shorter time intervals. In response to a 'burst' trigger from GBM during a high-energy solar flare, *Fermi* can autonomously be pointed at the Sun for up to five hours. In addition, when the Sun is in an unusually high state of activity, a Target of Opportunity can be declared where the spacecraft remains in the rocking orientation most favorable to solar observations, thus providing ~20-40 minute exposure during every 95 minute orbit.

2.1. *Analysis of Fermi LAT Data*

In performing both our temporal and spectral studies, we first accumulated >100 MeV photons with measured locations within 10° of the Sun using standard LAT analysis tools. For reference, we note that about 95% of all 200 MeV solar γ rays have measured locations within this disk of 10° radius (Atwood et al. 2009). We reduced the γ-ray background from the Earth's atmosphere in these accumulations by restricting events to those with angles <100° from the zenith. All of the accumulated data were then put into a format compatible with SSW IDL software[1] used by the solar community and operating within IDL[2]. Therefore, any scientist familiar with OSPEX[3] can study LAT solar data in the same way that they study *RHESSI* and GBM spectral data. We performed two types of analysis on these data in this paper.

The first is a temporal analysis designed to reveal the presence of solar transients on orbital time scales and to determine the time variation of the emission on minutes to hours time scales (§2.2 and §3.1). In producing what we call "light-bucket" time profiles, we simply divided the accumulated count-rate in each time interval by the default effective area provided in the LAT data products. This provides a simple and fast way to obtain an estimate of the >100 MeV γ-ray flux from within about 10° of the Sun. During solar quiet times, the flux comes from Galactic, extra-galactic, and quiescent solar photons (Abdo et al. 2011). This background flux varies seasonally from $\sim 3\times10^{-6}$ γ cm^{-2} s^{-1} in March to $\sim 4.5\times10^{-5}$ γ cm^{-2} s^{-1} in mid-December, as the Sun moves along the ecliptic and passes through the Galactic plane[4]. Any transient solar flux will therefore appear above this background in the plots. The effective area used to determine the light-bucket fluxes was for a hard celestial background spectrum and not for a softer solar transient spectrum. This affects the accuracy of the plotted flux during a solar transient. For the above reasons, we caution the reader not to use the light-bucket fluxes plotted in the body of the paper and appendices to make quantitative comparisons of solar fluxes. Instead, one should only use the >100 MeV solar fluxes provided in Table 3 derived using spectroscopic studies of background-subtracted data discussed below.

[1] http://www.lmsal.com/solarsoft/ssw_whatitis.html

[2] http://www.harrisgeospatial.com/ProductsandSolutions/GeospatialProducts/IDL.aspx

[3] https://hesperia.gsfc.nasa.gov/ssw/packages/spex/doc/ospex_explanation.htm

[4] The quiescent solar emission in March accounts for roughly 40% of the background flux. The remaining flux of $\sim 1.8\times10^{-6}$ γ cm^{-2} s^{-1} is consistent with what would be expected from the diffuse extragalactic contribution (Abdo & et al. 2010).

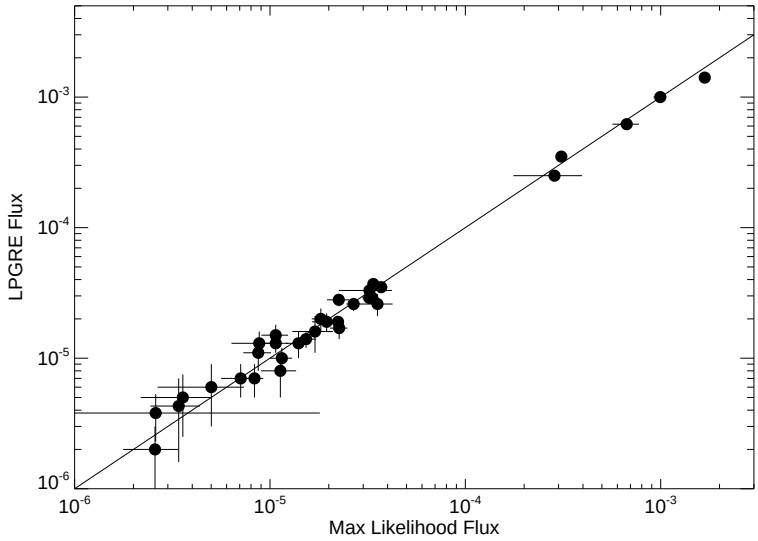

Figure 2. Comparison of the >100 MeV LPGRE fluxes reported here with those derived using the LAT Team's Maximum Likelihood analysis.

The second type of analysis involves detailed spectroscopic studies of background-subtracted data performed using OSPEX. The >100 MeV background in LAT Source class data from a 10° region around the Sun is relatively constant on timescales of hours (see Figure 3 in §2.2 below), as long as data <12° from the Earth's horizon (i.e., a zenith angle <100°) is excluded. Therefore, as background, we chose LAT observation intervals just before and/or after the LPGRE event with comparable solar exposures. The solar fluxes for the 30 LPGRE events listed in Table 3 were determined by fitting the background-subtracted spectra with plausible solar photon models as described in §4.1. As questions have been raised about the accuracy of our solar flux determinations, we compared the fluxes listed in Table 3 with the fluxes from the more sophisticated Maximum Likelihood method used by the LAT Team Ackermann et al. (2014); Ajello et al. (2014); Ackermann et al. (2017) for the same events. We plot a comparison of the fluxes in Figure 2. Even though the solar exposures for the two methods were not always identical, the agreement in flux is generally within the uncertainties and supports the validity of our method.

2.2. *Four-Day Plots of >100 MeV Solar Fluxes Observed by Fermi*

In Figure 3, we show an example of the four-day time histories of >100 MeV solar fluxes observed by LAT that are available for the entire *Fermi* Mission on the *RHESSI* Browser[5]. The top panel shows the >100 MeV light-bucket fluxes plotted as black data points with $\pm 1\sigma$ statistical uncertainties. As discussed above these fluxes include all photons $< 10°$ of the Sun including background from Galactic, extra-galactic, and quiescent solar sources. Although they accurately reveal the temporal variations, these light-bucket fluxes should not be used in quantitative solar studies. When the >100 MeV flux exceeds about 4.2 σ above background ($\sim 2 \times 10^{-5}$ probability for a random Gaussian distribution), as it did in three exposures separated by three hours on 2014 February 25, the plotted points are circled in red, identifying possible >100 MeV solar events. There were significant excesses in five exposures between 2011 November 7–11 when the active radio quasar, PKS 1510-089, passed near the Sun.

In the bottom panel of Figure 3 we plot the solar gamma-ray fluxes provided by the *FERMI* LAT team using their more sophisticated and sensitive Maximum-Likelihood method (Ackermann et al. 2014). This technique models and removes the background so that only upper limits (in black) are plotted unless there is a statistically significant solar transient when the points are plotted with $\pm 1\sigma$ errors and circled in red . Both methods also provide information on the LAT solar exposures shown in blue in each plot; the average effective area is given in the top panel and the effective area × exposure time in the bottom panel. More information about these plots can be found at http://hesperia.gsfc.nasa.gov/fermi/lat/qlook/LAT_qlook_plots.htm.

3. THE THIRTY EVENTS WITH LATE PHASE GAMMA-RAY EMISSION OBSERVED BY LAT

[5] http://sprg.ssl.berkeley.edu/~tohban/browser

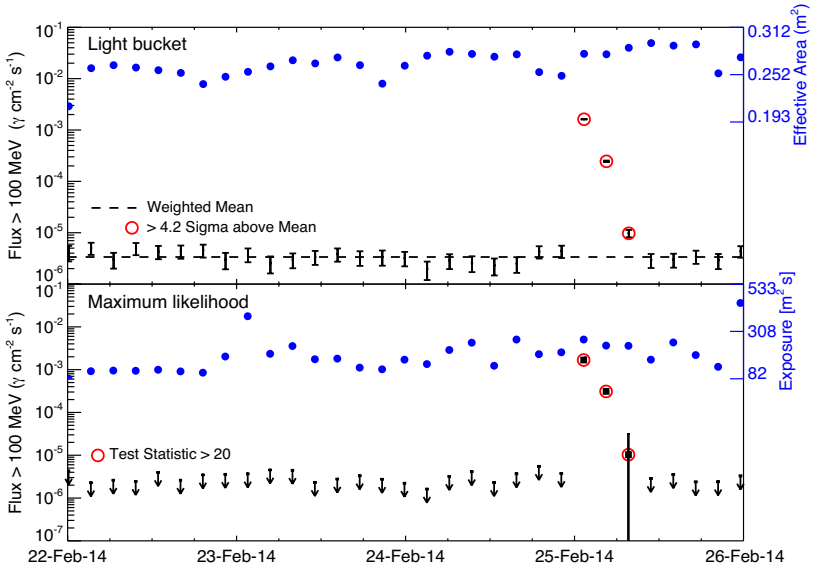

Figure 3. Example of *RHESSI* Browser 4-day plots of >100 MeV light-bucket fluxes (upper panel) and solar fluxes derived using the Maximum Likelihood technique described by Ackermann et al. (2014); Ajello et al. (2014) (lower panel). Note that the light-bucket fluxes include all photons < 10° of the Sun, including background (see text). The right ordinate provides the scale for the blue circles that give the average effective area (top panel) and effective area × time (bottom panel). The time period shown includes the solar eruptive event with LPGRE observed by *Fermi* on 2014 February 25 with fluxes and their $\pm 1\sigma$ uncertainties encircled in red in both plots.

We have identified 30 solar eruptive events with LPGRE from 2008 to 2016 from manual and automated searches of the LAT fluxes plotted in the *RHESSI* Browser (see the example in Figure 3). These events are listed in Table 1 and detailed in Appendix C. We do not include the behind-the-limb event on 2014 January 6 discussed by Ackermann et al. (2017) because it was not detected in our search of the LAT data and the emission was too weak to analyze. There were three other 20–40 minute solar exposures exhibiting fluxes $>4.2\sigma$ above the mean 4-day background that we found in our search of the light-bucket plots in the *RHESSI* Browser. Random fluctuations for a normal distribution would be expected to produce one to two such events in the 5 $\times 10^4$ exposures of the study.

Table 1. Solar Eruptive Events from June 2008 to December 2016 with >100 MeV Late Phase Gamma-Ray Emission

Number	Date, Location	*GOES* X-Ray	CME	Type II	SEP	Flare Hard X-ray
	yyyy/mm/dd, deg	Class, Start-End	Speed, km s^{-1}	M*, DH	Flux (pfu), Energy (MeV)	Energy (keV)
(1)	(2)	(3)	(4)	(5)	(6)	(7)
1	2011/03/07, N30W47	M3.7, 19:43–20:58	2125, H	3?, Y	39.6, >60	300–1000[d]
2	2011/06/02, S18E22	C3.7, 07:22–07:57	976, H	N, Y	∼0.1, <40[b]	–[e]
3	2011/06/07, S21W54	M2.5, 06:16–06:59	1255, H	2?, Y	60.5, >100	300–800
4	2011/08/04, N19W46	M9.3, 03:41–04:04	1315, H	2, Y	48.4, >100	300–1000[d]
5	2011/08/09, N16W70	X6.9, 07:48–08:08	1610, H	1?, Y	16.3, >10	800–7000
6	2011/09/06, N14W18	X2.1, 22:12–22:24	575, ∼1000[a,b,h], H	2, Y	5.6, >100	300–1000
7	2011/09/07, N18W32	X1.8, 22:32–22:44	792, PH	1, N	<1.7, >10[f]	300–1000[d]
8	2011/09/24, N14E61	X1.9, 09:21–09:48	1936, PH	2?, N	<77, >13[b,f]	800–7000
9	2012/01/23, N33W21	M8.7, 03:38–04:34	2175, H	N, Y	3280, >100	100–300[d,e]
10	2012/01/27, N35W81	X1.7, 17:37–18:56	2508, H	3, Y	518, >100	100–300[d,e]
11	2012/03/05, N16E54	X1.1, 02:30–04:43	1531, H	N, Y	<33, >13[b,f]	100–300[d,e]
12	2012/03/07, N17E27	X5.4, 00:02–00:40	2684, H	2?, Y	1800, >100	>1000[g]
		M7, 01:05–01:23	1825, H	2?, Y	1800, >100	>1000[g]
13	2012/03/09, N16W02	M6.3, 03:22–04:18	950, H	2, Y	<528, >10[f]	100–300
14	2012/03/10, N18W26	M8.4, 17:15–18:30	1296, H	N?, Y	<115, >10[f]	100–300[d]
15	2012/05/17, N05W77	M5.1, 01:25–02:14	1582, H	3, Y	180, >100	100–300[c]

Table 1 continued on next page

Table 1 *(continued)*

Number	Date, Location	*GOES* X-Ray	CME	Type II	SEP	Flare Hard X-ray
	yyyy/mm/dd, deg	Class, Start-End	Speed, km s^{-1}	M*, DH	Flux (pfu), Energy (MeV)	Energy (keV)
(1)	(2)	(3)	(4)	(5)	(6)	(7)
16	2012/06/03, N15E38	M3.3, 17:48–17:57	605, 892[b,h], PH	2, N	0.6, >60[b]	300–800
17	2012/07/06, S17W52	X1.1, 23:01–23:14	1828, H	3, Y	19.1, >100	>500[k]
18	2012/10/23, S15E57	X1.8, 03:13–03:21	–	Y, N	<0.1, >13[b]	>9000
19	2012/11/27, N05W73	M1.6, 15:52–16:03	–	N, N	<0.1, >10	300–1000
20	2013/04/11, N07E13	M6.5, 06:55–07:29	861, H	3, Y	184, >60[b]	100–300[d]
21	2013/05/13, N11E89	X1.7, 01:53–02:32	1270, H	1, Y	9.3, >60[b]	100–300
22	2013/05/13, N10E80	X2.8, 15:48–16:16	1850, H	2, Y	176, >60[b]	>1000
23	2013/05/14, N10E77	X3.2, 00:00–01:20	2625, H	1, Y?	306, >60[b]	300–1000[d]
24	2013/05/15, N11E65	X1.2, 01:25–01:58	1366, H	1, Y	<17, >13[b,f]	300–1000
25	2013/10/11, N21E103	M4.9[i], 07:01–07:45	1200, H	2, Y	156, >60[b]	– [j]
26	2013/10/25, S08E71	X1.7, 07:53–08:09	587, H	2, N	32.6, >60[b]	800–7000[c]
27	2013/10/28, S14E28	M4.4, 15:07–15:21	812, H	2, N	5.6, >13[b]	100–300[c]
28	2014/02/25, N00E78	X4.9, 00:39–01:03	2147, H	3, Y	219[b], >700	1000–10000
29	2014/09/01, N14E126	X2.1[i], 10:58–11:34	1901, H	Y?, Y	∼1000, >13	– [j]
30	2015/06/21, N13E16	M2.6, 02:03–03:15	1366, H	2?, Y	∼40, >10	100-300[d]

[a] *STEREO A*

[b] *STEREO B*

[c] *RHESSI*

[d] *Fermi*/GBM

[e] Missing hard X-ray data due to night time or SAA passage

[f] Preceding SEP

[g] *INTEGRAL*

[h] CACTUS

[i] Pesce-Rollins et al. (2015b)

[j] flare behind solar limb

[k] *Konus (Aptekar et al. 1995)*

[*] 1, 2, 3 ≃ <50, 50–500, >500 $\times 10^{-22}$ W m^{-2} Hz^{-1}

Much of the information in Table 1 comes from the NOAA solar event reports[6]. Column 1 lists the event number; column 2 lists the date of the event and location of the flare or centroid of the hard X-ray footpoints imaged by *RHESSI*; column 3 lists the *GOES* soft X-ray class (we used estimates made by Pesce-Rollins et al. (2015b) for the location and *GOES* class for the two events beyond the limb) and the *GOES* start and stop times; column 4 lists the projected CME speed from the *SOHO* LASCO coronagraph catalog[7] (unless noted) and whether the CME was a halo (H) or partial halo (PH); column 5 lists the Type II metric intensity from the solar event reports ("?" means that we could not confirm the detection spectroscopically), and whether decametric-hectometric (DH) Type II emission[8] was observed in space (Y/N); column 6 lists the peak SEP flux above 10 MeV in proton flux units (pfu; 1 pfu=1 proton cm^{-2} sr^{-1} s^{-1}) and the highest energy measured at the best magnetically connected spacecraft; and column 7 lists the highest X-ray energy channel that the impulsive phase was detected by *RHESSI* or GBM. Additional information about the sources of the data are provided in our discussion of Table B1 in Appendix B. We note that event 12 in Table 1 on 2012 March 7 was comprised of two flares and two episodes of LPGRE; the second flare, reported as an

[6] ftp://ftp.ngdc.noaa.gov/STP/swpc_products/daily_reports/solar_event_reports/

[7] https://cdaw.gsfc.nasa.gov/CME_list/index.html

[8] http://secchirh.obspm.fr/select.php,https://ssed.gsfc.nasa.gov/waves/data_products.html

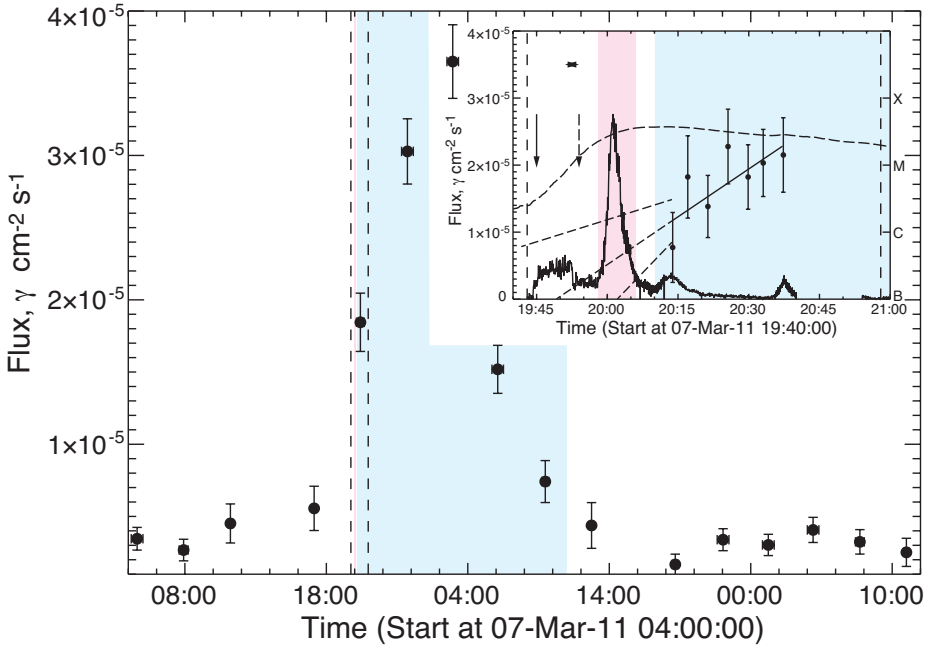

Figure 4. The main figure shows the time history of the >100 MeV light-bucket fluxes from $<10^{\circ}$ of the Sun, derived from Source class data, revealing LPGRE from the 2011 March 7 solar eruptive event. The fluxes are averaged over the ∼20–40 minute solar exposures and the uncertainties are $\pm 1\sigma$ statistical errors. As discussed in §2.1 care must be taken is using these light-bucket fluxes in quantitative solar studies. Vertical dashed lines show the *GOES* 1–8Å start and end times. The inset shows 4-minute accumulation light-bucket fluxes derived from Source class data. The best linear fit to the rising flux is shown by the solid line and its extrapolation back to background is shown by the dashed line; the other two dashed lines are extrapolations of $\pm 1\sigma$ deviations from the best fit. The combined 100–300 keV count rate observed by *RHESSI* and GBM during the impulsive flare, scaled to the γ-ray flux, is shown by the solid trace. The dashed curve shows the *GOES* time history (logarithmic scale on right ordinate). The $< - >$ symbol shows the range in CME onset times in the CDAW catalog derived for linear and quadratic extrapolations (the difference in times for this flare is small). The vertical solid arrow depicts our estimate of the CME onset from inspection of *SDO*/AIA images and the vertical dashed arrow shows the estimated onset of Type II radio emission. The blue-shaded region depicts our estimate of the duration of the LPGRE. The pink-shaded region depicts where we made estimates of the flux of >100 MeV impulsive-flare γ-ray emission listed in Table 3.
X1.3 *GOES*-class flare, is actually an M7 flare when the tail of the preceding X5.3 flare emission is subtracted.

3.1. *Time Histories and Details of Events with Late Phase Gamma-Ray Emission*

We present light-bucket time histories and observational details of each of the 30 events with LPGRE in Appendix C. In Figure 4 we provide an example of one of these time histories. The event occurred on 2011 March 7. It was the first event with LPGRE detected by LAT (Ackermann et al. 2014) and lasted about 14 hours. In the main part of the figure, we plot the >100 MeV γ-ray fluxes (with $\pm 1\sigma$ statistical uncertainties) within the 10° accumulation region centered on the Sun[9] for several hours before and after the flare. As discussed in §2.1 care must be taken is using these light-bucket fluxes in quantitative solar studies. Absolute solar fluxes for the events are provided in Table 3. It is clear from the main plot that the LPGRE began around the time of the flare and reached a peak about six hours after the flare, consistent with the time history presented by Ackermann et al. (2014). The six-hour delay to the peak of the LPGRE is in stark contrast with the two minute delay observed in the 1982 June 3 event (Figure 1). In addition the associated flare was only an M3.7 *GOES*-class event, compared to the X8 flare on June 3.

In the inset of Figure 4 we plot a blowup of data spanning the *GOES* soft X-ray event (dashed vertical lines). The relative LAT >100 MeV fluxes are plotted at 4 minute time resolution. The horizontal right- and left-pointing arrow heads show the estimated range of CME onset times using linear and quadratic extrapolations given in the CDAW LASCO CME Catalog[10]. We also studied *SDO* EUV images to visually determine the time when the CME lifted off with a one to two minute uncertainty; this time is shown by the downward solid arrow in the inset. The dashed downward arrow shows the estimated onset time of Type II radio emission given in the NOAA Solar Event Reports[11]

[9] The flux evaluation is done using the Sun's position at 12 UT on that day

[10] https://cdaw.gsfc.nasa.gov/CME_list/index.html

[11] ftp://ftp.ngdc.noaa.gov/STP/swpc_products/daily_reports/solar_event_reports/

or derived from studies of the radio spectra. We compare estimates of CME and Type II onset times for the 30 LAT events in Unlike the 1982 June 3 flare where pion-decay γ-rays were observed during the impulsive phase, GBM and *RHESSI* observed impulsive hard X-rays up to only 100–300 keV with no evidence for nuclear line emission. The combined GBM/*RHESSI* 100-300 keV time history is plotted as the solid trace in the inset and the rate peaks after the onsets of CME and Type II radio emission. LAT began observing the Sun at about 20:14 UT near the end of the impulsive hard X-ray emission. The >100 MeV fluxes plotted in the inset reveal that the LPGRE began within minutes of the hard X-ray peak. We estimated the range of LPGRE onset times by extrapolating the best linear fit and $\pm 1\sigma$ uncertainties, shown by the dashed lines, to background level. It is clear from the rising LPGRE flux that it is due to a distinct particle acceleration phase and is not just the tail of emission from the impulsive phase of the flare.

4. SPECTROSCOPIC STUDIES

Spectroscopic measurements made by LAT, *RHESSI*, and GBM are critical to our study of LPGRE. In §4.1 we describe the techniques used to analyze the >100 MeV solar emissions observed by LAT. We discuss how we used fits of calculated pion-decay spectra to background-subtracted impulsive and late phase spectral data to obtain the >100 MeV solar γ-ray fluxes, the power-law spectral indices of protons producing the emission, and the numbers of >500 MeV protons accelerated and entering the thick target during these two phases of the solar eruptive events (see Table 3). We discuss how we used fits of calculated pion-decay spectra to background-subtracted impulsive and late phase spectral data. We include a discussion of fits to a representative late phase emission spectrum above 100 MeV to demonstrate that it can be explained by pion-decay emission but not by bremsstrahlung from primary electrons (§4.1.1). This provides compelling support for the ion origin of the emission reached in studies of late-phase emission made prior to the launch of *Fermi* (e.g. Ryan (2000); Rank et al. (2001)) and discussed in Appendix A. All of the spectroscopic studies have been performed assuming that the protons producing the pion-decay emission had an isotropic angular distribution. In §4.1.2 we discuss how the results would change for anisotropic angular distributions. In §4.1.3 we discuss how we used neutron-capture line measurements from *RHESSI* and GBM spectra to estimate of the number of >500 MeV protons accelerated in the impulsive phase, whether or not LAT data are available, and to obtain information about the spectra, below 300 MeV, of the protons producing the LPGRE.

4.1. *Spectroscopic Studies of LAT LPGRE Data: Pion-Decay Fits*

In §2 and §2.1 we discussed how we processed LAT data to put them into a format for spectral analysis. In Figure 5, we show the background-subtracted count spectrum on 2014 February 25 (Event 28 Table 1, Appendix C.28) from one of the brightest episodes of LPGRE observed by LAT. The spectrum was accumulated over four minutes (01:13–01:17 UT) during the peak exposure to the Sun to avoid any instrumental issues near the edge of the field of view. As discussed in Ackermann et al. (2014) and Ajello et al. (2014), LPGRE photon spectra have the shape of a power-law with an exponential cutoff varying from several tens of MeV to a few hundred MeV. Such a shape arises naturally from the decay of neutral and charged pions produced when high-energy protons and α particles interact in the solar chromosphere and photosphere. A computer code developed by Murphy et al. (1987) calculates the yield of neutral and charged pions and the associated γ-ray spectra from neutral-pion decay, bremsstrahlung of positrons and electrons from charged-pion decay, and annihilation in flight of positrons from positive-pion decay. The calculations are performed assuming that the particles interact isotropically in a cold thick-target region and use nuclear data and models for the p + p and p + ^{4}He reactions (and the inverse reaction α + H). Both the accelerated and ambient ^{4}He/H abundance ratios are assumed to be 0.1. If the accelerated α/p ratio were 0.2, the pion-decay yield would increase by ∼10%. The pion-decay cross sections for p + heavier-ion interactions are significantly larger, and their threshold energies are lower than for the p-H reaction; however this is offset by the significantly lower heavy-ion abundances. Only for power-law ion spectra with indices steeper than 6 does the pion-decay gamma-ray yield from p-heavy and heavy-H reactions reach close to 15% of the yield from p-H reactions, for assumed coronal abundances (Reames 1995) for both the ambient medium and the accelerated-particles. For an impulsive-flare accelerated-particle composition (Reames 1995) the yield would not increase significantly due to Coulomb energy losses of the heavy ions.

Due to the high >300-MeV proton threshold for pion production, the pions are produced deep in the solar atmosphere. Because of the short pion decay times the photons are released at comparable depths. At these depths scattering effects on the escaping photons are significant, especially for flares observed at heliocentric angles >70°. We calculated the angle-dependent scattering effects on the spectra of the escaping photons from an estimated depth distribution for pion production and using a Monte Carlo N-Particle (MCNP6) photon-propagation code[12], employing a spherical geometry

[12] https://mcnp.lanl.gov/

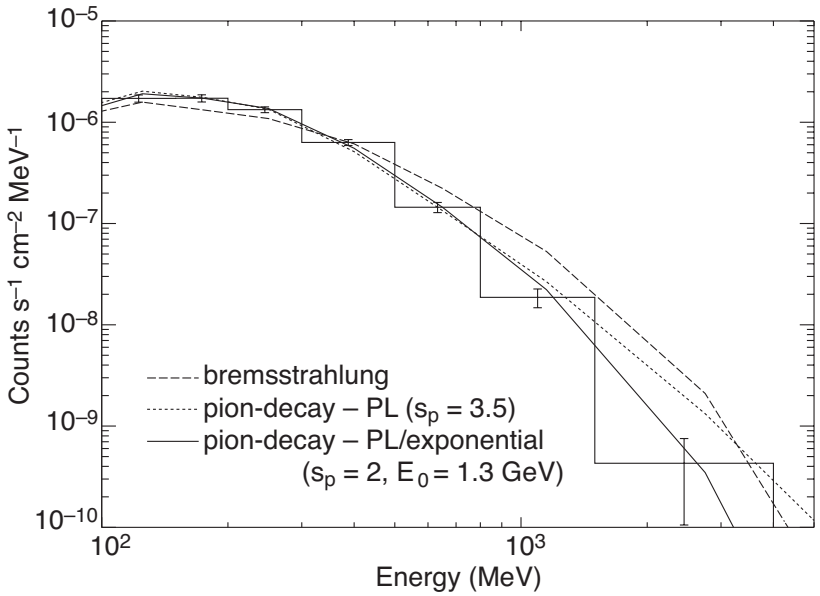

Figure 5. Background-subtracted LAT count spectrum with $\pm 1\sigma$ statistical uncertainties measured between 01:13:30 and 01:17:30 UT on 2014 February 25 during LAT's peak exposure to the Sun. Best fits to the spectrum after passing three different photon spectra through the instrument response are shown: 1) a pion-decay spectrum produced by a power-law spectrum of protons with spectral index, $s_p = 3.5$ (dotted curve); 2) a pion-decay spectrum produced by a power-law spectrum of protons with spectral index, $s_p = 2$ and 1.3 GeV exponential cutoff energy (E_0) (solid curve); and 3) a bremsstrahlung spectrum produced at a density 10^{16} cm^{-3} from a power-law spectrum of primary electrons with index, s = 1 and 1 GeV exponential cutoff energy (E_0) in a 10^3 G magnetic field (dashed curve).

model for the Sun. We isotropically released pion-decay spectra calculated with the Murphy et al. (1987) code and recorded escaping gamma-ray spectra at various angles relative to the normal to the solar surface at the flare-site; these angles correspond to flare heliocentric observation angles as observed from Earth. We found that there is only a small difference in the escaping >100 MeV photon spectral shape from flares at varying heliocentric angles. The primary effect is the reduction in the number of photons that escape. Only ∼82% of the 100 MeV pion-decay photons that escape at disk center can escape at a heliocentric angle of 70°. This number drops to ∼47% at 85° and to ∼8% at 90°.

Using the Murphy et al. (1987) code and attenuation corrections, we then calculated pion-decay spectral templates for the location of the associated active region and varied the proton spectral index to obtain the best fit to the LAT spectral data. As an illustration of our LAT spectral analyses we discuss our fits with these templates to the 2014 February 25 count spectrum plotted in Figure 5. We assumed that the 2014 February 25 emission came from the active region located at a heliocentric angle of 78° and fit the count spectrum with calculated pion-decay templates for unbroken proton power-law spectral indices, s_p. The χ^2 statistic was used to determine the proton spectral index and its estimated 1σ uncertainty was determined from the values where χ^2 increased by unity. The best-fitting spectrum was for a power-law index $s_p = 3.45 \pm 0.15$ (dotted curve). The fit is poor, χ^2/dof of 3.7; only 0.2% of random trials with this power-law form would have higher values of χ^2/dof. It is clear that the photon spectrum must steepen above ∼1 GeV, implying that the proton spectrum is not an unbroken power-law but rolls over at high energies. We found that a power-law proton spectrum with exponential cutoff ($(dN/dE \propto E^{-s_p} exp^{-E/E_0}$); used by Ellison & Ramaty (1985) in their study of shock acceleration in solar flares) having an index, $s_p = 2$, and an exponential cutoff, $E_0 =$ 1.3 GeV, provides a good fit to the spectral data (solid curve, 31% of random trials with this power-law exponential form would have higher values of χ^2/dof.) For the statistics available in most events in our study, fits with pion-decay spectra from protons with spectra following a unbroken power-law are adequate. Because of the threshold for pion production the information derived from these fits is only valid for proton energies above 300 MeV.

From the derived γ-ray flux and proton spectral index, we then applied the results of Murphy et al. (1987) to calculate the number of accelerated protons with energies >500 MeV at the Sun during each LAT exposure. The number of protons >500 MeV is relatively insensitive to uncertainties in spectral index because of the 300 MeV threshold. We also corrected the number of protons for atmospheric attenuation. Because of the limited duty cycle of the LAT observations, our knowledge of the temporal evolution of the LPGRE is limited. For events where only one LAT exposure is available, we estimated the number of accelerated protons by assuming that the flux onset occurred

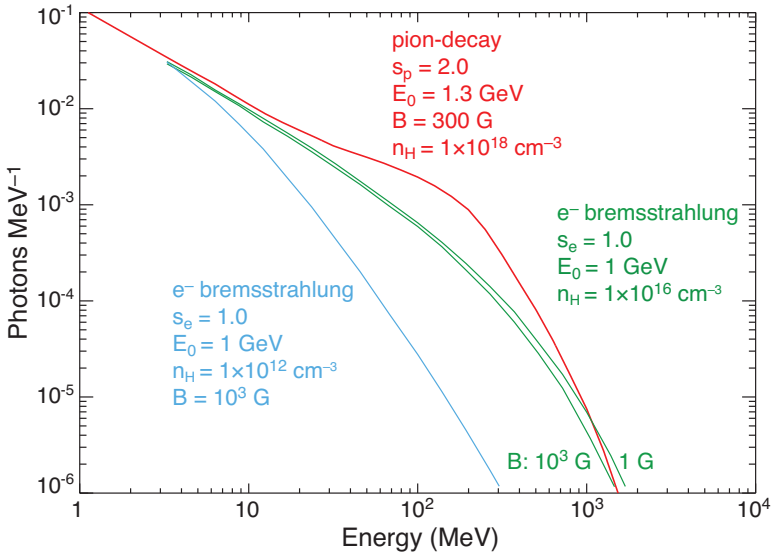

Figure 6. Comparison of calculated primary electron-bremsstrahlung spectra for two different assumed magnetic field strengths (green curves) at a density of 10^{16} cm^{-3} with the pion-decay production spectrum (red curve) that fits the γ-ray spectrum observed by LAT between 01:13:30 and 01:17:30 UT on 2014 February 25 shown in Figure 5. The pion-decay spectrum was produced by protons interacting at a density of 10^{18} cm^{-3} and having a power-law spectrum with 1.3 GeV exponential cutoff. For comparison we also plot the bremsstrahlung spectrum for the same electron spectrum but for a density of 10^{12} cm^{-3} and 1000 G field (blue curve).

at the end of the previous (null) LAT observation and increased linearly to the observed value that is assumed to be the peak. Similarly, we assumed that the flux decayed linearly from the peak to the beginning of the following (null) LAT observation. If there are higher time cadence LAT data available, as there are for the 2011 March 11 event (see Figure 4), we use them to estimate the onset time by linear extrapolation. For events where more than one exposure is available, we estimated the total number of protons by assuming that the flux changed linearly with time between measurements.

4.1.1. *>100 MeV LPGRE Spectra Cannot be Fit by Primary Electron Bremsstrahlung*

As discussed in §1 and above, pre-*Fermi* observations suggested that ions and not primary electrons are responsible for producing the late phase emission. We quantitatively addressed this question using the observed >100 MeV 2014 February 25 LPGRE spectrum. In Figure 6 we plot the calculated pion-decay photon spectrum (red curve) produced by interactions of protons with a power-law index s_p= 2 and an exponential cutoff, E_0 = 1.3 GeV, that provides a good fit to the LAT count spectrum observed at the peak of the LPGRE on 2014 February 25 (Figure 5). We attempted to find an electron bremsstrahlung spectrum that approximates the same shape. In order to duplicate the flat photon spectral shape at low energies, we chose a power-law electron spectrum with index, s_e = 1. In order to duplicate the roll-over in the pion-decay spectrum that fits the data well above a few hundred MeV, we introduced an exponential cutoff, E_0, in the electron spectrum. We varied the cutoff energy to provide the closest fit to the pion-decay spectrum and found that this occurred at about 1 GeV.

At these high electron energies, it is necessary to take into account the effect that synchrotron losses have on the shape of the resulting bremsstrahlung spectrum. The solid green curves in Figure 6 show how the bremsstrahlung spectrum changes with increasing magnetic field when the interaction region has a density of 10^{16} cm^{-3}. Electrons with energies >100 MeV can penetrate to these chromospheric densities. At such densities, bremsstrahlung dominates over synchrotron losses so that even with a magnetic field of 1000 G, the photon spectrum changes only marginally, as can be seen by the two green curves. The fit of this optimized bremsstrahlung spectrum to the LAT spectral data is poor (probability of $< 10^{-5}$). If the thick target has a lower density, 10^{12} cm^{-3}, the bremsstrahlung spectrum in a 1 G field has a shape similar to the green curve plotted for 1000 G and 10^{16} cm^{-3} density. If we increase the field strength to 1000 G at this lower density, the spectrum rolls over more rapidly at high energies (see blue curve) and is an even worse representation of the best-fit pion-decay spectrum. It is, therefore, clear that primary electron bremsstrahlung fails to reproduce the broad peak near 100 MeV resulting from π^0 decay. This poor fit of electron bremsstrahlung to the LAT count spectrum is shown by the dashed curve in Figure 5. We conclude that bremsstrahlung from plausible electron spectra cannot fit the shape of the LPGRE in the event on February 25 and that the source of >100 MeV

γ-rays is the decay of pions produced by proton interactions.

We made similar comparisons of pion-decay and bremsstrahlung spectral shapes for 16 separate LAT exposures where the >100 MeV LPGRE flux exceeded $>10^{-4}\gamma$ cm^{-2} s^{-1}. With >99.9% confidence, the pion-decay shape provided a significantly better fit to each γ-ray spectrum than did any plausible primary electron bremsstrahlung spectrum.

4.1.2. *Corrections for Non-Isotropic Particle Distributions*

Doppler shifts of nuclear de-excitation lines measured in impulsive flares occurring at a range of heliocentric angles show that the ions interacting to produce the excited nuclei are not isotropic. The shifts are instead consistent with a downward-isotropic angular distribution of interacting ions (Share et al. 2002). However, the angular distribution of the accelerated ions could still be isotropic, and the apparent anisotropic distribution of the interacting ions may be due to escape of upward moving protons. In any case, the magnetic loop transport and interaction model of Hua et al. (1989) shows that the angular distribution of the particles that interact are never isotropic.

Because of relativistic beaming of the pion-decay radiation, such anisotropic particle distributions can change both the intensity and spectral shape of the escaping pion-decay emission. We need to assess the effect of such anisotropic distributions on the results we obtained using the Murphy et al. (1987) isotropic code. Mandzhavidze & Ramaty (1992) calculated escaping pion-decay γ-ray emission using a solar-flare magnetic loop model similar to that used by Hua et al. (1989) for production of nuclear deexcitation-lines. The model accounts for ion energy losses due to Coulomb collisions, ion removal by nuclear reactions, magnetic mirroring of the ions in the converging flux tube, and pitch-angle scattering (PAS) of the ions due to MHD turbulence in the corona. Energetic ions are released isotropically at the top of the loop, and the angular distribution of the ions when they interact is determined by the magnetic-field convergence and the level of PAS. A downward-isotropic angular distribution results when there is no magnetic convergence. A converging magnetic field results in mirroring of the accelerated particles and an interacting-ion angular distribution that is peaked parallel to the solar surface (i.e., a broad fan beam) and in a more shallow interaction region. PAS repopulates the loss cone and results in both a more downward-directed ion angular distribution and a deeper interaction region. Mandzhavidze & Ramaty (1992) also included relativistic beaming of the pion-decay photons and Compton scattering of the escaping photons. While flare ions are transported and trapped in compact magnetic loops, the protons producing the LPGRE pion-decay emission may not be. In any case, the protons are still more likely to follow an approximately downward-isotropic distribution or, if magnetic mirroring dominates, a "fan beam" distribution when they interact.

The Mandzhavidze & Ramaty (1992) treatment provides the calculated pion-decay spectra needed to fit the LAT observations for anisotropic particle distribution, but spectra for a only limited set of parameters were presented in the paper. Unfortunately, we do not have access to the authors' code to calculate spectra over a wider range. However, Mandzhavidze & Ramaty (1992) provided the angle dependent escaping fluxes of pion-decay radiation for a proton spectrum following a power law proton spectrum with index 3 in Figure 10 of their paper. By comparing these heliocentric angle dependent fluxes, after removing the attenuation correction, with those calculated by Murphy et al. (1987), we can determine a heliocentric angle dependent factor to correct the number of protons required to produce the LPGRE. We use the neutral pion-decay component because it is dominant >100 MeV where the LAT measurements are made. For quasi downward-isotropic and fan beam distributions, this factor varies from unity at the solar limb to ~2.3 and 2.1 at disk center, respectively. These same factors can be applied to events with softer proton spectra because Mandzhavidze & Ramaty (1992) show that the heliocentric angular distribution of the flux of escaping pion decay radiation is relatively independent of spectral hardness. The charged pion component that produces lower energy positron and electron bremsstrahlung is more strongly attenuated on the solar disk for quasi downward-isotropic angular distributions than is the neutral component. This produces a total pion decay spectrum that is less steep below 100 MeV than calculated by Murphy et al. (1987), but not enough to account for what looks to be a pure neutral pion-decay spectrum observed by Akimov et al. (1996).

There is not enough information in Mandzhavidze & Ramaty (1992) to determine how much all the LPGRE power-law indices determined by the Murphy et al. (1987) code might change versus heliocentric angle for anisotropic proton distributions. From calculated γ-ray spectra produced by protons following a power law with index 3 that are plotted in Figure 15 of Mandzhavidze & Ramaty (1992), we can infer that there is no strong heliocentric angle dependence on the calculated pion decay spectrum for a fan beam particle distribution. However, for a quasi downward-isotropic particle distribution there is enough softening in the calculated pion decay photon spectrum for events near disk center so that a proton spectral index of 4 determined using the isotropic Murphy et al. (1987) code may actually be closer to 3. Whether such significant hardening at disk center occurs for even softer proton spectra is not known.

4.1.3. *Using the Neutron-Capture Line for Studying the Spectra of Impulsive- and Late-Phase Protons*

The 2.223 MeV neutron-capture line is usually the most prominent narrow-line feature in the 0.3–8 MeV γ-ray spectrum for flares far from the solar limb. It is produced by ions ranging in energy between about one and several hundred MeV nucleon^{-1}, depending on the steepness of the ion spectra (Murphy et al. 2007). Below we first describe how we used *RHESSI* and GBM measurements of the 2.223 MeV line to estimate the number of >500 MeV protons in the impulsive phase of events with LPGRE, especially when no LAT >100 MeV γ-ray observations were available.

We typically fit background-subtracted GBM and *RHESSI* impulsive phase spectra between 1.8 and 2.4 MeV with a continuum and a Gaussian peak to obtain the measured 2.223 MeV neutron-capture line flux, or its upper limit. For a few intense events, we fit the full 0.3 to 8 MeV spectrum with all the nuclear and bremsstrahlung components. As the capture line is produced deep in the chromosphere and in the photosphere, the flux is significantly attenuated. We used the code developed by Hua et al. (2002) to calculate the line flux (including attenuation) for the flare heliocentric angle and assumed spectrum of the accelerated protons producing the line. Using the measured 2.223 MeV line flux, we infer the number of protons >500 MeV for that assumed proton spectrum. The question is, what shall we use for the assumed impulsive phase energy spectrum over the broad two to several hundred MeV energy range?

Using the 1.63 MeV ^{20}Ne and 6.13 MeV ^{16}O deexcitation-line ratio obtained from a fit to the spectrum obtained by summing the 19 strongest gamma-ray flares observed with SMM, Murphy et al. (2016) found that the average 2–20 MeV proton spectrum, assuming it to be a power law and that the solar Ne/O abundance ratio is 0.15, has a index of 4.9. If the Ne/O ratio is closer to 0.25 then the 2–20 MeV index would be 4.2. Ramaty et al. (1996) studied γ-ray line ratios in the 19 flares observed with *SMM* (Share & Murphy 1995). Using the flux ratio of the 2.223 MeV neutron capture line to the 4.44 MeV ^{12}C deexcitation-line, the mean proton power-law index between about 5 and 40 MeV was ~4.1, consistent with the 2–20 MeV index assuming an Ne/O abundance ratio of 0.25 (Ramaty et al. 1996). Assuming a power law, Ackermann et al. (2012c,b) used the measured ratio of the neutron-capture line flux to pion-decay flux to infer that, during the impulsive flare on 2010 June 12 flare, the index between about 40 and 300 MeV was ~4.3. The index was calculated assuming an isotropic particle distribution for pion production; if a downward isotropic proton distribution had been used, the proton index would have been ~4.0. Both of these indices are consistent with the index obtained from nuclear line studies for a Ne/O abundance ratio of 0.25. Using fits to the measured pion-decay spectra, Ackermann et al. (2012c) provided evidence that the impulsive phase proton spectrum above 300 MeV had an index >4.5. Finally, there are two events in our study where LAT detected >100 MeV emission during the impulsive phase (§C.6 and §C.16). In each event, fits to the measured pion-decay spectra showed that the >300 MeV proton spectrum was consistent with a power law having an index of 6 or larger. Therefore, to estimate the number of impulsive-phase >500 MeV protons from the 2.223 MeV line flux, we shall assume that the proton spectrum is a power-law having an index of 4 below 100 MeV which steepens to an index of 5 at higher energies.

We also used upper limits on the 2.223 MeV neutron-capture line to constrain the steepness of the LPGRE proton spectrum <300 MeV. This can only be done for the most intense LPGRE events. We use the calculations of Murphy et al. (1987) to obtain limits on the 20–300 MeV proton spectral index, s_p, based on the ratio of the 2.223 MeV line flux to the >100 MeV γ-ray flux. The calculations assume that the >300 MeV protons producing the pion emission have an isotropic angular distribution. Based on calculations of Mandzhavidze & Ramaty (1992), the derived s_p will decrease by 0.3 (spectrum hardens) for flares at disk center if the protons have a downward isotropic angular distribution. In §5.3.2 we compare limits on the 20–300 MeV proton spectral index with measurements of the index >300 MeV to reveal how the LPGRE spectrum changes with increasing energy.

5. RESULTS

We identified 31 episodes of Late Phase Gamma Ray Emission (LPGRE) in 30 events occurring between 2008 and 2015 that we list in Table 1. Here we discuss the results of our study of these events. In §5.1 we discuss the relationship between LPGRE events, flares, CMEs, and SEPs and discuss the conditions under which the γ-ray emission is produced. We then provide details of the temporal characteristics of the LPGRE and compare them with other solar emissions in §5.2. In §5.3 we detail the spectral characteristics of the LPGRE and in §5.4 compare the numbers of protons in the LPGRE event with those in the associated flare and those in the SEP event. In §5.5 we discuss two LPGRE events associated with behind-the-limb flares and provide evidence that bremsstrahlung observed by GBM on 2014 September 1 was produced by electrons with energies reaching up to 10 MeV that were likely accelerated in the same process that produced the LPGRE.

5.1. *General Characteristics of Late Phase Gamma-Ray Emission Events*

A clear association of LPGRE events with either impulsive flares, CMEs, or SEP events would provide valuable information about the source of ion acceleration. The associated *GOES* soft X-ray flares ranged from a C3.7 to an X5.4, with one C-class, 14 M-class, and 16 X-class flares associated with the 31 emission episodes. There is no clear association between the intensity of flare soft X-ray emission and the occurrence of LPGRE events. By contrast, all of the pre-*Fermi* LPGRE events were associated with X-class flares. This may have just been due to the lower sensitivity of earlier >10 MeV instruments relative to FERMI/LAT. The listed *GOES* X-ray durations ranged from about 8 to 135 minutes.

All but two of the LPGRE events were associated with CMEs, with speeds ranging from about 600 to 2700 km s^{-1}. In every case where a CME was present, it was either a halo or partial-halo event (indicating very wide CMEs). Twenty four of the 30 events were associated with Type II metric radio emission and all but two were associated with either Type II metric or decametric-hectometric emission. Solar energetic particles were clearly observed in association with all but eight of the LPGRE events. A stronger preceding SEP event may have masked the particle emission in five or six of the events. The only two LPGRE events with no clear evidence for SEP protons occurred on 2012 October 23 and November 27, the two events when CMEs were not detected. However, AIA movies reveal evidence for the eruption of a magnetic loop in the low corona in both of these events and Type II metric radio emission, indicating shock formation, was detected following the magnetic eruption on 2012 October 23. This suggests that these LPGRE events may have been accompanied by failed CMEs (Ji et al. 2003). Hard X-ray observations during the impulsive phase are available for 27 of the 30 LPGRE events (28 of the 31 emission episodes) and in each case photons exceeding 100 keV were observed.

To further investigate this association of fast CMEs and >100 keV flares with LPGRE events, in Appendix §B we analyze a sample of solar eruptive events detected between 2010 and 2012 which have at least one of these characteristics. The sample consists of events that exhibit a wide CME faster than 800 km s^{-1}, SEPs exceeding 1 pfu at 10 MeV at Earth, or hard X-rays detected above 100 keV. This results in a list of 95 events, composed of 1 GOES-class B flare, 23 C flares, 38 M flares, 15 X flares, and 18 events with no flare identification (generally fast CMEs presumably from events over the limb). 19 of the 95 events exhibit both CME speeds above 800 km s^{-1} and flare emission above 100 keV. 14 of these 19 events produced LPGRE, indicating that the combination is not a sufficient condition for producing LPGRE. It is, however, possible that LAT's limited duty cycle for solar observations (see §2), i.e., solar data for 20-40 minutes out of every 90 or 180 minutes, could have resulted in LAT missing LPGRE emission in these five events (see Appendix B.1) if the duration of >100 MeV emission was less than about 50 minutes. The proximity of some of the five events to the solar limb could also result in diminished >100 MeV fluxes.

As noted earlier, the requirement for pion production by interaction of > 300 MeV protons with H implies that the pions are produced in high-density regions that must be relatively deep in the solar atmosphere, and in order for the resulting pion-decay photons to be detected these interactions must therefore be happening on regions of the solar disk visible from Earth. With the detection of the LPGRE events on 2013 October 11 and 2014 September 1 (Pesce-Rollins et al. 2015a; Ackermann et al. 2017) arising from flares with locations $\sim 10^\circ$ and $\sim 40^\circ$ beyond the limb, it is clear that the protons producing the LPGRE can interact tens of degrees from the flare site. Gamma-ray line emission from a flare $\sim 15^\circ$ beyond the limb was also observed by *SMM* on 1989 September 29 (Vestrand & Forrest 1993). From the study discussed in Appendix B of 70 eruptive events from 2008 to 2012 associated with CMEs with velocities $\gtrsim$800 km s^{-1}, we find that 35 were on the visible disk and 35 were beyond the limb of the Sun. There were 13 LPGRE events associated with the 35 fast CMEs arising from locations on the visible disk, but there were none associated with the 35 fast CMEs on the far side of the Sun. If we assume that about 1/3 of all fast CMEs are associated with LPGRE events and that LPGRE can be observed within tens of degrees from the flare location, we would expect to have detected up to seven LPGRE events from the 21 CME events located on the far side of the Sun but within $\sim 40^\circ$ of the limb. Since no LPGRE was detected in this sample, we conclude that the source of LPGRE usually lies within about ten heliocentric degrees of the active region location.

There is one peculiarity in the location of the flares associated with LPGRE: 24 out of the 30 events ($\sim$1% probability for a random distribution) occurred in the northern hemisphere even though sunspot activity was higher in the southern hemisphere during the same time period. Similarly, 79 of 95 the eruptive events discussed in Appendix §B occurred in the northern hemisphere, although this is less surprising since in the sample period 2010-2012 activity was markedly stronger in the northern hemisphere. We note, however, that such varying north/south asymmetries in solar indices is well known (see e.g. Verma (1993) and references within). There were roughly equal numbers of LPGRE events in the eastern (17) and western (13) hemispheres.

5.2. *Temporal Characteristics of Late Phase Gamma Ray Emission*

We provide time histories on minute and hour time scales for all 30 LPGRE events in Appendix C. They are plotted in the same format as Figure 4. Because the 2012 March 7 event (Table 1 number 12, Appendix C.12, Figure C17), has two separate LPGRE eruptions there are 31 cases to study. For each of the 31 episodes in the Appendix, we start by discussing the distinct nature of the LPGRE. In 17 of the 31 LPGRE episodes, the >100 MeV emission began after the impulsive phase hard X-rays. In four other episodes (event numbers 5, 16, 19, and 30), the >100 MeV LPGRE began during the impulsive hard X-ray peaks, but had a time history different from than that of the X-ray emission. Each of the remaining 10 LPGRE episodes were observed in only one 20–40 minute LAT solar exposure well after the flare. In seven of these events there is no evidence for temporal variation during the exposure, suggesting that the measurement may have been made near the peak of the LPGRE. In two of the events (event numbers 26 and 27) there is weak evidence at the 80–90% confidence level that the emission was falling with time during the exposure, and in one event (event number 17) the evidence for a falling flux is stronger. We could not determine if the emission in these three events came from the falling phase of a short LPGRE event or from the tail of the impulsive phase. However, in none of the 31 episodes did we find clear temporal evidence that the emission was the tail of >100 MeV γ-rays produced in the impulsive phase. In the following sections we: 1) compare CME, Type II radio, and LPGRE onset times; 2) study the LPGRE onset times and durations; and 3) discuss whether the LPGRE is due to a series of episodic events rather than continuous emission.

5.2.1. *CME, Radio, and LPGRE Onset Times*

We compared three methods for obtaining the time of rapid acceleration, or onset time, of CMEs: 1) CDAW extrapolations of LASCO coronagraphic observations of CME height vs. time, 2) our visual inspection of *SDO* AIA movies, and 3) the rise in flare soft X-rays (Zhang et al. 2001). We investigated these onset times in a sample of 28 eruptive events, including some in which LPGRE was observed, and we found that the CME onset times estimated from the EUV movies agreed well with the rise time of *GOES* 1–8Å emission; the mean difference is less then 0.5 minutes, with a maximum difference of four minutes. In contrast, the average of the CME onset times in the CDAW catalog, derived from linear and quadratic extrapolations, differ by as much as 20 minutes from the times based on the EUV movies, with an average difference of just over a minute. We therefore chose to use the CME onset times derived from the EUV movies as the reference time in determining the delays of Type II radio and late phase γ-ray emission. We list these CME onset times for the 30 LPGRE events in column 3 of Table 2. There were no CMEs reported for the 2012 October 23 (event 17; Appendix C.18, Figure C24) and 2012 November 27 (event 18, Appendix C.19, Figure C25) events, but there is clear evidence for the eruption of magnetic loops in AIA images at 03:15 UT and 15:56 UT, respectively, along with material moving away from the flare region. We, therefore, use these times as the eruption onsets for these two events.

Type II radio emission, discussed in Appendix E, is attributed to electrons accelerated at a shock and radiating in its vicinity as it moves through the corona. The onset time of Type II emission is often taken to mark the formation time of the shock as the CME moves outwards through decreasing Alfvén speed in the corona, and can be compared with the onset times of the CME and the LPGRE. In column 4 of Table 2, we list the Type II onset times, primarily derived from metric observations. Where these metric measurements are not available we list in italics the times derived from interplanetary decametric/hectometric (DH) observations. No Type II radio emission was observed from the 2012 November 27 event (event number 19), one of the two LPGRE events not accompanied by a CME. On average we find that metric Type II emission begins about six minutes after the CME onset times. Using these delays and the CME linear speeds from the CDAW catalog for the events in the study, we estimate that the shock, on average, was formed at a heliocentric distance of $\sim$1.7 $R_\odot$. Using a more sophisticated analysis of CMEs, Gopalswamy et al. (2013) found that the shock formation locations ranged from 1.20 to 1.93 $R_\odot$, with mean and median values of 1.43 and 1.38 $R_\odot$, respectively. These timing studies indicate that the CME shocks can form relatively low in the corona.

Table 2. Onset Times of CME, Type II Radio, and LPGRE

Event Number	Date	CME Onset UT	Type II Onset UT	LPGRE Onset UT
(1)	(2)	(3)	(4)	(5)
1	2011/03/07	19:45	19:54	$19{:}40\ ^{+00:22}_{-00:20}$
2	2011/06/02	07:43	*08:00*[a]	<09:40

Table 2 continued on next page

Table 2 *(continued)*

Event Number	Date	CME Onset UT	Type II Onset UT	LPGRE Onset UT
(1)	(2)	(3)	(4)	(5)
3	2011/06/07	06:16	06:25	<07:48
4	2011/08/04	03:46	03:54	<04:56
5	2011/08/09	08:02	08:01	08:02:40 ± 00:00:40
6	2011/09/06	22:18	22:19	22:20:00 ± 00:00:40
7	2011/09/07	22:36	22:38	<23:38:00
8	2011/09/24	09:34	09:35	09:40 ± 00:01
9	2012/01/23	03:40	*04:00*[a]	04:17 ± 00:01
10	2012/01/27	18:07	18:10	$19:31\ ^{+00:06}_{-00:22}$
11	2012/03/05	03:32	*04:00*[a]	04:30 ± 00:03
12	2012/03/07	00:07	00:17	$00:20\ ^{+00:08}_{-00:20}$
		01:01	01:09	$02:01\ ^{+00:07}_{-00:13}$
13	2012/03/09	03:38	03:43	$04:00\ ^{+00:30}_{-01:10}$
14	2012/03/10	17:24	*17:55*[a]	20:00 ± 01:20
15	2012/05/17	01:27	01:31	<02:15
16	2012/06/03	17:53	17:59	$17:55\ ^{+00:01}_{-00:04}$
17	2012/07/06	23:04	23:09	<23:26
18	2012/10/23	03:15[b]	03:17	<04:16
19	2012/11/27	15:56[b]	—	15:55 ± 00:01
20	2013/04/11	06:53	07:02	07:11 ± 00:01
21	2013/05/13	01:58	02:10	<04:30
22	2013/05/13	15:48	15:57	$17:07\ ^{+00:07}_{-00:09}$
23	2013/05/14	01:04	01:07	01:20 ± 00:03
24	2013/05/15,	01:29	01:37	03:00 ± 01:00
25	2013/10/11	07:08	07:11	07:15 ± 00:01
26	2013/10/25	07:57	07:59	<08:17
27	2013/10/28	15:00	15:10	<15:45
28	2014/02/25	00:43	00:56	$00:55\ ^{+00:06}_{-00:16}$
29	2014/09/01	10:57	*11:12*[a]	11:02 ± 00:01
30	2015/06/21	02:10	02:24	02:23 ± 00:03

[a] DH Type II start time in the absence of metric report

[b] No CME observed; onset time of magnetic eruption

The LPGRE onset times were derived by visual inspection of the >100 MeV fluxes plotted for the 30 events in Appendix C. In some cases the onset time can be clearly distinguished with an accuracy of one or two minutes. In other cases we fit the time history to estimate the onset and its uncertainty, as we did for the 2011 March 7 LPGRE event plotted in Figure 4 discussed in §3.1. For events for which there was only one solar exposure with detectable >100 MeV emission and no evidence for short-term variability, we used the start time of the exposure as an upper limit on the onset time. Our best estimates of the LPGRE onset times and their uncertainties are listed in column 5 of Table 2.

5.2.2. *Study of LPGRE Onset Delays and Durations*

We define the LPGRE onset delay as the difference between the LPGRE onset time and the CME onset time listed in column 3 of Table 2. As LAT had limited exposure to the Sun, our estimates of the durations are, in many cases, upper limits based on the time of the first LAT solar exposure with no detectable >100 MeV emission. This uncertainty does not impact the coarse comparisons that we are making. The durations are listed in column 6 of Table 3 for the "LPGRE Total" entries in column 2. In Figure 7, we plot the durations of the LPGRE events versus their onset delays. We include, separately, the delays and durations of the two post-flare LPGRE episodes on 2012 March 7, each

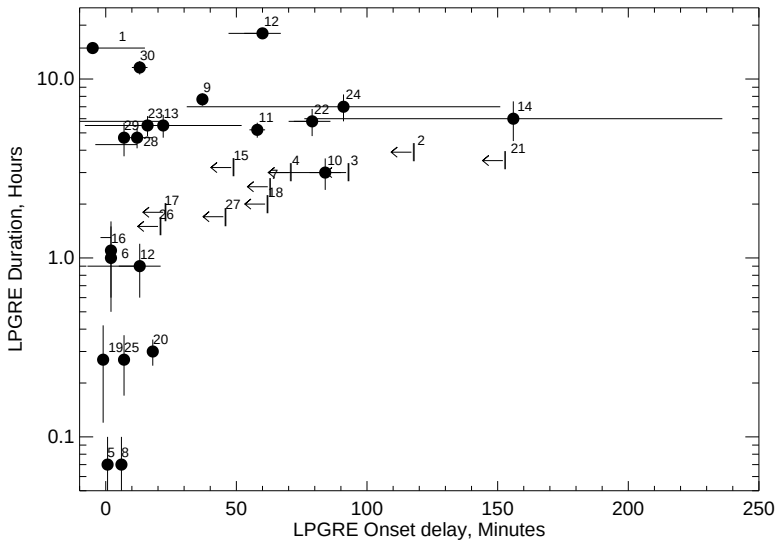

Figure 7. Estimated duration of >100 MeV LPGRE plotted against the delay in its start time from the onset of the CME determined from *SDO* AIA movies. When an onset time cannot be estimated, we place a horizontal upper limit symbol at the start time of the exposure in which LPGRE was first detected. The event numbers in Table 1 are printed adjacent to the data points.

identified by number 12 in the figure. Thus, there are 31 individual points in the plot. We were able to estimate the onset delays based on multiple flux observations for 21 of them (shown by filled circles). For ten of the events we only have upper limits on the delays. The measured LPGRE onset delays ranged from minutes to an hour or more. Sixteen of the 31 plotted events have onset delays shorter than 30 minutes. Four well-measured delays exceeded one hour.

The estimated LPGRE durations were as short as about 10 minutes and as long as ∼20 hours, with a mean duration of about 4.5 hours. As some of the longest lasting LPGRE events also had large onset delays, the durations and delays of the measured events (filled circles) exhibit a weak correlation (correlation coefficient 0.24). We also studied the approximate rise times of the LPGRE events (onset to estimated peak). They range from as short as a few minutes to as long as 6 hours.

We found no correlation between CME speed and LPGRE onset delay and only a weak correlation (correlation coefficient 0.3) between CME speed and LPGRE duration. We also compared the durations of ten >100 MeV SEP proton events observed by *GOES*, that were magnetically well-connected to the flare site, with the durations of the associated LPGRE events. The SEP duration was estimated from the time of onset to the time that the flux dropped to ∼10% of its peak value. The SEP and LPGRE durations plotted in Figure 8a) are correlated (correlation coefficient 0.93), with the SEP events lasting on average about five times longer. For comparison, in Figure 8b) we compare LPGRE durations with the durations of tails observed in soft X-rays from extended heating of the corona following flares (e.g. Ryan et al. (2013)). We defined the duration of the SXR emission to be from the time of the peak *GOES* 1–8Å flux to the time at which the flux had fallen back to the pre-flare background level. Small flares that occurred during this decay did not affect this study because of the relatively smooth exponential decay of the SXR emission from the flare of interest. There is a large scatter in the data points leading to a weaker correlation (correlation coefficient 0.32).

5.2.3. *Search for Short-Term Temporal Variations in LPGRE Events*

There were two distinct late phase emission episodes on 2012 March 7, one lasting about an hour and the second one about 18 hours. Otherwise the LAT time histories appear to be relatively smooth. Because of LAT's low duty cycle for solar observations, there are limited opportunities to study short-term variations. We searched LAT data at 4-minute temporal resolution for evidence that the gradually varying emission lasting for hours had such time structure. This study was best done for the longest duration LPGRE events on 2011 March 7 (event 1) and 2012 March 7 (second episode in event 12). We found no evidence for any short-term variations in any of the LPGRE exposures. Any temporal variations that we did find were instrumental and occurred as the Sun was leaving the field of view of the LAT, where the solar exposure was not well determined.

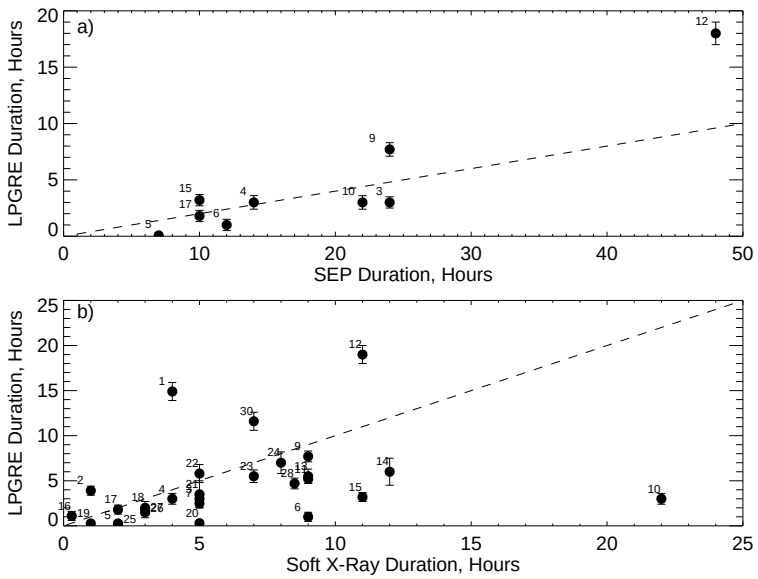

Figure 8. a) Estimated durations of LPGRE events plotted against durations of ten well-connected >100 MeV proton events observed by *GOES*. Dashed line: SEP duration 5× longer than LPGRE duration. b) Estimated durations of LPGRE events plotted against durations of SXR emission observed by *GOES*. Dashed line: equal LPGRE and SXR durations.

5.3. *Spectroscopic Studies of LPGRE*

In this section we summarize the *Fermi*/LAT spectroscopic measurements of >100 MeV γ-rays observed in the 30 LPGRE events and the related *RHESSI* and GBM observations in the nuclear γ-ray line energy range. These include observations made during both the impulsive and late phases of the events. Details of our analysis techniques are presented in §4. They are based on theoretical studies of pion decay emission for an assumed isotropic ion distribution (Murphy et al. 1987). Because the angular distribution of the ions producing the pion decay emission is likely to be anisotropic, we discuss how our results need to be modified for such distributions. We detail the results of these spectroscopic studies in Table 3 in §5.3.1. In §5.3.2 we discuss the inferred power-law indices of >300 MeV protons producing the LPGRE for all 30 events and of <300 MeV protons for seven intense events.

5.3.1. *Table of Spectral Characteristics of LPGRE in Solar Eruptive Events*

Table 3 provides the results of our spectroscopic study of the 30 events listed in Table 1. The listed values are based on our spectral fits with pion-decay templates derived for an isotropic particle distribution. The first column lists the date of the event and the event number in parentheses. In column two we indicate the type of emission for which we provide the information for that row. There are three types: 1) LPGRE, 2) impulsive phase emission indicated by its *GOES* class, and 3) SEP protons. If there is more than one LAT exposure for each event, we put the number of the exposure in parenthesis, e.g. LPGRE (2). As there were two LPGRE eruptions on 2012 March 7, we distinguish the individual exposures as A and B, e.g. LPGRE(A1) and LPGRE(B1). The third column gives the time interval of the LAT solar exposure providing the information. The measured >100 MeV γ-ray flux and uncertainty are listed in column 4.

In column 5, we list the best-fit spectral index and uncertainty of the >300 MeV protons producing the flux (with the exception of the 2014 February 25 event where a power-law times an exponential was necessary to fit the data, as discussed in §4.1). In the rows entitled LPGRE <300 MeV we provide the ∼20–300 MeV power-law spectral indices estimated for intense events, based on a comparison of measured fluxes of the 2.223 MeV neutron-capture line and >100 MeV emission (§4.1.3). As discussed in §4.1.2, Mandzhavidze & Ramaty (1992) calculated pion decay spectra for anisotropic distributions. We estimate for a downward isotropic distribution that the listed <300 MeV proton spectral indices should be reduced by as much as 0.3 for events near disk center.

From the >100 MeV γ-ray flux and its estimated attenuation for the flare location, the derived proton spectral index, and assumptions about the temporal structure of the LPGRE (§4.1), we estimated the numbers of >500 MeV protons required in each time interval and list them in column 7. These estimates were done using the results of Murphy et al. (1987) for an isotropic particle distribution and taking into account absorption of the photons in the solar atmosphere. In column 7 of the row labelled 'LPGRE Total' we list our estimate of the total number of >500 MeV protons and its

uncertainty, based on both statistical errors and our confidence in the time history and duration of the event, given in column 6. For a downward isotropic particle distribution, the Mandzhavidze & Ramaty (1992) calculations indicate that the number of protons required to produce the observed γ-ray flux would range from a factor of unity, for events near the solar limb, to a factor of $\sim$2.3 higher for events near disk center. We list this heliocentric-angle dependent correction factor in parentheses. In column 7, in the rows labelled 'SEP protons', we list estimates of the integrated number of >500 MeV protons in space and their uncertainties determined in Appendix D.

Table 3. Spectral Characteristics of LPGRE Events

Date (Event) yyyy/mm/dd (1)	Type (2)	Observing Interval, UT (3)	Flux >100 MeV $10^{-4}\gamma$ cm^{-2} s^{-1} (4)	Proton PL Index s[f] (5)	Emission Interval, UT (6)	>500 MeV Protons $\times10^{28}$ (Correction Factor)[a] (7)
2011/03/07 (1)	LPGRE (1)	20:10–20:39	0.17 ± 0.03	3.3 ± 0.45	20:00–20:39	0.1
	LPGRE (2)	23:21–00:03	0.29 ± 0.03	4.1 ± 0.4	20:39–00:03	1.6
	LPGRE (3)	02:32–03:13	0.35 ± 0.03	4.3 ± 0.4	00:03-03:13	2.4
	LPGRE (4)	05:43–06:25	0.14 ± 0.02	6.7 ± 1.4	03:13–06:25	2.0
	LPGRE (5)				06:25–11:00	1.1
	LPGRE Total				20:00–11:00	7.2 ± 2.1 (2.1)[a]
	M3.7 flare				19:58–20:06	<0.07[b]
2011/06/02 (2)	LPGRE	09:41–10:28	0.07 ± 0.02	4.2 ± 2.0	08:10 – 12:00	0.03 ± 0.02 (2.2)[a]
2011/06/07 (3)	LPGRE (1)	07:48–08:19	0.29 ± 0.03	4.5 ± 0.6	07:00 – 08:20	0.5
	LPGRE (2)				08:20–10:00	0.6
	LPGRE Total				07:00–10:00	1.1 ± 0.4 (2.0)[a]
	M2.5 flare				06:24–06:45	<0.2[b]
	SEP protons					4.3 ± 2.9
2011/08/04 (4)	LPGRE (1)	04:56–05:37	0.28 ± 0.03	4.6 ± 0.6	04:10–05:10	0.4
	LPGRE (2)				05:10–07:10	0.8
	LPGRE Total				04:10–07:10	1.2 ± 0.3 (2.1)[a]
	M9.3 flare				03:48–04:00	<0.1[b]
						<0.4 (2.1)[a]
	SEP protons					7.3 ± 5.0
2011/08/09 (5)	LPGRE	08:02:40–08:06:00	2.0 ± 0.2	5.8 ± 0.9	08:02:40–08:06:00	0.4 +- 0.1 (1.4)[a]
	LPGRE <300 MeV			4.3 ± 0.3[c]		
	X6.9 flare				08:02:00–08:02:20	<0.01 (1.4)[a]
	X6.9 flare				08:03:40–08:04:00	<0.01 (1.4)[a]
2011/09/06 (6)	LPGRE (1)	22:21–22:28	3.9 ± 0.2	5.3 ± 0.4	22:21–22:28	1.2
	LPGRE (1) <300 MeV	22:21–22:28		<4.0[c]		
	LPGRE (2)	22:28–22:34	4.4 ± 0.2	3.5 ± 0.3	22:28–22:34	0.6
	LPGRE (2) <300 MeV	22:28–22:34		<3.6[c]		
	LPGRE (3)	22:37–22:47	1.5 ± 0.1	3.5 ± 0.2	22:37–22:47	0.4
	LPGRE (3) <300 MeV	22:37–22:44		<3.9[c]		
	LPGRE Total				22:21–23:20	2.2 ± 0.4 (2.3)[a]
	X2.1 flare		6.6 ± 1.0	>6	22:18–22:20	0.13 ± 0.05(2.3)[a]
2011/09/07 (7)	LPGRE (1)	23:51–00:09	0.07 ± 0.02	4.4 ± 1.4	22:45–00:00	0.1
	LPGRE (2)				00:00–01:10	0.1
	LPGRE Total				22:45–01:10	0.2 ± 0.1 (2.2)[a]
	X1.8 flare				22:36–22:38	<0.1[b]

Table 3 continued on next page

Table 3 *(continued)*

Date (Event) yyyy/mm/dd (1)	Type (2)	Observing Interval, UT (3)	Flux >100 MeV $10^{-4}\gamma$ cm^{-2} s^{-1} (4)	Proton PL Index s[f] (5)	Emission Interval, UT (6)	>500 MeV Protons $\times10^{28}$ (Correction Factor)[a] (7)
2011/09/24 (8)	LPGRE	09:40–09:44	0.3 ± 0.09	3.4 ± 1.4	09:40–09:44	0.03 ± 0.01 (1.7)[a]
	X1.9 flare				09:35:30–09:37:00	<0.007 (1.7)[a]
2012/01/23 (9)	LPGRE (1)	05:46–06:10	0.19 ± 0.02	5.1 ± 0.8	04:20–05:59	0.8
	LPGRE (2)	07:18–07:48	0.16 ± 0.05		05:59–07:34	0.7
	LPGRE (3)	08:58–09:28	0.19 ± 0.03		07:34–09:14	0.8
	LPGRE (4)				09:14–12:00	0.7
	LPGRE Total				04:20–12:00	3.0 ± 0.6 (2.2)[a]
	M8.7 flare				03:53–04:09	<0.4[b]
	SEP protons					37 ± 23
2012/01/27 (10)	LPGRE (1)	19:36–19:56	0.26 ± 0.05	4.7 ± 0.7	19:00–19:50	0.5
	LPGRE (2)	21:06–21:37	0.05 ± 0.02	3.1 ± 0.6	19:50–21:21	1.1
	LPGRE (3)				21:21–22:00	0.05
	LPGRE Total				19:00-22:00	1.7 ± 1.0 (1.1)[a]
	SEP protons					100 ± 62
2012/03/05 (11)	LPGRE (1)	05:46–06:12	0.10 ± 0.015	4.9 ± 0.9	04:35–05:59	0.12
	LPGRE (2)	07:18–07:56	0.075 ± 0.019	3.6 ± 0.8	05:59–07:36	0.25
	LPGRE (3)				07:36–10:00	0.16
	LPGRE Total				04:30–10:00	0.53 ± 0.15 (2.0)[a]
	X1.1 flare				03:55–04:35	<0.3[b]
		04:28–04:35	<0.15		04:28–04:35	<0.04 (2.0)[a]
2012/03/07 (12)	LPGRE (A) Total	00:39–01:24	28.7 ± 0.4	3.6 +- 0.3	00:28–01:24	40 ± 15 (2.2)[a]
	LPGRE (B1)	02:18–02:48	5.8 ± 0.3	3.5 ± 0.2	02:00–02:34	3
	LPGRE (B1) <300 MeV			<3.3[c]		
	LPGRE (B2)	03:50–04:34	10.0 ± 0.2	3.85 ± 0.1	02:34–04:12	23
	LPGRE (B2) <300 MeV			<3.3[c]		
	LPGRE (B3)	05:34–06:01	8.7 ± 0.4	4.25 ± 0.2	04:12–05:46	30
	LPGRE (B4)	07:02–07:46	6.2 ± 0.2	4.5 ± 0.15	05:46-07:24	27
	LPGRE (B4) <300 MeV			<3.3[c]		
	LPGRE (B5)	08:42–09:12	4.1 ± 0.3	4.8 ± 0.5	07:24-08:48	18
	LPGRE (B5) <300 MeV			<3.7[c]		
	LPGRE (B6)	10:33–10:58	2.5 ± 0.2	5.2 ± 0.4	8:48–10:46	17
	LPGRE (B6) <300 MeV			<3.7[c]		
	LPGRE (B7)	13:23–13:33	0.6 ± 0.2		10:46–13:27	9
	LPGRE (B8)	16:35–16:49	0.22 ± 0.06		13:27–16:41	3
	LPGRE (B9)	19:46–20:14	0.07 ± 0.02		16:41-20:01	1
	LPGRE (B) Total				02:00–20:01	131 ± 15 (2.2)[a]
	X5.4 flare				00:16–00:28	1.4[b]
	M7 flare				01:11–01:20	1.1[b]
	M7 flare				01:12–01:17	<0.4 (2.2)[a]
	SEP protons					4075 ± 2590
2012/03/09 (13)	LPGRE (1)	05:10–05:58	0.06 ± 0.03	>6	04:30–06:00	0.1
	LPGRE (2)	06:46–07:32	0.11 ± 0.03	6 ± 1.5	06:00–07:09	0.3

Table 3 continued on next page

Table 3 *(continued)*

Date (Event) yyyy/mm/dd (1)	Type (2)	Observing Interval, UT (3)	Flux >100 MeV $10^{-4}\gamma$ cm^{-2} s^{-1} (4)	Proton PL Index s[f] (5)	Emission Interval, UT (6)	>500 MeV Protons $\times10^{28}$ (Correction Factor)[a] (7)
	LPGRE (3)	08:22–09:08	0.15 ± 0.03	6.7 ± 1.5	07:09–08:46	0.7
	LPGRE (4)				08:46–10:30	0.4
	LPGRE Total				04:30–10:30	1.5 ± 0.6 (2.3)[a]
	M6.3 flare				03:40–04:14	<0.1 (2.3)[a]
	M6.3 flare				03:30–04:06	<0.6[b]
2012/03/10 (14)	LPGRE (1)	20:59–21:33	0.02 ± 0.01	≥6	20:00–21:15	0.05
	LPGRE (2)	22:35–23:15	0.043 ± 0.027	≥6	21:15–22:55	0.18
	LPGRE (3)	00:10–00:56	0.038 ± 0.015	≥6	22:55–00:33	0.2
	LPGRE (4)				00:33-02:00	0.09
	LPGRE Total				20:00-02:00	0.5 ± 0.3 (2.2)[a]
	M8.4 flare				17:51–18:11	<0.1 (2.2)[a]
	M8.4 flare				17:41–18:05	<0.2[b]
2012/05/17 (15)	LPGRE (1)	02:10–02:48	0.08 ± 0.03	2.6 ± 0.6	02:05–02:29	0.02
	LPGRE (2)	03:46–04:22	0.05 ± 0.025	2.2 ± 1.0	02:29–04:02	0.1
	LPGRE (3)				04:02–05:20	0.03
	LPGRE Total				02:10–05:20	0.15 ± 0.1 (1.4)[a]
	M5.1 flare				01:40–01:55	<0.6[b]
	SEP protons					143 ± 92
2012/06/03 (16)	LPGRE (1)	17:51–17:53	0.24 ± 0.08	$2.5\ ^{+1.5}_{-?}$	17:51–17:53	0.01?
	LPGRE (2)	17:54–18:02	0.54 ± 0.06	4.3 ± 0.7	17:54–18:02	0.15
	LPGRE (3)				18:02–19:00	0.58
	LPGRE Total				17:54–19:00	0.74 ± 0.35 (2.2)[a]
	M3.3 flare		3.3 ± 0.4	6.4 ± 1.0	17:53–17:54	0.19 ± 0.05 (2.2)[a]
2012/07/06 (17)	LPGRE (1)	23:27–23:54	0.37 ± 0.04	5.1 ± 0.6	23:14–23:40	0.2
	LPGRE (2)	23:27–23:40		4.7 ± 0.8		
	LPGRE (3)	23:40–23:54		>6.0		
	LPGRE (4)				23:40–01:00	0.7
	LPGRE Total				23:14–01:00	0.9 ± 0.3 (2.1)[a]
2012/10/23 (18)	LPGRE (1)	04:10–04:40	0.13 ± 0.03	4.6 ± 1.2	03:20–04:25	0.18
	LPGRE (2)				04:25–05:20	0.15
	LPGRE Total				03:20–05:20	0.33 ± 0.2 (1.9)[a]
	X1.8 flare				03:15–03:17	<0.06[b] (1.9)[a]
2012/11/27 (19)	LPGRE Total	15:55–16:11	0.13 ± 0.03	2.9 ± 0.6	15:55–16:11	0.04 ± 0.02 (1.4)[a]
	M1.6 flare				15:55:40–15:56:44	<0.002 (1.4)[a]
2013/04/11 (20)	LPGRE (1)	07:10–07:14	1.0 ± 0.1	5.8 ± 0.8	7:10–07:14	0.21
	LPGRE (1) <300 MeV	07:10–07:30		<4.5[c]		
	LPGRE (2)	07:14–07:20	1.1 ± 0.09	5.2 ± 0.5	07:14–07:20	0.30
	LPGRE (3)	07:20–07:30	0.53 ± 0.06	5.0 ± 0.7	07:20–07:30	0.23
	LPGRE Total				07:10–07:30	0.74 ± 0.3 (2.3)[a]

Table 3 continued on next page

Table 3 *(continued)*

Date (Event) yyyy/mm/dd (1)	Type (2)	Observing Interval, UT (3)	Flux >100 MeV $10^{-4}\gamma$ cm^{-2} s^{-1} (4)	Proton PL Index s[f] (5)	Emission Interval, UT (6)	>500 MeV Protons $\times10^{28}$ (Correction Factor)[a] (7)
	M6.5 flare				07:07–07:11	<0.03 (2.3)[a]
	SEP protons					41 ± 25
2013/05/13 (21)	LPGRE Total	04:30–05:15	0.10 ± 0.02	6.0 ± 2.0	02:30–06:00	2.2 ± 1.5 (1.0)[a]
2013/05/13 (22)	LPGRE (1)	17:15–17:28	0.11 ± 0.05	4 ± 2	17:00–17:22	0.06
	LPGRE (2)	17:41–17:59	0.25 ± 0.05	2.9 ± 0.6	17:22–17:50	0.2
	LPGRE (3)	20:25–21:10	0.2 ± 0.04	6.2 ± 1.0	17:50–20:45	2.0
	LPGRE (4)				20:45–23:00	1.0
	LPGRE Total				17:00–23:00	3.3 ± 1.8 (1.3)[a]
	X2.8 flare				16:00–16:07	<0.6[b]
2013/05/14 (23)	LPGRE (1)	01:30 – 01:47	0.06 ± 0.02	6 ±2	01:20–01:40	0.05
	LPGRE (2)	02:58–03:23	0.42 ± 0.03	5.0 ± 0.5	01:40–03:10	1.3
	LPGRE (3)	04:20–05:06	0.26 ± 0.03	6.6 ± 0.9	03:10–04:43	2.1
	LPGRE (4)	06:01–06:41	0.08 ± 0.02	>6.5	04:43–06:20	1.2
	LPGRE (5)				06:20–07:00	0.1
	LPGRE Total				01:20–07:00	4.8 ± 2.0 (1.4)[a]
	X3.2 flare				01:06–01:16	<0.2[b]
2013/05/15 (24)	LPGRE (1)	02:37–03:23	0.02 ± 0.01	4.5±2	02:00–03:00	0.02
	LPGRE (2)	04:13–04:58	0.06 ± 0.02	5±1.5	03:00–04:35	0.15
	LPGRE (3)	05:52–06:34	0.03 ± 0.01	<2.5	04:35–06:13	0.12
	LPGRE (4)	07:33–08:09	0.03 ± 0.01	<2.5	06:13–07:51	0.12
	LPGRE (5)				07:51–09:00	0.04
	LPGRE Total				02:00-09:00	0.45 ± 0.25 (1.3)[a]
	X1.2 flare				01:36–01:46	<0.01 (1.3)[a]
	X1.2 flare				01:30–01:55	<0.36[b]
2013/10/11 (25)	LPGRE Total	07:14–07:30	2.6 ± 0.2	4.3 ± 0.2	07:14–07:30	3.0 ± 1.7 [e] (1.0)[a]
	LPGRE <300 MeV	07:14–07:30		<4.2 [c,e]		
2013/10/25 (26)	LPGRE (1)	08:14–08.59	0.13 ± 0.02	5.6 ± 1.4	08:02–08:30	0.11
	LPGRE (2)				08:30–09:30	0.21
	LPGRE Total				08:02–09:30	0.32 ± 0.15 (1.5)[a]
	X1.7 flare				07:58–08:02	<0.32[b]
2013/10/28 (27)	LPGRE (1)	15:46–16:06	0.07 ± 0.02	2.5 ± 0.5	15:20–15:55	0.014
	LPGRE (2)				15:55–17:00	0.026
	LPGRE Total				15:20–17:00	0.04 ± 0.02 (2.2)[a]
2014/02/25 (28)	LPGRE (1)	01:13–01:17	14.1 ± 0.5	∼3.5 [d]	00:55–01:15	6
	LPGRE (1) <300 MeV	01:10–01:26		<3.5 [c]		
	LPGRE (2)	04:21–04:40	3.5 ± 0.2	∼7	01:15–04:30	73
	LPGRE (2) <300 MeV	04:21–04:40		<3.8 [c]		
	LPGRE (3)				04:30–05:30	9
	LPGRE Total				00:50–05:30	88 ± 40 (1.3)[a]
	X4.9 flare				00:43–00:52	3 ±1.5[b]

Table 3 continued on next page

Table 3 *(continued)*

Date (Event) yyyy/mm/dd (1)	Type (2)	Observing Interval, UT (3)	Flux >100 MeV $10^{-4}\gamma$ cm^{-2} s^{-1} (4)	Proton PL Index s[f] (5)	Emission Interval, UT (6)	>500 MeV Protons $\times10^{28}$ (Correction Factor)[a] (7)
	SEP protons					30600 ± 22700
2014/09/01 (29)	LPGRE (1)	11:06–11:12	40 ± 2	4.75 ± 0.2	11:06–11:12	20
	LPGRE (2)	11:12–11:20	50 ± 2	4.35 ± 0.15	11:12–11:20	29
	LPGRE <300 MeV	11:04–11:30		<3.4[c,e]		
	LPGRE (3)	12:26 – 12:58	0.30 ± 0.03	3.65 ± 0.3	11:20–12:42	149
	LPGRE (4)				12:42–15:52	1
	LPGRE Total				11:02–15:52	199 ± 90[e] (1.0)[a]
2015/06/21 (30)	LPGRE (1)	02:20–02:41	0.12 ± 0.04	?	02:20–02:41	0.07
	LPGRE (2)	05:20–05:53	0.13 ± 0.03	3.2 ± 0.7	02:41–05:37	0.57
	LPGRE (3)	08:30–09:02	0.09 ± 0.02	2.7 ± 0.7	05:37–08:46	0.38
	LPGRE (4)	11:41–12:14	0.07 ± 0.02	3.3 ± 1.3	08:46–11:56	0.27
	LPGRE (5)				11:56–14:00	0.08
	LPGRE Total				02:20–14:00	1.4 ± 0.7 (2.3)[a]
	M2.6 flare				02:11–02:20	<0.2 (2.3)[a]
	M2.6 flare				02:09–02:25	<0.6[b]

[a] Multiplicative factor to correct number for a downward isotropic angular distribution

[b] from 2.223 MeV line flux assuming protons follow a power-law spectrum with index s=4 above ∼30 MeV that steepens to an index of 5 >300 MeV see §4.1.3

[c] 95% confidence limit on index between 30 and 300 MeV based on comparing 2.223 MeV line flux upper limit and >100 MeV γ-ray flux, see §4.1.3

[d] Better fit E^{-2}*exp-(E/1300 MeV)

[e] Assuming a heliocentric angle of 85°

[f] >300 MeV unless noted in column 2

5.3.2. *Spectral Indices of Protons Producing Late Phase Gamma-Ray Emission*

In this section we review the properties of the spectra and variability of >300 MeV protons producing the LPGRE. We assume that the >300 MeV protons interact in a thick target and have an unbroken power-law spectrum, even though there is evidence that the spectra in the most intense events steepen above about 1 GeV. The derived power-law spectral indices and uncertainties are listed for each LAT solar exposure in column 5 of Table 3 and plotted in Figure 9 by event number. These were calculated for an assumed isotropic proton angular distribution. As discussed in §4.1.2, for a downward isotropic angular distribution of protons, the proton spectral indices for events near disk center will be smaller by as much as unity (harder spectra) than those listed in the Table and plotted in the figure. There is not enough information given in Mandzhavidze & Ramaty (1992) to provide event-by-event correction factors. Recall that there are two LPGRE episodes associated with the two flares on 2012 March 7 (event 12). For events where there is more than one LAT solar exposure, and statistics are sufficient, we plot the derived spectral index and error for both the first (filled circle) and last (unfilled circles) exposures. The values of the event-averaged proton power-law index have a large scatter relative to the uncertainties and range from ∼2.5 to 6.0, with a mean index of 4.5 for an isotropic angular distribution of protons. We would expect the average index to be harder for a downward isotropic distribution of protons.

One of the hardest of the LPGRE proton spectra is associated with the 2012 May 17 GLE (event 14). The proton spectral index measured between 02:10 and 02:48 UT had a value of 2.6 ± 0.6. As this event was close to the solar limb, we do not expect the calculated index to be significantly different for a downward isotropic angular distribution. Over a 0.3 to 1 GeV energy range, this differential power-law index in energy is equivalent to a differential rigidity index of 3.4. Neutron monitors recorded rigidity indices ranging from 2.1 to 3.8 from 01:40 to 03:30 UT in this event (Plainaki et al. 2014), consistent with that implied by the γ-ray measurement.

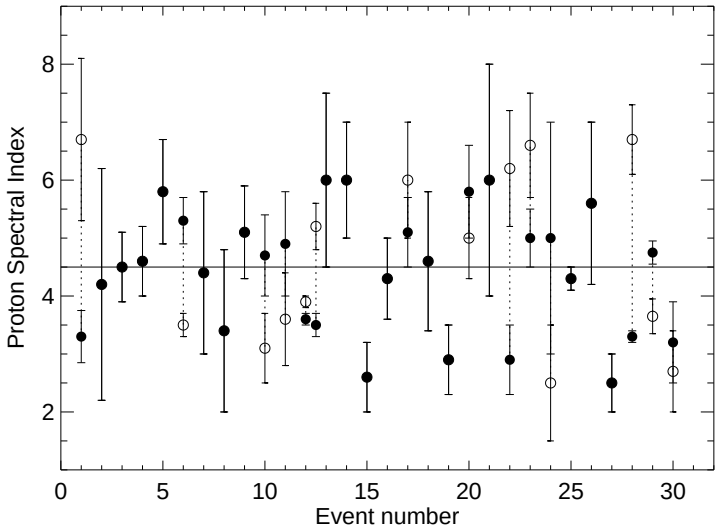

Figure 9. Estimated >300 MeV proton spectral indices and $\pm 1\sigma$ statistical uncertainties for the LPGRE events. Filled circles are the measured indices when there is only a single measurement or if the index does not vary significantly through the event. When the spectral index varies through the event the filled circle gives the first index and the open circle gives the last index. The event averaged spectral index varies from ∼2.5 to 6.0. The mean index is 4.5 and is plotted as the solid line.

There are six events in which there appears to be significant variation in proton spectral index with time. Four of these showed spectral softening with time: 2011 March 7 (event 1), 2012 March 7 (2^{nd} episode event 12), 2013 May 13 (event 22), and 2014 February 25 (event 28). All of these events had durations longer than four hours. As can be seen in Table 3 the spectrum of the second 2012 March 7 event gradually softened from an index of ∼3.5 to an index of ∼5.2 over a nine-hour period. This is consistent with the observations of Ackermann et al. (2014). The second event on 2013 May 13 (event 21), associated with the flare at 16 UT, also showed clear evidence of softening between 17:50 UT, when the power-law index was ∼3, and 20:50 UT, when the index was ∼6. A similar spectral softening from a power-law index of ∼3 to an index of ∼6 also occurred over a three hour period in the event on 2014 February 25.

There are two events that showed evidence for spectral hardening: 2011 September 6 (event 6) and 2014 September 1 (event 29). These two events were of shorter-duration than the four discussed above. The September 6 event had a duration of less than an hour and had a much softer proton spectrum, power-law index 5.3, during the rise to maximum than it did during the decaying phase, when the index was 3.5. A similar, but less significant spectral variation was observed during the behind-the-limb 2014 September 1 event, where the proton spectrum hardened from an index of 4.75 ± 0.20 during the six-minute rise phase to 4.35 ± 0.15 during the eight minute decline phase. The protons producing weak emission an hour later also appeared to have a harder index, 3.65 ± 0.3.

We studied other LPGRE events with durations shorter than an hour in a search for spectral hardening with time. As shown in Figure C10 panel d), there are two 20 second LAT exposures at the peak of the 6–10 minutes long >100 MeV LPGRE event on 2011 August 9 (event 5). The spectrum of the first exposure appears to be softer than the second one. The spectral evolution of the first LPGRE event on 2012 March 7 (1^{st} point; event 12 in Figure 9), following the X5.7 flare (see inset of Figure C17) is complicated because there were only a few measurements before the peak. The proton spectrum from 00:39 – 00:44 UT, in what appears to be the rising phase of the emission, is harder than the spectrum during the falling phase before the M7 flare, but the statistical significance is not compelling (see also Table 1 in Ajello et al. (2014)). The 2012 November 27 event (19) exhibits a clear rise and fall, but the measured spectra during those times are both consistent with power laws with indices of ∼3. The event on 2013 April 11 (event 20) also showed a clear rise and fall and there is a suggestion that the proton spectrum hardened after the peak flux, but it is not statistically significant. There was no evidence for spectral hardening from the rise to the fall of the behind-the-limb event on 2013 October 11 (event 25), with the power-law indices both being consistent with an index of 3.7 ± 0.2. Thus, there is no clear pattern of spectral hardening with time in LPGRE events with durations shorter than about one hour.

Due to the threshold for pion production, LAT only provides spectral information on protons with energy above 300 MeV. As discussed in §4.1.3, spectral information on lower energy protons can be obtained by comparing *RHESSI* and GBM flux measurements of de-excitation lines and the 2.223 MeV neutron capture line with the >100 MeV γ-ray

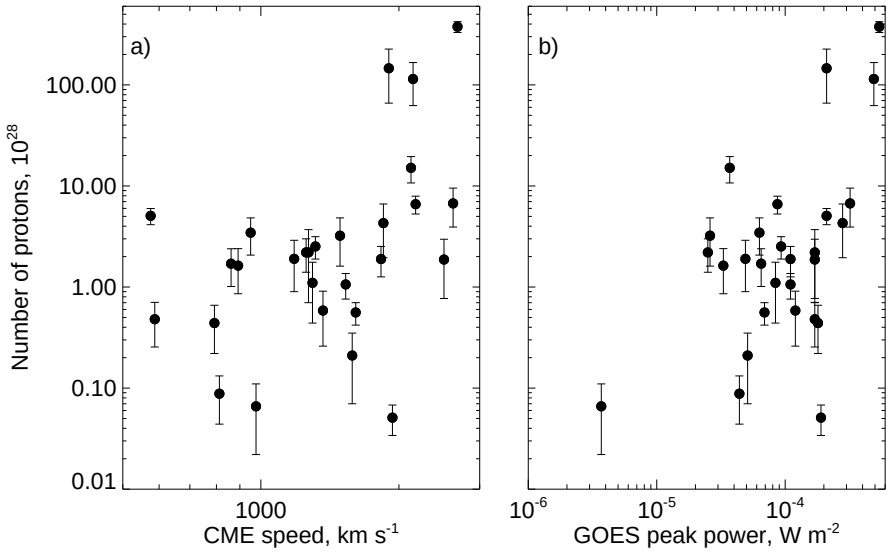

Figure 10. Number of protons >500 MeV producing the LPGRE plotted against CME speed (panel a) and against peak soft X-ray power (panel b). For reference a *GOES* X-class flare has a peak power of 10^{-4} W m^{-2}.

fluxes measured by LAT. Because those instruments are much less sensitive in their energy domains than LAT is above 100 MeV, suitable spectral information can only be obtained for the seven most intense LPGRE events with peak >100 MeV fluxes $\geq 1 \times 10^{-4}\gamma$ cm^{-2} s^{-1}: 2011 August 9 (event 5); 2011 September 6 (event 6); 2012 March 7 (event 12); 2013 April 11 (event 20); 2013 October 11 (event 25); 2014 February 25 (event 28); and 2014 September 1 (event 29). We discuss these events below and provide evidence that the spectrum of protons producing the LPGRE softens between 20-300 MeV and several hundred MeV.

GBM detected de-excitation and 2.223 MeV neutron-capture line emission during the short LPGRE event on 2011 August 9 (Appendix C.5, Figures C9 and C10). After subtracting the contribution from the impulsive phase, we found that the relative 2.223 MeV line and >100 MeV fluxes were consistent with LPGRE produced by 20–300 MeV protons with a spectral index 4.0 ± 0.3 for an isotropic particle distribution. This value is listed in the second row for the event in Table 3 and denoted by the footnote 'c'. For comparison, the proton spectrum measured above 300 MeV, using our pion-decay fits, had an index of 5.8 ± 0.9. Because the flare is relatively close to the solar limb neither of the two spectral indices will change significantly for a downward isotropic proton distribution. Although GBM detected the 2.223 MeV line during the impulsive phase on 2011 September 6, it did not detect the line at any time during the LPGRE event. We list 95% confidence limits on the 20–300 MeV proton spectral indices (denoted by the footnote 'c') at three different times during the event in Table 3. Only during the rise of the LPGRE, when the >300 MeV proton spectrum had a power-law index of ∼5, is it clear that the lower energy spectrum was significantly harder: index <4.0. Because the event occurred near disk center both spectral indices should decrease for a downward isotropic distribution: the >300 index to ∼4.3 and the 20-300 MeV index upper limit to ∼3.7. Thus even for a downward isotropic proton distribution, the LPGRE proton spectrum softened at higher energy. The 20-300 MeV LPGRE proton spectrum were also significantly harder than the >300 MeV spectrum between 04:21 and 04:40 UT on 2014 February 25, independent of the angular distribution because the event were close to the solar limb. For emission at an assumed heliocentric angle of 85° the proton spectrum also steepened significantly above a few hundred MeV between 11:06 and 11:20 UT on 2014 September 1. For larger assumed heliocentric angles, attenuation of the 2.223 MeV line becomes severe and the evidence for steepening is diminished. For an assumed isotropic proton distribution, the 20-300 MeV LPGRE proton spectra were also significantly harder than the >300 MeV spectra in the six hours after 04 UT on 2012 March 7; between 07:10 and 07:30 UT on 2013 April 11. Because these two events are located near disk center, the significance of the change in spectral index between the two energy bands is less if the interacting particles have a downward isotropic particle distribution.

5.4. *Numbers of >500 MeV LPGRE Protons*

We estimate the number of >500 MeV protons in the LPGRE events using techniques discussed in §4.1 and §4.1.3 and list the number in each 20–40 minute LAT exposure for the 30 events in column 7 of Table 3. The total number

of protons at the Sun responsible for the LPGRE events ranges from $\sim 2 \times 10^{26} - 1.5 \times 10^{30}$, assuming that the protons have an isotropic angular distribution. For a downward isotropic particle distribution, the number of protons increases from a factor of unity for events near the solar limb to about 2.3 near disk center (§4.1.2). We list this heliocentric-angle dependent factor in parentheses for each event in Table 3.

It is of interest to determine whether the number of LPGRE protons is correlated with other event parameters such as CME speed and peak *GOES* soft X-ray power. In Figure 10 we plot the number of >500 MeV protons for a downward isotropic angular distribution versus CME speed in panel a) and peak *GOES* power in panel b). The scatter is large and there is no clear correlation of proton number with either CME speed or X-ray power, with the exception of the three largest LPGRE events on 2012 March 7, 2014 February 25, and September 1 that had large associated CME speeds and X-ray powers. This may just be a manifestation of what Kahler (1982) called "the big flare syndrome", i.e., the most energetic events tend to exhibit all forms of activity, irrespective of causally connections.

In the next section, §5.4.1, we compare the numbers of >500 MeV protons producing the late phase γ-ray emission with the numbers of protons producing pion-decay radiation in the impulsive phase of the flare. In §5.4.2 we compare the number of LPGRE protons with the number of >500 MeV protons in space inferred from SEP observations.

5.4.1. *Comparison of Numbers of Protons in the LPGRE and Impulsive Flare*

In this section we compare the number of >500 MeV protons that produce LPGRE with the number in the impulsive phase of the flare. In making this comparison we assume that the protons follow a downward isotropic angular distribution in both phases. Our sample includes the 19 events for which there was near complete exposure to the impulsive phase with either LAT observations >100 MeV (8 events) or with *RHESSI* or GBM measurement of the 2.223 MeV neutron capture line (11 events). In §4.1.3 we discussed how we obtain estimates of the number of impulsive >500 MeV protons from 2.223 MeV line measurements. The measured impulsive phase proton numbers or upper limits are given in column 7 of Table 3 in the row listing the *GOES* X-ray class. We plot the derived impulsive/late phase proton number ratios versus event number in Figure 11. The red and blue symbols give the ratios for events where LAT and 2.223 MeV line impulsive phase observations were used, respectively. In most instances we only have 95% upper limits on the ratios and only one of them was >0.2.

LAT observed impulsive phase >100 MeV emission on 2011 September 6 (event 6; Appendix C.6) and 2012 June 3 (event 16; Appendix C.16). The LPGRE in the hour following the flare on 2011 September 6 was produced by ∼15 times the number of protons responsible for the impulsive emission. The number of protons producing LPGRE on June 3 was ∼ 4 times higher than the number in the impulsive phase. The 2.223 MeV neutron-capture line was detected by the SPI detector on *INTEGRAL* (Zhang et al. 2012) during the the X5.4 and M7 flares on 2012 March 7 (event 12, Appendix C.12, Figure C17). From these observations, we estimate that there were 1.4 and 1.1 $\times 10^{28}$ protons with energies >500 MeV in the X5.4 and M7 flares on 2012 March 7, respectively. We note that the number derived for the M7 flare is consistent with the upper limit of 0.9 $\times 10^{28}$ obtained from LAT observations. There was a 45-minute long LPGRE event following the X5.4 flare produced by ∼50 times the number of impulsive phase protons and a second 18 hr LPGRE that began within an hour of the flares. We summed the proton numbers in the two impulsive flares and the numbers in the two LPGRE events to estimate the ratio plotted in the figure. The neutron-capture line was detected by GBM during the impulsive phase on 2014 February 25 (event 28, Appendix C.28) and for that event the number of protons in the LPGRE was ∼40 times larger.

Overall, most of the observations suggest that the number of >500 MeV protons producing the LPGRE is at least a factor of ten larger than the number producing impulsive phase >100 MeV γ-ray emission.

5.4.2. *Comparison of Numbers of Protons in the LPGRE and the Associated SEP Event*

Most SEP measurements are made at energies below 100 MeV. Satellite experiments such as *PAMELA* (Adriani et al. 2015) and *AMS* (Aguilar et al. 2013) provide sensitive observations >100 MeV, but results on the total number of protons in space are not yet available. Determination of the total number of particles in an SEP event requires knowledge of the spatial distribution of high-energy SEPs. Using data from the *GOES* HEPAD experiment and from neutron monitors, Tylka et al. (2014) developed a method to estimate the total number of >500 MeV SEP protons in space for some of the LPGRE events. We updated this study in Appendix D and provide estimates of the number of protons in eight SEP events with emission that can be studied above 100 MeV. There are systematic uncertainties in the numbers listed in column 7 in Table 3 in the rows labelled SEP protons in column 2 that are not reflected in the quoted errors. This is due to the estimate in the transport, or crossing correction. We have used neutron monitor data to infer that the >500 MeV crossing correction is ∼2. Values as large as eight are inferred from Monte Carlo calculations (Chollet et al. 2010) that would reduce the estimated number of SEP protons. However, these larger

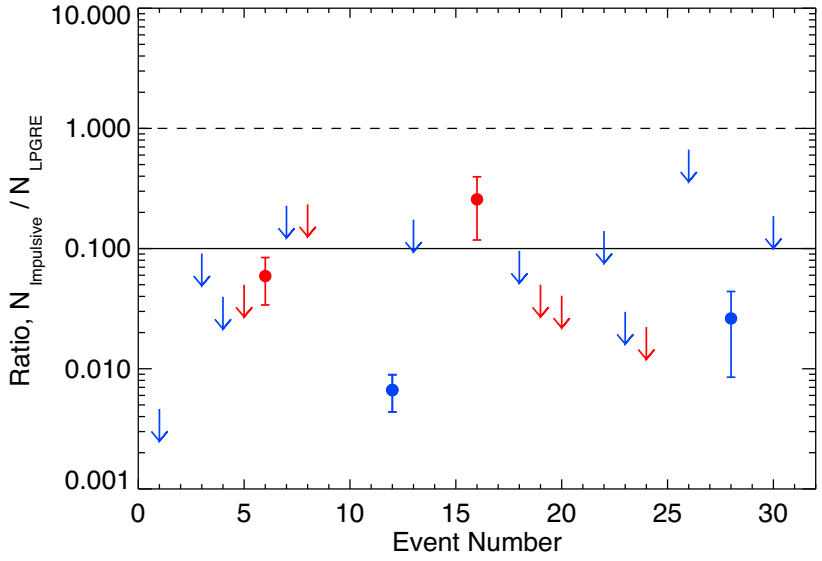

Figure 11. Ratio of the number of >500 MeV protons in the impulsive phase to the number in the late phase for events where there were LAT (red symbols) or 2.223 MeV line (blue symbols) observations during the flare. Filled circles give the ratios in four events where impulsive phase γ-ray fluxes were measured. 95% confidence upper limit symbols are plotted at the ratios where impulsive phase γ-ray emission was below the sensitivity of the instruments.

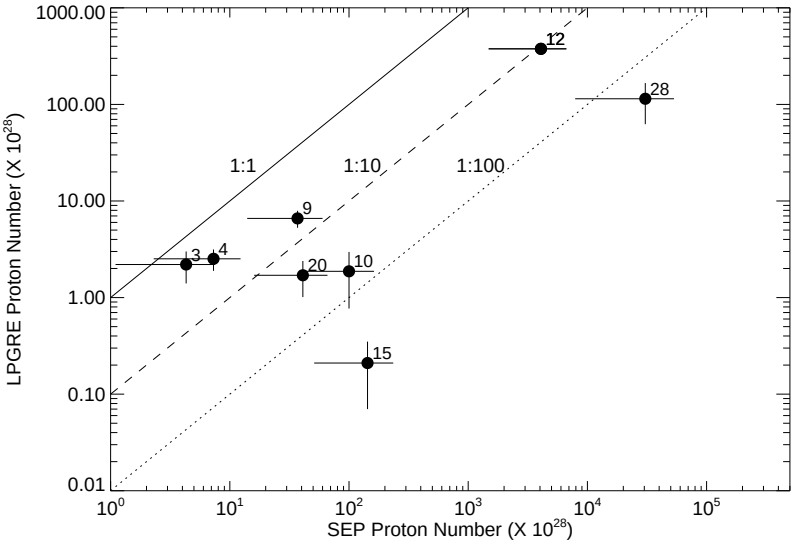

Figure 12. Number of >500 MeV protons producing the late phase gamma ray emission plotted vs. the estimated number in the associated SEP event. The lines represent ratios of 1:1, 1:10, and 1:100.

factors also implies significantly more interplanetary scattering, producing a radial dependence in SEP flux that falls faster than the r^{-2} dependence assumed. The estimated number of interplanetary protons would then increase.

With these uncertainties in mind, we plot the number of >500 MeV LPGRE protons versus the number observed in eight accompanying SEP events in Figure 12. In estimating the number of LPGRE protons, we have assumed that the protons followed a downward isotropic angular distribution. Even though the two largest SEP events are associated with the two largest LPGRE events, the overall probability that LPGRE and SEP proton numbers is correlated is small (correlation coefficient 0.3). The LPGRE/SEP proton number ratio ranges from 0.0015 to 0.5 with an average of 0.14. Systematic uncertainties, primarily due to the transport correction, could increase these ratios by as much as a factor of five.

5.5. *Evidence for Late Phase Bremsstrahlung in a Behind-the-Limb Event*

Detection of >100 MeV LPGRE from behind-the-limb events on 2013 October 11 (event 25) and 2014 September 1 (event 29) (Pesce-Rollins et al. 2015a,b; Ackermann et al. 2017) demonstrates that this emission can be produced by protons interacting far from the flare site. Plotnikov et al. (2017) detailed the characteristics of these events and showed that the onsets of the LPGRE emission are consistent with the times when CME shock-accelerated protons interacted at the locations visible from Earth after transport on magnetic fields returning to the Sun.

We plot the time histories of these two behind-the-limb events in Figures C30 and C34 and discuss the detailed observations in Appendix C.25 and Appendix C.29. Before the onset of LPGRE, the NaI detectors on GBM observed hard X-rays from high coronal sources associated with both flares after they appeared over the solar limb. Direct on-disk observations of the flares themselves were made by the Solar Assembly for X-rays (SAX) instrument on *MESSENGER* (Schlemm et al. 2007). The LPGRE on 2013 October 11 began about seven minutes after the 50–100 keV coronal source rose above the solar limb, lasted 15 minutes, and showed no evidence for spectral evolution. The >100 MeV γ-ray spectrum is consistent with the decay of pions produced by >300 MeV protons with a power-law spectral index, s = 3.8 ± 0.2 throughout the observation (Table 3). Because the emission came from close to the solar limb, the spectrum is not significantly different for isotropic, downward isotropic, or fan beam angular distributions of protons.

The most intense portion of the LPGRE on 2014 September 1 lasted about 30 minutes and its peak flux was about ten times larger than that of the 2013 October 11 event. It was one of the most intense LPGRE events observed by LAT, even though the active region was more than 30° beyond the solar limb. Our studies summarized in Table 3 and in §5.3.2 provide evidence that the proton spectrum producing the pions hardened from a power-law index ∼4.3 to ∼3.3 from 11 to 13 UT. During the peak emission time, we also found that the proton power-law spectrum steepened from one with an index harder than 3.4 between 20 and 300 MeV to one with an index of ∼4 above 300 MeV.

What is significantly different about the 2014 September 1 event is that the >100 MeV LPGRE was accompanied by hard X-ray emission extending to energies above 10 MeV that began within a minute of the >100 MeV emission and peaked about five minutes earlier (see Figure C34 in Appendix C.29). The spectrum of the hard X-rays measured by the GBM NaI detectors from onset to the peak of the LPGRE was fit acceptably by thick-target bremsstrahlung from a power-law electron spectrum with index 3.2 ± 0.1 and a low-energy electron cutoff of ∼130 keV (Appendix C.29. There is no evidence for variation of the spectrum with time. The spectrum could not be fit acceptably by thin target bremsstrahlung, suggesting that the electrons interacted in the low corona and the chromosphere. (The fits were done using SSW OSPEX "Thick2" and "Thin2" electron bremsstrahlung routines.) Additional evidence for the thick target nature of the emission comes from fits to the GBM BGO spectrum from 200 keV to 30 MeV over the same time interval. Our spectral fits to these high-energy data yielded the same 3.2 ± 0.1 electron power-law index observed at lower energy. Ackermann et al. (2017) showed that the hard X-ray and microwave time histories match one another and that the electrons producing the >1 GHz emission had a power-law index of ∼3, the same value we found for electrons producing the bremsstrahlung. Although Ackermann et al. (2017) focus most of their discussion on a thin target origin from a source high in the corona, they leave open the possibility that the emission could be due to bremsstrahlung produced by electrons radiating in the chromosphere, as we suggest.

There is evidence that the hard X-ray source may have been extended over tens of heliographic degrees. After emerging from the SAA radiation belts at 11:11 UT, *RHESSI* detected >20 keV X rays from the Sun. *RHESSI* derives spatial information from the modulation of the photon flux in grids sensitive to different spatial scales as the satellite rotates. RHESSI detected a sufficient number of photons in this case to yield an image of the source (Hurford et al. 2002), but the only modulation observed was derived by taking the differences in the fields of view parallel and perpendicular to the slit axis. This localized the source to the northeast quadrant of the Sun, consistent with LAT centroid (Ackermann et al. 2017), but no image could be made. The absence of rotational modulation in *RHESSI* detector 9, which has the coarsest grids, implies that the source size had to be larger than 300 arcsec. This indicates that the > 20 keV hard X-ray emission was distributed over a broad region and not confined to the relatively small (< 50 arcsec) loop top source imaged in the 6-12 keV range by Ackermann et al. (2017). If the association of this electron bremsstrahlung with the LPGRE is valid, then these measurements provide evidence that the protons producing the emission can be distributed over tens of heliographic degrees in some events. Additional evidence for a distributed source comes from the LAT observation of the westward shift by tens of degrees in the location of the LPGRE late in the 2012 March 7 event (event 12) (Ajello et al. 2014).

The fact that both the protons producing the LPGRE and the late phase electrons producing bremsstrahlung interacted in a thick target on the visible disk and that both emissions commenced near the same time, suggests that they had a common origin. If they were energized by the CME shock that also produced the intense electron and proton SEP event observed by *STEREO*, we would expect the relative numbers of the protons and electrons at the

Sun and in space to be comparable. The *STEREO* 0.7–4 MeV electron and 13–100 MeV proton SEP fluxes each rose to a peak after the flare and the electron-to-proton flux ratio during these peaks was about 4.5 as measured in these energy bands. From our fits to the bremsstrahlung spectrum, we estimate that about 3 $\times 10^{33}$ electrons with energies between 0.7–4.0 MeV interacted in the solar atmosphere. Assuming that the proton spectral index had a value of 3.0 from 10 MeV to 200 MeV and softened to 4.0 above 200 MeV, as suggested by our spectral measurements, we estimate that there were about 5 $\times 10^{33}$ protons with energies between 13–100 MeV that interacted at the Sun. From this admittedly uncertain estimate we find that the electron-to-proton ratio at the Sun is about 0.6. Thus, the measured electron/proton ratios at the Sun and in space are within a factor of ten of one another. This is reasonable agreement given the uncertainties involved, and further suggests that the electrons producing the late phase bremsstrahlung and protons producing the LPGRE had a common origin with the SEP electrons and protons observed in interplanetary space.

We did not observe late phase bremsstrahlung during the LPGRE from the behind-the-limb flare on 2013 October 11 where the peak pion-decay γ-ray flux was about 20 times lower than that on 2014 September 1. The SEP 0.7-4.0 MeV electron flux on October 11 was between 50 and 100 times lower than it was on September 1. Bremsstrahlung from an electron flux two orders of magnitude smaller than observed on September 1 would not have been detectable above the background by GBM. The LPGRE events on 2012 March 7 (Appendix C.12) and on 2014 February 25 (Appendix C.28) were of intensity comparable to the 2014 September 1 event, but we did not detect any evidence for late-phase bremsstrahlung emission. However, flare-related and instrumental background could have affected the GBM sensitivity to late-phase bremsstrahlung. We estimate the expected late-phase bremsstrahlung flux from these events by assuming that the (peak LPGRE)/(peak-late-phase-bremsstrahlung) ratio was the same as that measured in the 2014 September event, modified by the relative SEP proton/electron ratio measured in space. For the first LPGRE event on 2012 March 7 the estimated second phase bremsstrahlung flux was about a factor six lower than the upper limit that could be set from the background at that time. For the second event on March 7 the estimated bremsstrahlung flux was about the same as the upper limit based on the background. In contrast, we estimate that the late phase bremsstrahlung during the peak of the LPGRE on 2014 February 24 should have exceeded the upper limit set by background by a factor of five. Thus, we have evidence for late phase bremsstrahlung emission only during the peak of the LPGRE on 2014 September 1, and there is one event where we might have expected to detect the bremsstrahlung, but did not.

6. DISCUSSION

6.1. *Summary of results*

Below we list the primary results of our study of LPGRE properties.

- The spectra of >100 MeV LPGRE can be fit by the shape expected from decay of neutral and charged pions produced by protons interacting in a thick target and having a power-law spectrum in energy (§4.1). However, there is evidence in the most intense events that the >300 MeV proton spectrum steepens from an unbroken power-law near 1 GeV. LPGRE >100 MeV spectra (§4.1.1) cannot be fit by bremsstrahlung from high-energy primary electrons with synchrotron losses.

- In all 27 LPGRE events for which there were available hard X-ray measurements of the accompanying impulsive phase, hard X-rays with energies in excess of 100 keV were detected (§5.1).

- $\gtrsim$800 km s^{-1} CMEs that were either full or partial halo events accompanied 28 of the 30 LPGRE events. No CMEs were observed in the 2 remaining events, but there is evidence for magnetic eruptions, suggesting that they were failed CMEs. Thus a fast-broad CME is not a necessary condition for LPGRE (§5.1).

- Neither an accompanying flare with detectable >100 keV hard X-rays (HXR) nor an accompanying fast CME is a sufficient condition for LAT detection of LPGRE. However, this conclusion may be influenced by the limited duty cycle of LAT observations.

- LPGRE from behind-the-limb flares (Ackermann et al. 2017) indicate that LPGRE can extend up to a few tens of degrees from the active region. However, a study of solar eruptive events with >800 km s^{-1} CME on the near and far sides of the Sun suggests that >100 MeV emission over such a spatial extent is not common (§5.1).

- The LAT LPGRE time histories are incomplete due to its limited duty cycle for solar observations. However, it is clear that the LPGRE begins after the impulsive-phase hard X-ray emission (17 of 21 eruptions; two on 2012

March 7) and/or has a time profile distinctly different from, or extends in time well beyond, the impulsive phase emission. None of the LPGRE events has a time history that clearly represents the decay of impulsive-phase flare emission (§5.2). There is no evidence that the LPGRE is due to a series of episodic short-duration high-energy outbursts masquerading as steady emission (§5.2.3).

- The LPGRE begins as early as the onset of the CME and as late as about two hours after CME onset (§5.2.2). The rise times range from a few minutes to 6 hours. The duration of the emission ranges from about five minutes to 20 hours. There is no correlation between onset delay and duration.
- The LPGRE durations appear to be correlated with the durations of the accompanying >100 MeV SEP proton events, but the SEP durations are on average five-times longer (§5.2.2).
- The average power-law index of >300 MeV protons producing the LPGRE is 4.5 for an assumed isotropic proton distribution, but there is a large statistically significant flare-to-flare scatter in index with an RMS value of 1.8 (§5.3.2). For downward isotropic and fan-beam proton distributions near disk center, the proton spectra are significantly harder.
- Analysis of nuclear lines in the γ-ray spectra of LPGRE events indicates that the proton spectrum between 20 and 300 MeV tends to be flatter than it is above 300 MeV (§5.3.2).
- The spectral index of the >300 MeV protons producing the LPGRE associated with the ground level enhancement (GLE) on 2012 May 17 is consistent with the spectrum determined from neutron monitor data (§5.3.2).
- The spectrum of the LPGRE emission softened with time in four of the events with durations >4 hours and hardened in two events with shorter durations (§5.3.2).
- The number of >500 MeV protons producing the LPGRE is typically about an order of magnitude larger than the number producing any impulsive γ-ray emission during the associated flare (§5.4.1).
- Type II metric or DH radio emission, indicating the presence of a shock, accompanied all of the LPGRE events except the 2012 November 27 event, which also did not have an associated CME (see Appendix E).
- Type III metric or DH radio emission, indicating that flare electrons reached open field lines, accompanied all the LPGRE events except the two events which did not have associated CMEs (see Appendix E).
- SEP protons were observed from all LPGRE events that were accompanied by a CME and for which the proton flux was not masked by the remnants of a previous SEP event.
- The number of >500 MeV protons needed to produce the LPGRE ranges from 0.1 to 50% of the number of protons observed in SEPs in interplanetary space (§ 5.4.2). There are significant systematic uncertainties in the SEP estimates, however.
- There is evidence that late-phase emission electrons with energies in excess of 10 MeV producing bremsstrahlung in a thick target were accelerated along with the protons producing the >100 MeV LPGRE on 2014 September 1 (§5.5). *RHESSI* imaging studies indicate that the bremsstrahlung was distributed over tens of degrees in heliographic longitude (§5.1), suggesting that the LPGRE was similarly distributed.

6.2. *Models for LPGRE*

Fermi LAT's high sensitivity to >100 MeV γ-ray emission allows the study of significantly weaker late-phase emission than was possible with previous instruments. In contrast to pre-*Fermi* LPGRE events, which were all associated with X-class flares, only about 50% of the events observed by *Fermi* are associated with such intense flares. Studies of LPGRE events made prior to *Fermi* discussed by Ryan (2000) and Chupp & Ryan (2009) (see also Appendix A) indicated that the emission came primarily from ion interactions. Spectra of intense >100 MeV LPGRE events observed by LAT are consistent with pion-decay emission, and are not compatible with any plausible spectrum from primary electron bremsstrahlung. One of the limitations of LAT, however, is its limited duty cycle for solar observations. Here we discuss the constraints imposed by the characteristics summarized above on models for the late phase emission (e.g., Ryan 2000; Chupp & Ryan 2009). The two critical issues are the nature of the mechanism that can accelerate protons

to GeV energies, and the long duration of >100 MeV emission compared with most flare properties (we note that all known LPGRE events have flare associations).

One early model can be described as a magnetic trap: it invoked delayed precipitation into the chromosphere of high-energy particles that were accelerated in the impulsive phase of the flare and then stored in magnetic structures high in the corona (e.g., Ryan 1986). The nature of impulsive-phase acceleration is still under debate, but γ-ray observations confirm that it can accelerate protons to high energies within seconds of the electrons producing bremsstrahlung (e.g., Ackermann et al. 2012a). The trapping mechanism could be magnetic mirroring in a large loop combined with very slow pitch-angle diffusion (i.e., weak wave turbulence), or perhaps very strong wave turbulence that inhibits proton escape by imposing a slow random walk process on propagation. The difficulty with this model is that it does not provide a natural way to explain the LPGRE events displaying a distinct increase in >100 MeV flux beginning after the impulsive phase. Such a passive trap also cannot explain the much larger number of late-phase protons than impulsive-phase protons inferred from the pion-decay γ-ray observations.

What is required is a mechanism that can accelerate particles after the impulsive phase is over. Ryan & Lee (1991) studied a model in which particles are injected into a large loop (10^5 km) that is dominated by magnetic hydrodynamic turbulence. These particles diffuse and precipitate to the footpoints producing the impulsive phase emission with intensities depending on where along the loop they were injected. The turbulence also accelerates the particles by the 2^{nd} order Fermi process to energies high enough to produce pion-decay emission over a longer timescale. The parameters of the loop and the turbulence can be adjusted to account for the time profiles of the impulsive and late phase emission observed on 1982 June 3. More recently Ryan et al. (2015) has applied this model to some of the events observed by *Fermi*. With enough turbulent energy in the loop, the model can account for the factor of ten increase in the number of >500 MeV protons in the late phase emission over that found in the impulsive phase. However, this model requires a very high level of turbulence filling a large volume for a long period of time. It is not clear what the source of such a high energy density of turbulence is. The mean free path due to turbulent scattering needed in the Ryan & Lee (1991) model to precipitate impulsively injected particles and accelerate the protons producing late phase emission is 2×10^4 times smaller than in magnetic loop models for impulsive-phase electron bremsstrahlung and nuclear γ-ray line emission (Miller & Ramaty 1989; Hua et al. 1989; Murphy et al. 1997). The long loops in the Ryan & Lee (1991) model can account for detection of LPGRE far from the flare site in behind-the-limb events and the smooth time profiles, but may not be able to explain emission that is spatially extended over tens of heliographic degrees.

As initially conceived, this high-turbulence loop model is not dependent on the presence of a CME. However, one of the features of the LPGRE events is their association with fast CMEs and with SEP production. All but two of the thirty events are associated with fast wide CMEs. Because the energy carried by a CME is comparable to or larger than that of the flare-accelerated particles (Emslie et al. 2012), and because CME-driven shocks are generally believed to produce SEPs, CMEs are clearly candidates as the energy source for the >300 MeV protons that produce LPGRE. An accompanying CME is not necessary to produce late phase emission in the Ryan & Lee (1991) model, but it is possible that the passing CME could impart additional magnetic turbulence to the large loops and enhance the acceleration of the protons to the high energies necessary to produce the observed pion-decay radiation. The eruption of a fast CME also naturally provides two mechanisms for accelerating particles to high-energies (e.g., Ryan 2000).

The first mechanism is acceleration by the strong electric fields in the current sheet formed behind the receding CME. Akimov et al. (1996) suggested that the late phase γ-ray emission observed by the *GAMMA* satellite on 1991 June 15 was due to particles accelerated in the current sheet behind the receding 1100 km s^{-2} CME. Such a mechanism could also account for the extended duration of the events, but it would have difficulty explaining the longer onset delays of hours or more since we expect the current sheet to form once the CME launches. The mechanism might account for LPGRE far from the flare site in behind-the-limb events, but may not be able to explain emission that is spatially extended over tens of heliographic degrees. It is also not clear whether electric fields in the current sheet would be strong enough to accelerate protons to hundreds of MeV.

The second mechanism is acceleration of particles by the shock produced by a fast CME. Type II radio emission indicating the presence of such a coronal shock was observed in all but one of the 30 LPGRE events (the 2012 November 27 event without an accompanying CME). SEPs were detected in all of the LPGRE events that were accompanied by fast CMEs, except for those where the SEPs were masked by particles from a previous event. The correlation between the duration of LPGRE events and the duration of SEP events observed above 100 MeV also suggests a common CME-shock origin, even though the LPGRE durations are on average about five times shorter than those of the SEPs. Thus, a plausible scenario for production of LPGRE is shock acceleration of seed particles onto magnetic field lines that reach the visible disk and precipitation of these particles into the chromosphere. A shock origin for the LPGRE

explains other characteristics of LPGRE events. Particle acceleration across a wide fast CME can account for the variations in observed arrival times and spectra of SEPs at widely separated spacecraft (Rouillard et al. 2012). It can, therefore, explain how >300 MeV protons interacted at the Sun to produce the first LAT LPGRE event on 2011 March 7 while the energies of the SEP protons measured in space barely exceeded 100 MeV. In addition, Plotnikov et al. (2017); Jin et al. (2018) have explained LPGRE from behind-the-limb flares by the passage of a CME shock that accelerates protons onto front-side-connected field lines. A CME-shock model also addresses the wide range of delays observed in LPGRE onset times: short LPGRE onset delays represent shock acceleration low in the corona (e.g., Gopalswamy et al. 2013), while long LPGRE onset delays indicate that the CME had to expand over several solar radii before accelerating >300 MeV protons that could return to the Sun. Deposition of shock accelerated particles onto field lines returning to the Sun may have difficulty explaining the smooth time histories of the LPGRE events lasting several hours because it implies that the shock continues to accelerated protons to energies >300 MeV at several tenths of an AU from the Sun and that these particles were able to return to the Sun. Such long-duration events can be explained by precipitation of particles that are magnetically trapped in a reservoir (Reames 2013) behind the expanding CME.

One of the main difficulties with this model is transporting the protons back to the Sun against the magnetic mirror force, well after the flare, when the CME is many solar radii above the surface with magnetic field strengths much lower than at the solar surface. Quantitative estimates indicate that only a very small fraction of accelerated protons can return to interact in the chromosphere (e.g., Hudson 2018). The way around this objection is to assume that there is significant MHD turbulence on the field lines connecting the CME to the Sun such as required in the model of Ryan & Lee (1991). Kocharov et al. (2015) presented a shock-wave model to estimate the ratio of the number protons that return to the Sun and interact to the number that escape into interplanetary space. They estimate that the ratio for >100 MeV protons ranges from about 0.2 to 10% depending on the amount of turbulence in the corona. This range is consistent with the 0.1 to 50% range that we estimate in our comparison of the number of >500 MeV protons producing LPGRE and those detected as SEPs in space.

A variant on the magnetic trap model was proposed by Hudson (2018), called the "lasso" model. In this case the SEP particle accelerator crosses both open (SEP) and closed (LPGRE) field lines, leaving energetic protons on both. The closed-field region can be large, perhaps extending out to several $R_\odot$, and rather than requiring that the protons themselves find their way back to the solar surface, Hudson (2018) suggests instead that the loop structure holding the protons contracts back downwards towards the solar surface as the corona recovers from the launch of a CME. The contraction of the closed field lines leads to an increase in magnetic field strength that eases the problem of magnetic mirroring, as well as possibly supplying additional acceleration of the protons.

The fact that two LPGRE events were observed without accompanying CMEs presents a problem for the CME-shock magnetic-field scenario. Neither the event on 2012 October 23 (event 17; Figure C24, Appendix C.18) nor the event on 2012 November 27 (event 18; Figure C25, Appendix C.19) had an accompanying CME or detectable SEP event. The *GOES* soft X-ray durations for these events were two of the three shortest in our sample of 30 LPGRE events, and such short-duration soft X-ray flares are less likely to have CMEs Sheeley et al. (1983). It is unlikely that the flares were directly responsible for the LPGRE because the numbers of protons required to produce the October 23 and November 27 LPGRE were 5 and 20 times larger, respectively, than the upper limits on the numbers of protons accelerated during the flare impulsive phase. AIA movies reveal evidence for the eruption of a magnetic loop in both events, at the times denoted by the downward arrows in the inset of Figures C24 and C25. In addition, Type II metric radio emission, indicative of shock formation, was detected following the magnetic eruption on 2012 October 23. This suggests that the two LPGRE events may have been accompanied by failed CMEs (Ji et al. 2003). Such events can still accelerate protons, but presumably only for a short period of time while the mass is still moving outwards, and then only onto field lines in the relatively low corona. The LPGRE event on 2012 October 23[13] requires that the protons be stored in the low corona for over an hour after the flare.

There is one feature of the LPGRE events that is puzzling: the observation of impulsive flare hard X-rays with energies greater than $\gtrsim$100 keV in every LPGRE event for which there were flare measurements. Such an association may simply be a manifestation of the Big-Flare Syndrome (Kahler 1982), but there may also be a physical explanation that we offer here. Detection of >100 keV X-ray emission indicates the presence of hundreds of keV electrons in the flare, but it also may indicate the presence of sub-MeV ions. This follows by analogy because nuclear de-excitation line γ-rays, produced by >1 MeV protons, are detected with high probability in flares only when the accompanying

[13] It is of interest that the 2012 October 23 event was accompanied by the largest helio-seismic event of Cycle 24 that was believed to be produced by the energy release of electrons in the solar atmosphere during the impulsive phase (Sharykin et al. 2017).

electron bremsstrahlung exceeds 300 keV (e.g. Vestrand et al. (1999); Share & Murphy (2000); Shih et al. (2009)). Such sub-MeV to MeV flare protons can provide the seed population for further acceleration in the Ryan & Lee (1991) loop model. To provide a seed population for subsequent acceleration by a CME shock, the protons must escape from the flare site. Electrons can escape from the flare site as evidenced by their presence in radio plumes containing both open and closed field lines (Fleishman et al. 2017) and their large number higher in the corona and further from the hard X-ray footpoints than previously detected (Gary et al. 2018), and by the fact that they have been shown to be the source of heating of a CME (Glesener et al. 2013). The presence of electrons on open field lines is also inferred in 27 of the 30 LPGRE events by the accompanying Type III radio emission. In addition, acceleration of flare-produced electrons by CME shocks was suggested by Petrosian (2016) to explain the harder electron spectra in the associated SEP events. Thus it is possible that hundreds of keV flare electrons accelerated to MeV energies by the CME shock onto field lines returning to the visible disk produced the observed late phase $\sim$ MeV bremsstrahlung emission in the 2014 September 1 behind-the-limb flare. In like manner flare-accelerated sub-MeV ions, which do not produce detectable γ rays, may provide the seed population for further acceleration in one of the scenarios discussed above to produce the LPGRE. This would explain the LPGRE association with >100 keV hard X-rays from flares. We discuss other aspects of this association in Appendix B.

It is possible that such a seed population of sub-MeV ions accelerated in the flare may also in part explain the delay in the onset of the LPGRE because of the time it would take them to catch up to the CME shock where they can be further accelerated. If we assume that the protons are ejected into space at the time of the mid-point of flare 100–300 keV X-ray emission, we can estimate the energy they would require in order to reach the shock by the time of the onset of the LPGRE. From a comparison of CME and LPGRE onsets and hard X-ray time profiles in 18 events where the LPGRE onset was determined, we estimate that these protons would need to have an energy of $\sim$75 keV. This energy would be even higher if the LPGRE onset delay is in part due to the time it takes for the shock accelerated particles to reach a magnetic field line returning to the Sun and the time it takes to accelerate the protons to energies >300 MeV.

Due to the broad range of LPGRE characteristics, we deem it unlikely that any one of the mechanisms discussed above alone will be able to account for the emission in all of the observed events. The acceleration and transport process is complicated and will require detailed modeling that will need to draw upon those and other processes to explain the emission and its relationship to flares, CMEs, and SEP events.

G. Share conducted this research with financial support from NSF Grant 1156092, NASA Fermi/GI grant GSFC #71080, the EU's Horizon 2020 research and innovation program under grant agreement No 637324 (HESPERIA), a PRAXIS sub-contract, and the U.S. Civil Service Retirement System. R. Murphy was supported by a NASA Fermi/GI DPR and by the Chief of Naval Research. P. Shea and D. Smart acknowledge support from NRL under Praxis Contract N00173-05-C-2084 for their work on the SEP Appendix. We thank Allan Tylka for his work characterizing the SEP events early in the program, prior to his retirement. We acknowledge stimulating conversations with Eric Grove and the hospitality of the NRL Space Science Division, the Solar Physics Laboratory (Code 671) of NASA GSFC, and the Department of Astronomy of the University Maryland. This work would not have been possible without the efforts of the *Fermi* teams that built the highly successful LAT and GBM detectors and provided the data products and calibrations. We especially acknowledge to work of Nicola Omodei and Melissa Pesce-Rollins who provided the custom solar data sets. We also acknowledge our use of data from NASA's *Ramaty High Energy Solar Spectroscopic Imager* and *Solar Dynamics Observatory*, and from the LASCO instrument on ESA's and NASA's *Solar Heliospheric Observatory*. We also acknowledge insights on our analysis and interpretation provided by discussions with D. Reames, H. Hudson, S. Kahler, G. DeNolfo, and J. Ryan.

APPENDIX

A. LATE PHASE GAMMA-RAY EMISSION EVENTS PRIOR TO *FERMI*

Ryan (2000); Chupp & Ryan (2009) list thirteen nuclear γ-ray events lasting from a fraction of an hour up to eight hours. All of them were associated with *GOES* X-class soft X-ray flares. Four of them, detected by *SMM*, had phases of high-energy γ-rays consistent with pion-decay emission (Dunphy & Chupp 1994). There was a brief impulsive phase of emission in the 1984 April 24 event followed by a phase of high-energy emission consistent with pion-decay that lasted about 15 minutes, similar to that observed on 1982 June 3. Nuclear γ-ray emission was observed in five distinct peaks over an hour (Vestrand et al. 1999) in the 1988 December 16 flare. The second peak, lasting about ten minutes, was spectrally harder than the others with high energy emission consistent with pion decays (Dunphy & Chupp 1994).

A similar peak consistent with high-energy emission from pion decays began about five minutes after the start of the 1989 March 6 flare (Dunphy & Chupp 1994); it was the hardest of several discrete MeV emission peaks observed over the hour-long duration of the flare. These last two flares were similar to two other long-duration impulsive gamma-ray flares observed by *SMM* on 1981 April 27 and 1982 December 7, each lasting close to an hour (Vestrand et al. 1999). The only difference was that one of the many peaks in 1988 December 16 and 1989 March 6 events had harder spectra with emission consistent with pion-decay emission. Whether these high-energy peaks were produced by a distinct acceleration process from the other impulsive peaks is debatable. De-excitation lines and the neutron capture line, along with > 25 MeV emission were observed in what appears to be an extended phase of the behind-the-limb 1989 September 29 flare observedby *SMM* (Vestrand & Forrest 1993).

The 1990 April 15 event observed by the SIGMA and PHEBUS experiments on *GRANAT* exhibited several impulsive phase hard X-ray peaks between 2:50 and 3:10 UT and one-hour long late phase emission, not detected above 10 MeV, that began near the end of the impulsive phase Talon et al. (1993); Trottet (1994). Two peaks with energies >15 MeV were observed by PHEBUS on 1990 May 24 within 48 seconds of one another, with the latter one being much harder and likely to be due to pion-decay radiation (Talon et al. 1993; Trottet 1994; Vilmer et al. 2003; Ryan 2000). There is a delayed phase of what appears to be >15 MeV γ-ray emission, beginning about two minutes later, but this radiation is, in part, due to solar neutrons arriving at Earth. GAMMA-1 observed a clear phase of >100 MeV gamma-rays beginning about eight minutes after an impulsive phase of emission on 1991 March 26 Akimov et al. (1994). The impulsive phase spectrum is consistent with a power-law extending up to 300 MeV while the delayed phase spectrum is consistent with an origin due to pion-decays . The peak of this delayed phase emission occurred at the time of a peak in 9.5 GHz microwave radiation.

The five flares in 1991 June listed by Ryan (2000); Chupp & Ryan (2009) were all from the same active region. Nuclear line emission was observed during the impulsive phase in the four flares where there were measurements (Murphy et al. 1993) and later in the 1991 June 15 event (Rank et al. 2001). Neutron-capture 2.223 MeV γ rays were observed from the 1991 June 4 solar eruptive event for up to four hours after the onset of the flare by the OSSE detector on *CGRO*, with evidence for an additional acceleration phase that began 30 to 60 minutes after the onset of the flare (Murphy et al. 1997). Although >16 MeV bremsstrahlung was observed during the flare, there is no evidence for pion decay emission during the flare or at later times (DelSignore 1995). Impulsive 20–200 MeV γ-ray emission on 1991 June 6 was observed by the EGRET calorimeter on *CGRO* (Schneid et al. 1996), but the spectrum is relatively soft and is likely due to electron bremsstrahlung (DelSignore 1995). What appears to be delayed phase γ-ray emission beginning just after the impulsive peak may in part be due to the arrival of solar neutrons, similar to what was observed on 1991 June 4 (Murphy et al. 1999). However, there is weak evidence for time-extended >16 MeV γ-ray emission in the hours after the flare (DelSignore 1995). The time histories of nuclear de-excitation lines and the neutron capture line in the 1991 June 9 event were observed by COMPTEL (Rank et al. 2001). They revealed an impulsive phase peak followed by an exponential decay visible for 25 minutes. After that time, a second more gradual exponential phase dominated. There is no evidence for pion-decay emission at any time during the flare and at later times (Rank et al. 2001; DelSignore 1995). The longest duration event was observed on 1991 June 11 by *CGRO* EGRET at energies >30 MeV and lasted about eight hours with a spectrum containing pion-decay emission that dominated at late times (Kanbach et al. 1993). EGRET and COMPTEL observed both fast and slowly decaying components of γ-ray emission similar to that observed on June 9. There appears to be an hour long flaring phase of emission in the 1991 June 15 event as evidenced by the good agreement between the COMPTEL and *GAMMA-1* γ-ray, the BATSE hard X-ray, and the microwave time profiles (Akimov et al. 1994; Rank et al. 2001; Kocharov et al. 1998). The high-energy spectrum observed by GAMMA-1 appears to be consistent with neutral pion-decay with no evidence for the low-energy continuum from the decay of charged pions. Following that hour-long interval, COMPTEL observed the neutron capture line flux over the next four hours with a much longer exponential decay rate. The late emission is what we refer to as LPGRE and is clearly of nuclear origin.

From this discussion we see that there is a delayed and time-extended phase of γ-ray emission in the events on 1982 June 3, 1984 April 24, 1990 April 15, 1990 May 24, 1991 March 26, 1991 June 4, 1991 June 6, and 1991 June 11. An onset of delayed γ-ray emission can also be inferred from the time histories of the neutron capture line in the 1991 June 9 and 1991 June 15 events that revealed short and long time exponential decays (Rank et al. 2001). There were individual peaks of high-energy emission consistent with pion-decay radiation observed in the impulsive phases of the 1988 December 16 and 1989 March 6 flares that in other respects resemble hour-long nuclear γ-ray flares. Whether these high-energy peaks represent a distinct phase of γ-ray emission is not clear. Only the tail of the 1989 September 29 was observed; thus no conclusions can be reached about it might have been the decay of the impulsive phase emission. It is clear from both spectroscopic studies of >20 MeV γ-rays and the presence of the 2.223 MeV neutron-capture line

in the late-phase events that ions and not electrons were responsible for the observed emission.

The phrase Long Duration Solar Gamma-Ray Flares (LDGRF) was first used by Kanbach et al. (1993) and by Akimov et al. (1996) to describe the hours-long emission associated with the 1991 June 11 and June 15 events. Ryan (2000) used this phrase to identify the 13 events discussed above. He defined such an event as "a solar flare exhibiting gamma-ray (and/or neutron) emission (> 1 MeV) for time periods of a fraction of an hour to hours after the impulsive phase while other common flare emissions (e.g., X-rays) are absent or greatly diminished". This latter emission is what we refer to as LPGRE. The launch of the *Fermi* Large Area Telescope (LAT) in 2008 provided the opportunity to study a larger sample of solar eruptive events with Late Phase Gamma-Ray Emission (LPGRE). Similar to the pre-*Fermi* observations, the LPGRE that we study is temporally distinct from the impulsive phase of the solar eruptive event, with onset times from minutes to hours later, and durations of minutes to tens of hours. We note that some of the late phase emission events included in our study begin while the impulsive phase is still in progress. The key factor is that the LPGRE time profile is distinct from the impulsive hard X-ray emission. The LPGRE spectrum is also harder than that in the impulsive phase of the flare, and is consistent with pion-decay emission.

B. LPGRE RELATIONSHIP TO FLARES, CMES, AND SEPS

Early in our research program, as a step in understanding the origin of LPGRE, we identified high-energy eruptive events between June 2008 and May 2012, having at least one of the characteristics found in the three originally-reported LAT events. Specifically, we searched for: (1) CMEs with projected speeds $\gtrsim$ 800 km s^{-1} and widths >90° in the *SOHO* LASCO CME Catalog[14], (2) SEP events with proton flux >1 pfu at energies $\gtrsim$10 MeV measured at the best magnetically connected spacecraft, or (3) hard X-ray flares with energies >100 keV. We manually identified the SEP events from the *GOES* >10 MeV proton plots for the four years of the study and performed an automated search of proton fluxes >13 MeV in the IMPACT instrument (Luhmann et al. 2008) on *STEREO* from 2010 to 2012, when the two spacecraft were at large angular separations from Earth. We identified the flares with >50 keV hard X-ray emission observed by *RHESSI* and GBM using the flare lists [15] and events that triggered the GBM onboard burst mode. We then visually inspected the RHESSI Browser [16] plots to determine the highest-energy band detected.

We identified 95 solar eruptive events between having at least one of the three characteristics and list them in Table B1[17]. The first column of the table gives the sequential event number. The second column contains the date of the associated event and location of the flare from the NOAA Solar Event Reports[18]. Where *RHESSI* data are available, we list the centroid of the highest-energy quick-look hard X-ray image in the *RHESSI* Browser. Where the emission appears above the limb and there is no evidence for footpoints, we list the longitude as E91 or W91. For backside events, we list flare locations from the *STEREO* EUVI catalog developed by Aschwanden et al. (2014). The third column lists the *GOES* soft X-ray class and its start and end times as given in the NOAA Solar Event Reports. For behind-the-limb events we list the estimated *GOES*-class range based on *STEREO A/B* data, where available (Nitta et al. 2013). When the flare occurred behind the solar limb, and there is no associated *GOES* X-ray event, we list the linearly extrapolated CME onset time given in the *SOHO* LASCO CME Catalog or from the EUVI flare image in *STEREO A/B*.

The fourth column lists linear speeds from the *SOHO* LASCO CME Catalog. The uncertainty in speeds is a few hundred km s^{-1} based on a comparative study of different CME catalogs by Richardson et al. (2015). In the fifth column we list the relative strength of any observed metric Type II slow drift ∼20 to 200 MHz (1.5m to 15m) radio emission in the corona observed by ground-based radio observatories as reported in the NOAA Solar Event Reports. If we cannot confirm the Type II emission in our studies of the radio spectra, we add a "?" next to the entry. We also enter a "Y" when decameter-hectometric (DH) Type II emission was observed by *Wind* and *STEREO* spacecraft, as given in the Wind/WAVES type II bursts and CME catalog[19]. The sixth column lists the estimated peak SEP proton flux (>10 MeV for *GOES* and >13 MeV for *STEREO*) in protons cm^{-2} s^{-1} (pfu) followed by the highest energy or energy range where protons were observed. We list the measured flux from the spacecraft that was best magnetically connected to the flare site. Fluxes are from *GOES* unless otherwise specified. These peak fluxes were obtained after background subtraction and do not include energetic particle fluxes from local shocks. We identify events for which only flux limits can be obtained because they were preceded by a much stronger SEP event (footnote 'f'). The seventh

[14] http://cdaw.gsfc.nasa.gov/CME_list/index.html

[15] http://hesperia.gsfc.nasa.gov/rhessi2/

[16] http://sprg.ssl.berkeley.edu/~tohban/browser

[17] Event 72 contained an X- and M-class flare, each with distinct CME emissions but unresolved SEP contributions

[18] ftp://ftp.ngdc.noaa.gov/STP/swpc_products/daily_reports/solar_event_reports/

[19] https://cdaw.gsfc.nasa.gov/CME_list/radio/waves_type2.html

column lists the maximum hard X-ray energy band detected by the *RHESSI* and GBM hard X-ray detectors based on the *RHESSI* Browser plots. A dash indicates that no hard X-rays were detected, either because the active region was beyond the limb of the Sun or hard X-ray data were missing.

Table B1. Solar Eruptive Events from June 2008 to May 2012

Number	Date, Location yyyy/mm/dd, deg	*GOES* X-Ray Class, Start-End	CME Speed, km s^{-1}	Type II M*, DH	SEP Protons Flux (pfu), Energy (MeV)	Hard X-ray Energy (keV)
(1)	(2)	(3)	(4)	(5)	(6)	(7)
A1	2010/02/08, N22W02	M4.0, 07:36–07:46	N	N, N	<0.2, <10	100–300[d]
A2	2010/02/12, N25E11	M8.3, 11:19–11:28	509	N, N	0.1, <35[b]; <0.2, <10	300–800[c]
A3	2010/06/12, N22W57	M2.0, 00:30–01:02	486	2, N	0.6, <60	1000–40000
A4	2010/08/01, N13E21	C3.2, 07:55–09:35	850	N, Y	5.3, <60[b]	12–25
A5	2010/08/07, N12E31	M1.0, 17:55–18:47	871	2, Y	5.0, >60[b]	12–25[e]
A6	2010/08/14, N11W65	C4.4, 09:38–10:31	1205	1, N	9.5, >100	25–50
A7	2010/08/18, N19W97	C4.5, 04:45–06:51	1471	1, Y	2.5, <60	12–25[c]
A8	2010/08/31, S22W146	M8.4–X2.5, 20:41–?	1304	N, Y	0.6, >60[a]	–
A9	2010/12/14, N20W56	C2.3, 15:03–16:55	835	N, N	<0.2, <10	6–12
A10	2011/01/28, N17W91	M1.3, 00:44–01:10	606	1, Y	1.9, >100	25–50[c]
A11	2011/02/13, S20E04	M6.6, 17:28–17:47	373	1, Y	0.3, <60[b]	100–300[d]
A12	2011/02/14, S19W05	M2.2, 17:20–17:32	326	2, N	<0.2, <10	100–300[d]
A13	2011/02/15, S20W12	X2.2, 01:44–02:06	669	2, Y	5.4, >60[b]	100–300
A14	2011/02/18, S20W55	M6.6, 09:55–10:15	N	N,N	<0.2, <10	100–300[c]
A15	**2011/02/24, N15E84**	**M3.5, 07:23–07:42**	**1186**	**2, Y?**	**0.06, <35[b]; <0.2,<10**	**800–7000**
A16[**] **(1)**	**2011/03/07, N30W47**	**M3.7, 19:43–20:58**	**2125**	**3?, Y**	**39.6, >60**	**300–1000[d]**
A17	2011/03/09, N09W11	X1.5, 23:13–23:29	332	N, N	<14.7, >10[f]	100–300[d]
A18	2011/03/14, N15W49	M4.2, 19:30–19:54	512	N, N	<0.2, <10	100–300[d]
A19	2011/03/21, N20W128	M1.3–X1.3, 02:11–?	1341	N, Y	702, >60[a]	–
A20	2011/03/27, N19E101	?, ∼ 05:16	877	1, N	<0.2, <10	–
A21	2011/03/29, N21E115?	?, ∼20:14	1264	N, N	1.3, >60[b]	–
A22	2011/04/27, N19E59	C2.0, 02:26–03:01	924	2, N	<0.2, <10	25–50
A23	2011/05/09, N19,E91	C5.4, 20:42–21:19	1318	N, Y	0.3, <41[b]	25–50
A24	**2011/05/29, S18E75**	**C8.7, 21:04–21:45**	**1407**	2?, Y	**5.6, <35[b]**	**100–300[d]**
A25[**] (2)	2011/06/02, S18E22	C3.7, 07:22–07:57	976	N, Y	0.1, <40[b]; <0.2, <10	–[e]
A26	2011/06/04, N15W140	M5.2–X1.6, 07:06–?	1407	N, Y	55.8, >60[a]	–
A27	2011/06/04, N17W148	X4–X12 ,21:51–?	2425	N, Y	2060, >60[a]	–
A28[**] **(3)**	**2011/06/07, S21W54**	**M2.5, 06:16–06:59**	**1255**	**2?, Y**	**60.5, >100**	**300–800**
A29	2011/06/13, S18E131	?, ∼ 03:55	957	N, Y	<3.6, >10[f]	–
A30	2011/07/30, N14E34	M9.3, 02:04–02:12	N	N, N	<0.2, <10	100–300
A31	2011/08/02, N19W11	M1.4, 05:19–06:48	712	2, Y	1.3, >100	25–50[c]
A32[**] **(4)**	**2011/08/04, N19W46**	**M9.3, 03:41–04:04**	**1315**	**2, Y**	**48.4, >100**	**300–1000[d]**
A33	2011/08/08, N15W64	M3.5, 18:00–18:18	1343	1, Y	1.5, >100	50-100[d,e]
A34[**] **(5)**	**2011/08/09, N16W70**	**X6.9, 07:48–08:08**	**1610**	**1?, Y**	**16.3, >10**	**800–7000**
A35	2011/09/06, N14W07	M5.3, 01:35–02:05	782	3, Y	1.5, >100	50–100[d]
A36[**] **(6)**	**2011/09/06, N14W18**	**X2.1, 22:12–22:24**	**575, ∼1000[a,b,h]**	**2, Y**	**5.6, >100**	**300–1000**
A37	2011/09/07, N22E66	B9.1, 18:24–18:33	924	N, Y	<1.6, >10[f]	25–50[c]
A38[**] **(7)**	**2011/09/07, N18W32**	**X1.8, 22:32–22:44**	**792**	**1, N**	**<1.7, >10[f]**	**300–1000[d]**
A39	2011/09/08, N14W41	M6.7, 15:32–15:52	351	N, N	<0.4, >10[f]	100–300
A40	2011/09/08, N19W134	?, ∼ 21:50	983	N, Y	<0.4, >10[f]	–
A41	2011/09/21, N19W114	?,∼ 22:00	1007	N, N	0.2, <60[a]	–
A42	2011/09/22, N10E91	X1.4, 10:29–11:44	1905	2, Y	1220, >60[b]	25-50[c,e]
A43[**] **(8)**	**2011/09/24, N14E61**	**X1.9, 09:21–09:48**	**1936**	**2?, N**	**<77, >13[b,f]**	**800–7000**
A44	**2011/09/24, N11E61**	**M7.1, 12:33–14:10**	**1915**	**N, Y**	**<70, >13[b,f]**	**100–300[d]**

Table B1 continued on next page

Table B1 *(continued)*

Number	Date, Location	*GOES* X-Ray	CME	Type II	SEP Protons	Hard X-ray
	yyyy/mm/dd, deg	Class, Start-End	Speed, km s^{-1}	M*, DH	Flux (pfu), Energy (MeV)	Energy (keV)
(1)	(2)	(3)	(4)	(5)	(6)	(7)
A45	2011/09/24, N12E42	M3.0, 19:09–19:41	972	2, Y	<127, >13[b,f]	50–100
A46	2011/09/25, S27W67	M4.4, 02:27–02:37	613	N, N	<118, >13[b,f]	100–300[d]
A47	2011/09/25, N08E71	M7.4, 04:31–05:05	788	N, Y	<180, >13[b,f]	50–100
A48	2011/09/26, N13E33	M4.0, 05:06–05:13	N	N, N	<27, >10[f]	100–300[c]
A49	2011/09/28, N15W01	C9.3, 12:26–12:38	562	N, N	<2.5, >10[f]	100–300[d]
A50	2011/10/01, N20E169	?, ∼ 20:30	1238	N, Y	<0.2, <10	–
A51	2011/10/04, N23E146	?, ∼ 12:40	1101	N, N	12.4, >60[b]	–
A52	2011/10/14, N12E133	?, ∼ 12:00	814	N, N	<0.20, <10	–
A53	2011/10/20, N19,W91	M1.6, 03:10–03:44	893	N, N	<0.20, <10	50–100
A54	2011/10/22, N29W91	M1.3, 10:00–13:09	1005	N, N?	8.1, <60	12–25
A55	2011/11/03, N08E156	M4.7–X1.4, 22:41–?	991	N, Y	127, >60[a]	–
A56	2011/11/17, N11E102	?, ∼ 20:15	1041	N, N	1.2, >60[b]	–
A57	2011/11/26, N11W48	C1.2, 06:09–07:56	933	N, N	48.1, >100	25–50[d,e]
A58	2011/12/21, S19E164	?, ∼ 03:10	1064	N, Y	<0.2, >13[a,f]	–
A59	2011/12/25, S22W25	M4.0, 18:11–18:20	366	2, Y	1.6, >100	100–300[d]
A60	2011/12/27, S16E32	C8.9, 04:11–04:31	147	N, N	<0.2, <10	100–300
A61	2012/01/02, N11W104	C2.4, 14:31–16:04	1138	N, Y	0.5, <60	12-25
A62	2012/01/12, N20E115	C2.5, 07:54–12:16	814	N, N	<0.2, <10	6–12
A63	2012/01/16, N09E143	C6.5, 02:36–06:46	1060	N, N	0.4, <60[b]	12–25
A64	2012/01/19, N32E22	M3.2, 13:44–17:50	1120	N, Y	4.6, >60[b]	25–50[d]
A65[**]**(9)**	**2012/01/23, N33W21**	**M8.7, 03:38–04:34**	**2175**	**N, Y**	**3280, >100**	**100–300**[d,e]
A66	2012/01/26, N26W73	C6.4, 03:58–07:03	1194	N, N	<41, >10[f]	12–25[d]
A67[**]**(10)**	**2012/01/27, N35W81**	**X1.7, 17:37–18:56**	**2508**	**3, Y**	**518, >100**	**100–300**[d,e]
A68	2012/02/24, S16W165	?, ∼03:15	800	N, N	2.3, <50	–
A69	2012/03/03, N18E91	C1.9, 18:13–20:46	1078	N, N	0.1, >24[b] ; <0.2, <10	12–25
A70	**2012/03/04, N17E68**	**M2.0, 10:29–12:16**	**1306**	**N, Y**	**74.7, >60**[b]	**100–300**
A71[**]**(11)**	**2012/03/05, N16E54**	**X1.1, 02:30–04:43**	**1531**	**N, Y**	**<33, >13**[b,f]	**100–300**[d,e]
A72[**]**(12)**	**2012/03/07, N17E27**	**X5.4, 00:02–00:40**	**2684**	**2?, Y**	**1800, >100**	**>1000**[g]
		M7, 01:05–01:23	**1825**	**2?, Y**	**1800, >100**	**>1000**[g]
A73[**]**(13)**	**2012/03/09, N16W0**	**M6.3, 03:22–04:18**	**950**	**2, Y**	**<528, >10**[f]	**100–300**
A74[**]**(14)**	**2012/03/10, N18W26**	**M8.4, 17:15–18:30**	**1296**	**N?, Y**	**<115, >10**[f]	**100–300**[d]
A75	**2012/03/13, N19W59**	**M7.9, 17:12–18:25**	**1884**	**3?, Y**	**271, >100**	**300–1000**[d]
A76	2012/03/16, N20W104	?, ∼ 20:30	862	N, N	<0.5, >10[f]	–
A77	2012/03/18, N20W110	?, <00:24	1210	N, Y	<0.2, <10	–
A78	2012/03/21, N21W152	?, ∼07:20	1178	N, Y	38.5, >60[a]	–
A79	2012/03/24, N12E154	?, ∼ 00:00	1152	N, Y	71, >60[a]	–
A80	2012/03/26, N18E123	M8.2–X2.5, 22:16–?	1390	N, Y	<45, >13[b,f]	–
A81	2012/03/27, N21W17	C5.3, 02:50–03:22	1148	N, N	<45, >13[b,f]	12-25[d]
A82	2012/03/28, N19E106	?, ∼ 01:25	1033	N, Y	<26, >13[b,f]	–
A83	2012/04/05, N18W29	C1.5, 20:49–21:57	828	N, N	0.2, <50	50-100[d]
A84	2012/04/07, N13W152	?, ∼16:15	765	N, Y	3.2, >60[a]	–
A85	2012/04/09, N20W67	C3.9, 12:12–13:08	921	1, Y	<0.2, <10	12–25[c]
A86	2012/04/15, N10E108	C1.7, 02:16–02:45	1220	1, Y	0.2, <60[b]	12–25[c]
A87	2012/04/16, N12E91	M1.7, 17:24–18:00	1348	N, N	<0.2, <10	25-50[c]
A88	2012/04/18, S26W31	C5.9, 14:51–15:18	840	N, N	0.05, <35[a]; <0.2, <10	25–50[d]
A89	2012/04/30, S16W91	C3.9, 06:56–08:19,	992	1, N	<0.2, <10	25–50
A90	2012/05/09, N13E31	M4.7, 12:21–12:36	N[h]	N, N	<0.2, <10	100–300[e]
A91	2012/05/09, N08E19	M4.1, 21:01–21:09	N[h]	N, N	<0.2, <10	100–300[d]
A92	2012/05/10, N12E23	M5.7, 04:11–04:23	N[h]	N, N	<0.2, <10	100–300[c]

Table B1 continued on next page

Table B1 *(continued)*

Number	Date, Location	*GOES* X-Ray	CME	Type II	SEP Protons	Hard X-ray
	yyyy/mm/dd, deg	Class, Start-End	Speed, km s^{-1}	M*, DH	Flux (pfu), Energy (MeV)	Energy (keV)
(1)	(2)	(3)	(4)	(5)	(6)	(7)
A93	2012/05/11, N05W13	C3.2, 23:02–00:33	805	N, N	<0.2, <10	12-25
A94** **(15)**	**2012/05/17, N05W77**	**M5.1, 01:25–02:14**	**1582**	**3, Y**	**180, >100**	**100–300**[c]
A95	2012/05/26, N12W118	?, ∼ 20:35	1966	1, Y	8.5, <60	–

* 1, 2, 3 ≃ <50, 50–500, >500 $\times 10^{-22}$ W m^{-2} Hz^{-1}

**Fermi/LAT LPGRE event

[a] *STEREO A*

[b] *STEREO B*

[c] *RHESSI*

[d] *Fermi*/GBM

[e] Missing Data

[f] Preceding SEP event

[g] *INTEGRAL*

[h] No LASCO data; no clear associated CME in *STEREO A/B*

Of the 95 events presented in Table B1 70 are associated with broad CMEs $\gtrsim$ 800 km s^{-1}, 38 with measured peak SEP proton fluxes >1 pfu, and 38 with flare X-rays >100 keV. In addition, 58 of the 95 are on the visible disk. Entries in bold print denote the 19 events for which the CME speed was $\gtrsim$ 800 km s^{-1} and flare hard X-rays reached energies above 100 keV. The 14 events listed in the Table with their event numbers in red, and with a double asterisks, had accompanying >100 MeV LPGRE detected by LAT. For reference we list the associated event number in Table 1 in parenthesis in column 1. The LPGRE event A25 on 2011 June 2 was not in bold print because there were no observations available to determine if the emission exceeded 100 keV. From this four-year study, we would conclude that both an impulsive flare with emission exceeding 100 keV and a CME with speed exceeding about 800 km s−1 are necessary conditions for an LPGRE event. Because there were two LPGRE events found with no accompanying CMEs after this study was completed, we can no longer conclude that a fast CME is a necessary condition for an LPGRE event.

It is puzzling an associated impulsive flare with hard X-ray emission >100 keV would be a necessary condition for late phase γ radiation. We therefore studied the complete sample of 32 events between 2008 June and 2012 May with CME speeds $\gtrsim$800 km s^{-1} where hard X-ray measurements of the accompanying flare were made. In Table B2 we list the characteristics of the 32 events depending on whether the flare's X-ray energy exceeded 100 keV or not. The numbers of events in the two categories are comparable, but the characteristics are distinctly different. In addition to not producing LPGRE , the mean peak soft X-ray power for <100 keV flares is fifteen times smaller, the mean CME speed is 40% less and the number of events with metric Type II emission is 3-times smaller. There are 22 events where the SEP proton flux was measured without a preceding strong SEP event. The mean/median proton fluxes are about two orders of magnitude larger when the flares emit hard X-rays >100 keV. Not only does flare emission >100 keV appear to be a necessary condition for LPGRE but it also significantly affects the associated CME speed and SEP flux. This association could just be a manifestation of the Big Flare Syndrome (BFS) defined by Kahler (1982) to be "energetic flare phenomena are more intense in larger flares, regardless of the detailed physics."

One way to explore the BFS explanation is to look for systematic differences in the X-ray spectra of the two groups. Of the fourteen events listed in the table with hard X-ray emission that did not exceed 100 keV, only two had emission exceeding even 50 keV: the M3 flare on 2011 September 24 (event number 45 in Table B1) and the C1.5 flare on 2012 April 5 (event number 83). The best fitting electron spectra had power-law indices of 4.8 and 6.0, respectively. These compare with power-law indices close to 3.5 for the three weakest *GOES* class flares observed above 100 keV (events 15, 24 and 70). Thus, the flares with hard X-ray emission that does not exceed 100 keV have significantly steeper non-thermal electron energy spectra than the flares where the emission exceeds 100 keV. This suggests that the BFS

may not the primary reason why detection of impulsive >100 keV emission is a necessary condition for production of LPGRE and why the associated SEP proton flux is so high.

Table B2. Characteristics of Events in Table B1 Where Maximum HXR Energy is <100 keV and >100 keV

	Maximum HXR Energy	
	<100 keV	>100 keV
Number	14	18
Number with LPGRE	0	13
Mean *GOES* Class	C8	X1.4
Mean CME speed, km s^{-1}	964	1635
Number With Type II radio	4	13
Mean/Median SEP proton flux, pfu	6.8/ 0.2[a]	525/75[b]

[a] 10 measured fluxes

[b] 12 measured fluxes

It is clear that neither a flare with hard X-ray emission exceeding 100 keV nor a CME with speeds in excess of 800 km s^{-1} are sufficient conditions for LPGRE, as there are five events meeting both these criteria with no late phase emission. In §B.1 below, we discuss the characteristics of these five events and reasons why LPGRE might not have been detected.

B.1. *Characteristics of the Five Events Identified in the Study with no Detectable LPGRE*

If the dual requirements, $\gtrsim$800 km s^{-1} CME speed and impulsive >100 keV hard X-ray emission, are physically related to the production of LPGRE , we need to explain the five events (black numbers with bold print: A15, A24, A44, A70, A75) in Table B1; events, meeting these requirements that did not exhibit LPGRE. The first question to address is whether there is any difference between the average characteristics of the 14 LAT events (red numbers with bold print) with observed LPGRE and these five events. We use median values to compare these characteristics because of the small number of events in the samples. Events associated with LPGRE had a higher median *GOES* X-ray class (X1.1 vs. M3.5), comparable median CME speeds (1582 vs. 1407 km s^{-1}) and peak SEP proton fluxes (61 vs 75 pfu), and median heliographic longitudes closer to disk center (47° vs 68°) than events with no LPGRE. The higher *GOES* class for LPGRE events might be just a manifestation of the Big Flare Syndrome.

The higher heliographic longitude of the five events with no detectable LPGRE can be explained by detectability of γ rays near the solar limb. The transmission of >100 MeV γ rays from the lower chromosphere and photosphere, through the overlying solar atmosphere decreases from about 95% at 45° to 82% at 70° and to 15% at 89° relative to disk center. In addition, if the LPGRE does not all come from the flare site, but is distributed over tens of degrees in heliographic angle, then γ-ray fluxes from events near the solar limb may be weaker due to attenuation and occultation.

The lack of a LAT detection of >100 MeV emission in the five events might also just be due to the limited duty cycle for good LAT solar exposures: 20–40 minutes every 90 or 180 minutes. LAT would have the highest probability of missing a short 30-minute, transient than it would one that lasted several hours. Below we plot and discuss the LAT, GBM, and *RHESSI* observations of the five events to determine whether these duty-cycle considerations could have played a role in the failure to detect LPGRE. We identify the event by its date, the standard naming convention for the accompanying flare (Leibacher et al. 2010), and its number in the table.

2011 February 24, SOL2011-02-24T07:23, Event A15.

Why might the LPGRE have been missed? LAT had good solar exposure that ended just before the impulsive phase and no >100 MeV emission was detected at that time. Any LPGRE with duration less than one hour following the impulsive phase would not have been detected because the next solar exposure began at 08:35 UT. The flare was near the solar limb (E84), thus some of the emission might have been beyond the solar limb or attenuated by at least a factor of two in the overlying atmosphere.

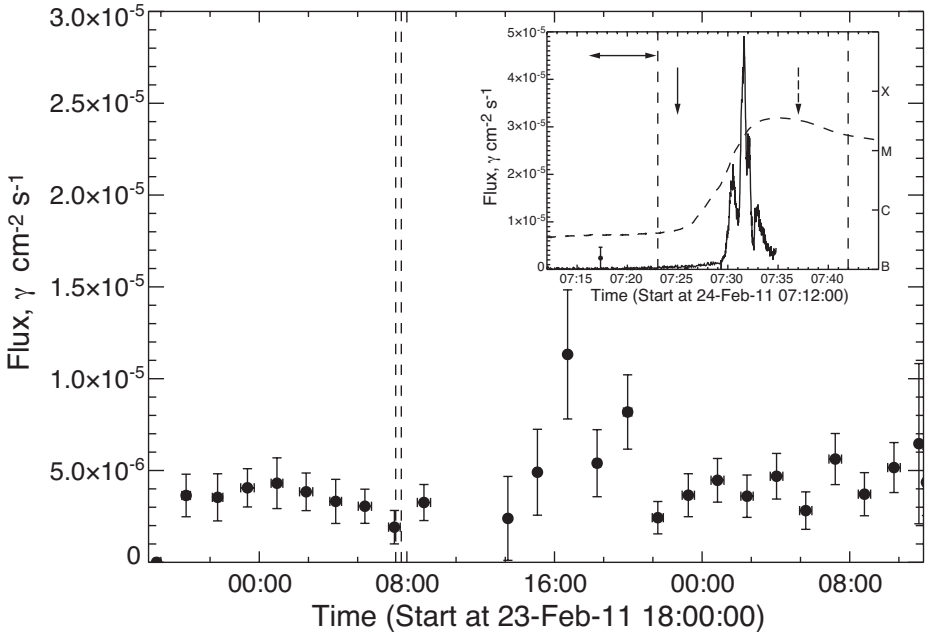

Figure B1. Time history of 2011 February 24 event with no LPGRE detected by LAT. Main figure displays the time history of >100 MeV flux (data points and uncertainties) accumulated in 10 to 40 minute LAT exposures $\leq 10^{\circ}$ of the Sun using Source class data. Vertical dashed lines show the *GOES* start and end times. The inset shows an expanded plot around the impulsive phase with LAT source class data plotted at 4-minute resolution. The solid trace is the GBM 100-300 keV count rate scaled to the LAT flux. The vertical dashed lines show the *GOES* start and end times and the dashed curves show the *GOES* 1–8Å time history; the *GOES* scale on right ordinate. The $< - >$ symbol shows the range in CME onset times in the CDAW catalog derived for linear and quadratic extrapolations. The solid vertical arrow shows our estimate of the CME onset time estimated from *SDO*/AIA movies and the dashed vertical arrow shows the onset of Type II radio emission.

Details Event A15 is plotted in Figure B1. M3.5 class flare at E84 (limb flare) lasting ∼20 minutes; ∼1200 km s^{-1} CME with onset ∼5 minutes before the 100–300 keV X-ray onset; M (metric) and DH (decameter-hectometric) Type II emissions observed with the M onset about 12 minutes after the CME onset; marginal evidence for solar energetic protons; impulsive γ-ray emission up to 1 MeV was observed by GBM (100–300 keV rates plotted in inset) and *RHESSI* with no evidence for 2.223 MeV neutron-capture line, as is expected for such a location near the limb. Good LAT solar exposure 07:05 – 07:35 UT, that overlaps the early part of the impulsive phase ; however, LAT solar exposure ends just before the rise of the hard X-rays. No evidence for >100 MeV emission 08:35 – 09:10 UT, one hour after impulsive phase. No additional LAT solar exposure until 14 UT. Both 2.223 MeV line and >100 MeV emissions would be strongly absorbed if produced at flare site.

2011 May 29, SOL2011-05-29T21:04, Event A24.

Why might the LPGRE have been missed? LAT had poor solar exposure to the impulsive phase and the first good *Fermi* solar exposure was at 22:54 UT (see Figure B2; therefore we have no information about the presence of >100 MeV emission from about 21:04–22:54 UT, for about two hours after the impulsive peak. The active region was also relatively close to the solar limb (E75), with consequences for attenuation and missed radiation behind the solar limb if the late phase gamma rays were broadly distributed. We also note that there was only a weak (6 pfu) SEP observed by magnetically well-connected *STEREO B*.

Details Event A24 is plotted in Figure B2. C8.7 class flare at E75 lasting ∼39 minutes; ∼1400 km s^{-1} CME with estimated onset within minutes of the soft X-ray rise; GBM entered sunlight at 21:07 revealing 100–300 keV emission plotted in inset; M (metric) and DH (decameter-hectometric) Type II emissions observed with the M onset ∼10 minutes after the CME launch; small flux of solar energetic protons up to energies >40 MeV at *STEREO B* for which the flare site was well connected. Poor LAT solar exposure 21:14–21:40 UT after the hard X-ray peak with no evidence for >100 MeV emission. Good LAT exposure 22:54–23:36 UT but no evidence for >100 MeV emission. Cannot rule out >100 MeV emission up until 22:54 UT.

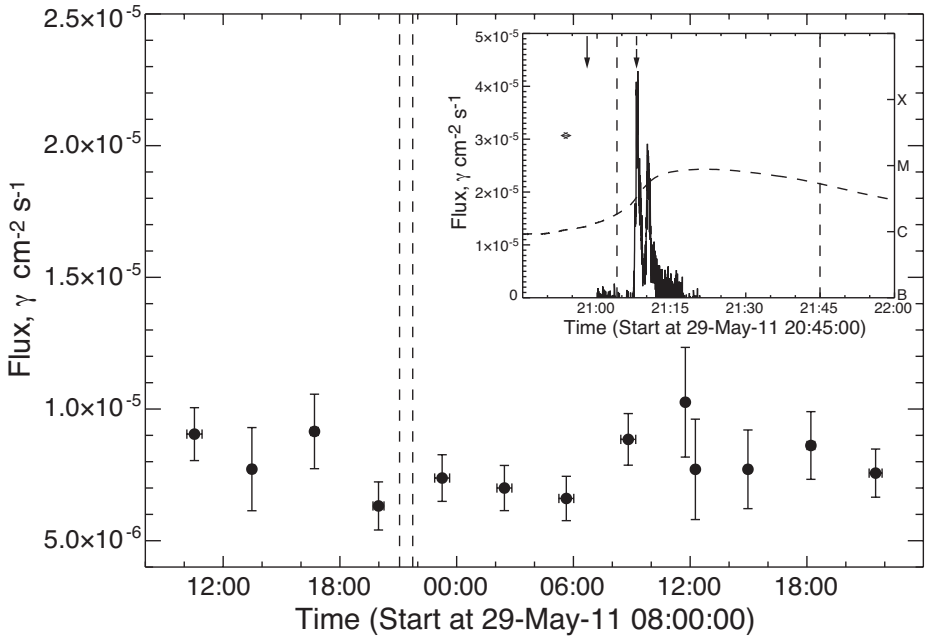

Figure B2. Time history of the 2011 May 29 event with no LPGRE detected by LAT. Arbitrarily scaled GBM 100-300 keV rates are shown by solid trace in the inset. Otherwise the same caption as Figure B1

2011 September 24, SOL2011-09-24T12:33, Event A44.

Why might the LPGRE have been missed? LAT had good solar exposure at the beginning of the impulsive phase between 12:37–13:00 UT and poor exposure near the end between 14:10–14:30 UT. There is no evidence for LPGRE in both source class and Solar Flare Transient class data in these time intervals. The next good solar exposure was an hour later and no LPGRE was observed. LAT would have missed any LPGRE during the flare from 13:10–14:10 UT and for about an hour after the flare.

Details Event A44 is plotted in Figure B3. M7.1 class flare at E61 lasting ∼37 minutes; the CME speed was ∼1936 km s^{-1} with estimated onset about 14 minutes before the first intense 100–300 keV X-ray peak; only DH Type II emission; only an upper limit on the SEP proton flux was obtained because of the large event on September 22. GBM observed emission up to 100–300 keV from the beginning of the flare until nighttime at 13:05 (time history plotted in the inset). LAT had good solar exposure 12:37–13:00 UT, poor exposure 14:10–14:30 UT, and good exposure 15:30–16:10 UT. There is no evidence for >100 MeV emission in the Source class data in any of these intervals. The Source class data in the first two exposures were compromised because high ACE rates. We therefore plot the Solar Flare Transient class >100 MeV fluxes during these time periods in the inset. There is no evidence for LPGRE in any of the exposures.

2012 March 4, SOL2012-03-04T10:29, Event A70.

Why might the LPGRE have been missed? LAT had limited exposure during the impulsive phase, ending near the rise of the impulsive X-ray peak and there is no evidence for impulsive emission in our plots of Source class and LLE data. The ability to search for >100 MeV emission following the impulsive phase was compromised by the shortened solar exposure split by an SAA passage beginning about an hour after the impulsive phase , and again during the next orbit.

Details Event A70 is plotted in Figure C16 in Appendix C.11 where both the full plot and inset used Pass8 Source class data in hopes of improving sensitivity and detecting weak LPGRE ; there was no significant improvement over Pass7. M2.0 class flare at W68 lasting ∼107 minutes; ∼1300 km s^{-1} CME with onset coincident with GBM 50-100 keV X-ray rise (plotted in inset in lieu of the 100–300 keV band); no Type II radio emissions; moderate solar energetic proton event with emission observed >60 MeV; impulsive hard X-ray emission up to 100-300 keV (*RHESSI*, GBM) with no evidence for the 2.223 MeV neutron-capture line. LAT peak solar exposure from 10:40–11:10 UT only 50% of the exposure of the adjacent orbits. Exposure very small at the time of the 100–300 keV impulsive peak at 11:05

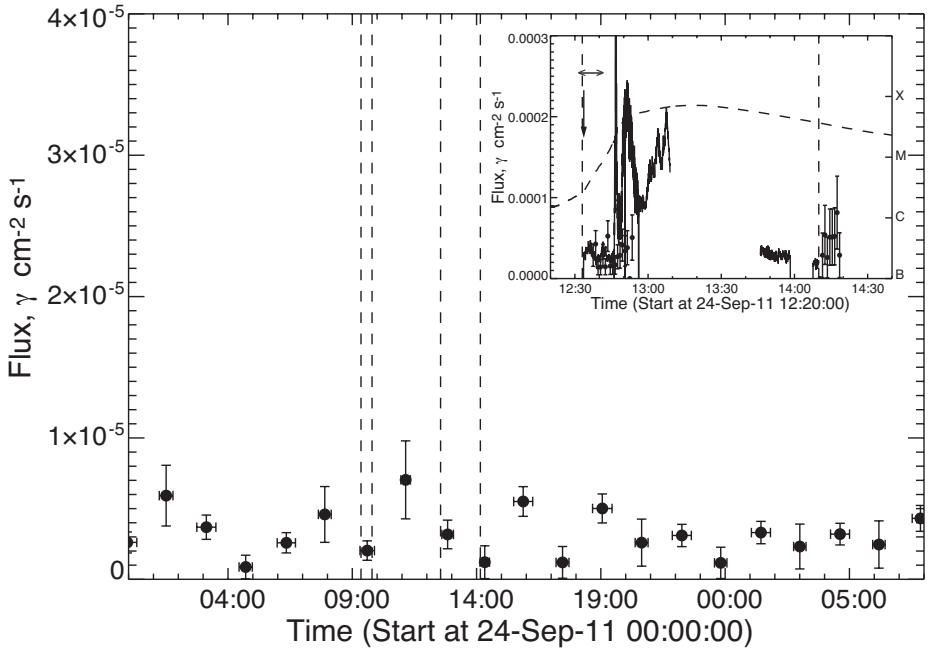

Figure B3. Time history of LAT > 100 MeV fluxes on 2011 September 24. LPGRE was observed during the first flare beginning at 09:21 UT (see Appendix C.1). No LPGRE was detected by LAT during and after the flare beginning at 12:33 UT. The inset plots GBM 100–300 keV count rates on the same scale as >100 MeV fluxes derived from Solar Flare Transient class data. Otherwise the same caption as Figure B1

UT. No reported impulsive >100 MeV (Ackermann et al. 2014) or observed in our study of the Pass8 Solar Flare Transient class data. LAT exposures in the next orbits truncated by SAAs: 12:10–12:20, 12:40–12:50 UT; 13:50–13:57 UT causing large uncertainties in the flux. No clear evidence for LPGRE during these exposures.

2012 March 13, SOL2012-03-13T17:12, Event A75.

Why might the LPGRE have been missed? This event was the most likely of the five to have produced LPGRE because of its association with a 1900 km s^{-1} CME and 271 pfu SEP event. Unfortunately, the first good LAT solar exposure occurred about 90 minutes after the impulsive phase. Thus, it is possible that any LPGRE lasted less than 90 minutes. There is an alternative explanation, assuming that the particles responsible for the LPGRE are produced along with SEPs. Because of different shock and magnetic field geometries (Rouillard et al. 2012)), it is possible that the protons on field lines reaching the Sun may not have been accelerated to energies sufficient to produce pions even though the protons observed in space reached energies >100 MeV. This same process might also explain why >300 MeV protons reached the Sun during the 2011 March 7 LAT event (number 1 in Table 1, A16 in Table B1 while few SEP protons were observed in space with energies >100 MeV.

Details Event A75 is plotted in Figure B4. M7.9 class flare at W59 lasting ∼73 minutes; ∼1600 km s^{-1} CME with estimated onset ∼2 minutes after the *GOES* start time and six minutes before GBM hard X-ray data become available; M (metric) and DH (decameter-hectometric) Type II emissions observed with the M onset within one minute of the CME launch; strong SEP event with emission >100 MeV that appeared to steepen at higher energy because it was not observed in the *GOES* HEPAD data; impulsive hard X-ray emission observed up to 1 MeV by GBM (100–300 keV time history plotted in inset). No LAT solar exposure during the flare. Good LAT solar exposures only made every other orbit: 19:08–19:30, 22:17–23:00, and 01:28–02:12. No evidence for LPGRE at a flux level in excess of 3 $\times 10^{-6} \gamma$ cm^{-2} s^{-1} about 90 minutes after the flare and in the ensuing hours. However, it is possible that there was time-extended >100 MeV emission during the 90 minutes between the time of the hard X-ray peak and first LAT observation at 19:08 UT. GBM spectrum during the impulsive hard X-ray peak can be fit by bremsstrahlung from the sum of two power-law populations of electrons >200 keV: one containing about 2.6 $\times 10^{35}$ electrons and having an index of 5.3 and the second containing about 1.4 $\times 10^{34}$ electrons having an index of 3.2. The 5.3 index of the soft component is the same as derived by Kaufmann et al. (2013) in their paper discussing the discovery of 30 THz emission that has a time history somewhat broader than observed in the hard X-rays. Kaufmann et al. (2013) point

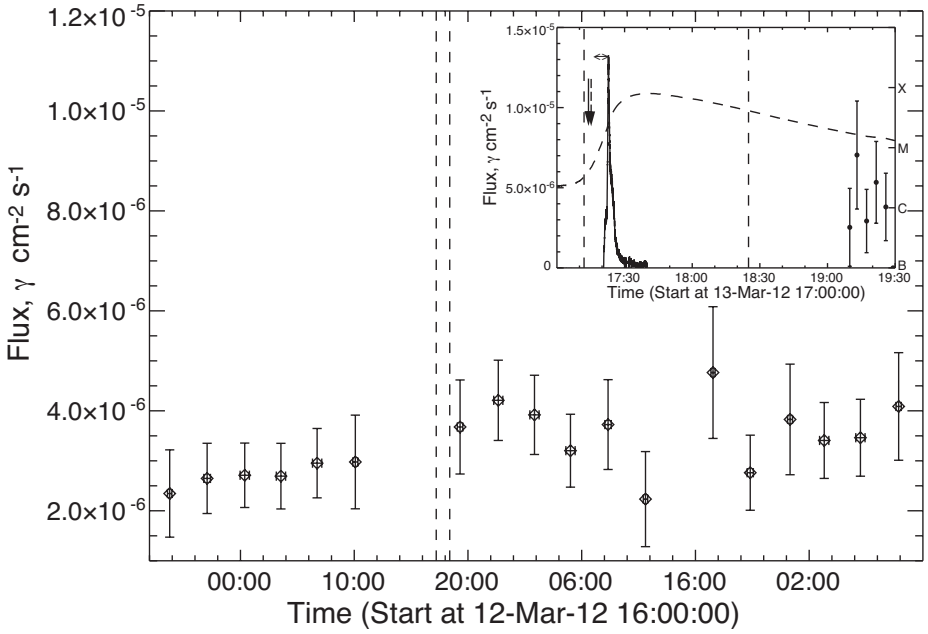

Figure B4. Time history of the 2012 March 13 event with no LPGRE detected by LAT. Otherwise same caption as Figure B1

out that the softer spectrum of electrons cannot penetrate to depths where the THz emission can be produced. The fact that there may be a harder spectrum of electrons that is suggested by our fits may provide a source that could penetrate to the depths needed. However, the time history of the 30 THz emission is significantly more extended in time than the γ-ray emission observed by GBM. There is weak evidence (95% statistical confidence) for the 2.223 MeV neutron capture line in GBM impulsive-phase spectrum, but this could be due to the strong background line. There is also structure in the spectrum that Trottet et al. (2015) attribute to nuclear lines, but the features do not appear at the energies of the expected nuclear lines.

C. DETAILS OF THE THIRTY LATE PHASE GAMMA RAY EVENTS

In this Appendix we plot and discuss the light-bucket time histories of the 30 LPGRE events observed by *Fermi* LAT from 2008 to 2016 and listed in Table 1. These plots lead us to conclude that the LPGRE is temporally distinct from the accompanying impulsive phase in at least 67% of the events. For each event, we also provide details of the LAT, GBM, and RHESSI observations, as well as a brief summary of related solar and heliospheric measurements. We identify the event by its date and the standard naming convention for the accompanying flare (Leibacher et al. 2010)).

The main plot accompanying each event shows the time history of >100 MeV light-bucket flux from hours before to hours after the associated solar eruption, including the entire duration of any late phase emission. The plotted fluxes, derived from Source class data, are averages integrated over the LAT solar exposures and the $\pm 1\sigma$ uncertainties are statistical. The solar exposures were made either each orbit or every other orbit, depending the viewing geometries of the spacecraft's two rocking positions. There are times when LAT solar observations can be made every orbit, e.g., when the orbital procession provides comparable exposures for both rocking positions, as a targeted observation for a few hours after an Autonomous Repoint Request (ARR) following a cosmic gamma-ray/solar flare trigger from GBM, or during a Target of Opportunity (ToO) when the favorable rocking position for solar observations is maintained for days due to high solar activity. The plotted vertical dashed lines are the *GOES* soft X-ray start and stop times.

The insets in the figures either show blowups of the *GOES* flare region (vertical dashed lines) or later solar exposures exhibiting temporal variation of the >100 MeV emission. The dashed curves within the flare interval depict the *GOES* 1–8Å X-ray flux histories with its logarithmic scale on the right ordinate. The horizontal arrow heads designate the range in CME onset times given in the CDAW catalog estimated from linear and quadratic extrapolations to the surface of the Sun (1 $R_\odot$). We have also visually studied movies of SDO 171Å, 193Å, and 211Å images to provide an alternate estimates of the CME onset times. These times are based on motions of field lines from which the CMEs were released and are shown by the vertical arrows; these times are subjective and are accurate to about two minutes. The onsets derived using the two methods are not always consistent. There is an alternative method for estimating the CME onset that uses the *GOES* soft X-ray data (Zhang et al. 2001); these times are are in good agreement with what

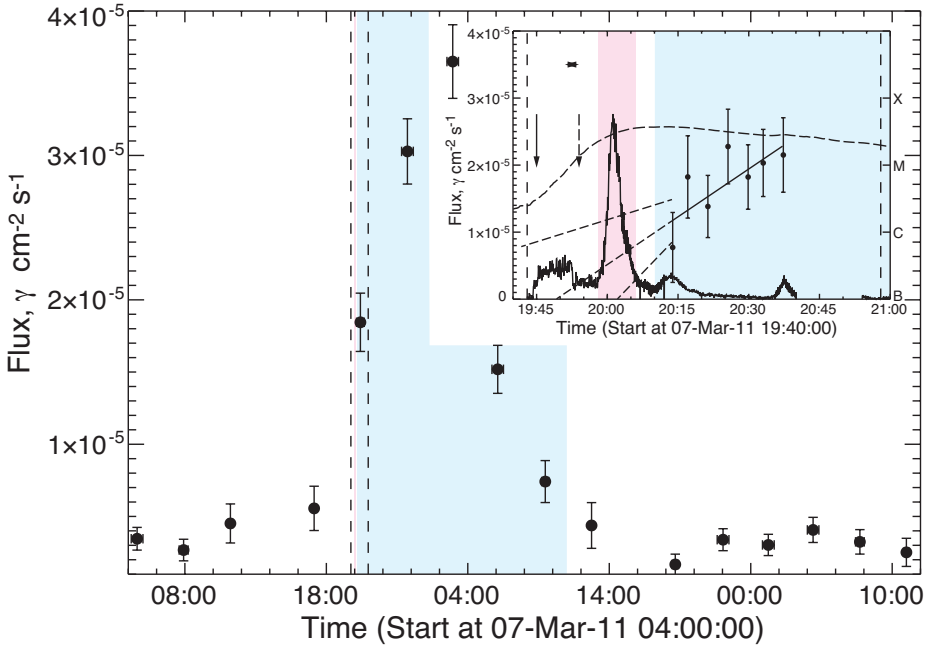

Figure C5. The main figure shows the time history of the >100 MeV flux from $\leq 10^{\circ}$ of the Sun, derived from Source class data, revealing the 2011 March 7 LPGRE event. (All of the fluxes plotted in the Figure accurately reflect temporal variations but should not be used in quantitative solar studies. They include background from Galactic, extra-galactic, and quiescent solar sources. See Table 3 for absolute fluxes and other spectral information.) The fluxes were averaged over the ∼20-40 minute solar exposures and the uncertainties are $\pm 1\sigma$ statistical errors. Vertical dashed lines show the *GOES* 1–8Å start and end times. The inset shows 4-minute accumulation LAT >100 MeV fluxes derived from Source class data. The best fit to the onset of the >100 MeV emission is shown by the solid line and its extrapolation to zero flux is shown by the dashed line; the other two dashed lines are extrapolations of $\pm 1\sigma$ deviations from the best fit. The combined 100-300 keV count rate observed by *RHESSI* and GBM during the impulsive phase, scaled to the γ-ray flux, is shown by the solid trace. The dashed curve shows the *GOES* 1–8Å time history (scale on right ordinate) and the $< - >$ symbol shows the range in CME onset times in the CDAW catalog[b] derived for linear and quadratic extrapolations. The vertical solid arrow depicts our estimate of the CME onset from inspection of *SDO*/AIA images and the vertical dashed arrow shows the estimated onset of Type II radio emission. The solid time history is the arbitrarily scaled 100-300 keV count rates from *RHESSI* and GBM. The blue-shaded region depicts our estimate of the duration of the LPGRE. The pink-shaded regions depict where we made estimates of the flux of >100 MeV impulsive-phase γ-ray emission. The dotted trace shows the high-energy γ-ray timer history of the 1991 June 11 flare normalized to the first LAT 4-minute accumulation point at 20:14 UT. We do not show this curve in time histories of other LAT events.

[a] https://cdaw.gsfc.nasa.gov/CME_list/index.html

[b] https://cdaw.gsfc.nasa.gov/CME_list/index.html

we found using the *SDO* data. The dashed vertical arrow depicts the onset of Type II radio emission. The solid traces typically plot arbitrarily scaled rates in the 100-300 keV band from *RHESSI* or GBM. When they are not available, we plot a representative hard X-ray time history. Where LAT Source class, LLE data, or Solar Flare Transient class data are available during the flare, we plot the >100 MeV fluxes accumulated over either one or four minute intervals; the uncertainties are statistical. We use the adopted naming convention (Leibacher et al. 2010) for the accompanying solar flare to identify each event.

As discussed in §2.1 care must be taken is using these light-bucket fluxes in quantitative solar studies. Absolute fluxes for the events are provided in Table 3.

C.1. *SOL2011-03-07T19:43*

Distinct nature of the LPGRE The >100 MeV flux began sometime during or after the impulsive phase and lasted several hours. The LPGRE is clearly not the decay of the impulsive phase emission. The estimated number of >500 MeV protons in the LPGRE is at least an order of magnitude higher than in the impulsive phase.

Details of the observation Plotted in Figure C5. This was the first late phase emission event detected by the LAT. Additional details in §3 and Ackermann et al. (2014)). M3.7 class flare at W47 lasting 15 minutes; ∼2100 km s^{-1} CME with onset from *SDO*/AIA 171Å and 211Å images consistent with the rise in 100-300 keV X-rays and ∼15 minutes before its peak; M (metric) and DH (decameter-hectometric) Type II emissions observed with the M onset about nine minutes after the CME launch; moderate SEP event with proton energies barely exceeding 100 MeV;

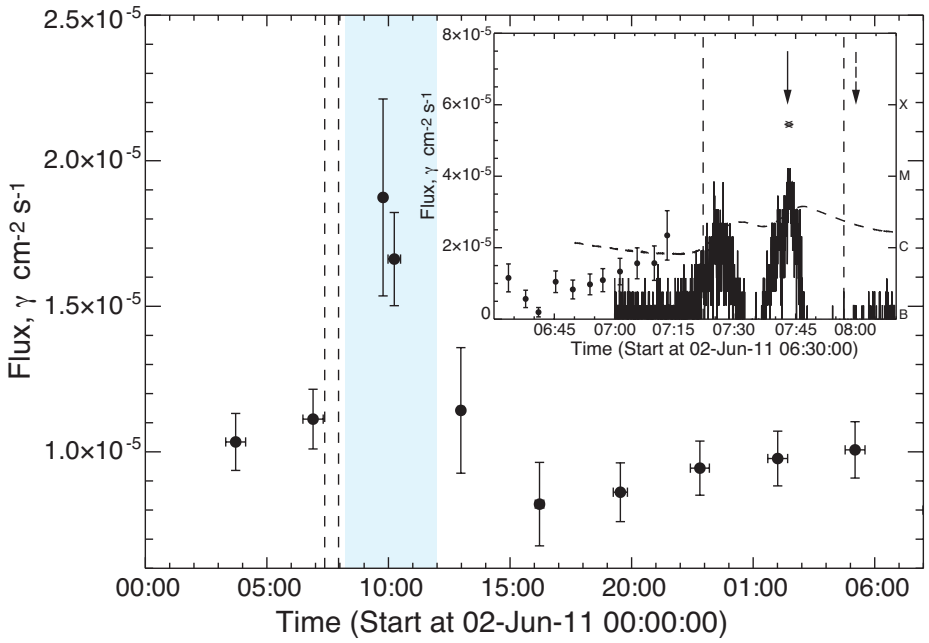

Figure C6. Time profile of the 2011 June 2 LPGRE event observed by LAT. The inset shows a blowup of the region around the flare. >100 MeV fluxes at 4-minute resolution with $\pm 1\sigma$ statistical errors are shown just before the flare. As neither *RHESSI* nor GBM had significant exposure to the flare, we plot an arbitrarily scaled derivative of the *GOES* 1–8Å power that is a proxy for the hard X-ray time history. Plotted by the dashed downward arrow is the DH Type II onset time; there were no metric Type II observations. See caption for Figure C5 for more details.

impulsive γ-ray emission up to 1 MeV with no evidence for 2.223 MeV neutron-capture line (limit on line flux is used to estimate a limit on number of >500 MeV protons during the impulsive phase of the flare). Note that the CME onset time derived from AIA is about seven minutes earlier than the CDAW onset times. In plotting the 100-300 keV time history, we used *RHESSI* data from the onset of the flare until 20:08, when the satellite entered the radiation belts of the South Atlantic Anomaly (SAA) and normalized GBM 100–300 keV fluxes after ∼20:02 UT when *Fermi* entered sunlight.

There was good LAT solar exposure between 20:10–20:40 UT following the impulsive phase ; >100 MeV emission appears to increase (90% confidence) after about 20:14 UT and continues rising to a peak flux of $\sim 3.5 \times 10^{-5}\gamma$ cm^{-2} s^{-1} near 03:00 UT (consistent with Ackermann et al. (2014)) and was observable until about 13:00 UT on March 8. The fluxes plotted in the figure and inset used Source class data; we confirmed the fluxes measured just after the flare using Solar Flare Transient class data. The celestial background level $\sim 3 \times 10^{-6}\gamma$ cm^{-2} s^{-1} in March was low and is about 50% higher than the quiescent solar flux from cosmic-ray interactions (Abdo et al. 2011). From our extrapolations, the LPGRE onset appears to have occurred before 20:05 UT. The best fitting pion-decay spectra suggest that the >300 MeV proton spectra softens during the duration of the event (Table 3). Number of protons >500 MeV in the LPGRE exceeds the number in the impulsive phase, determined by the upper limit on the 2.223 MeV line flux, by at least a factor of ten. We note that the SEP proton energies only reached 100 MeV, significantly below the threshold for producing the pion-decay photons observed by LAT.

.

C.2. *SOL2011-06-02T07:22*

Distinct nature of the LPGRE The >100 MeV γ rays were only weakly observed in one spit exposure two hours after the flare; there is no evidence for flux variability. We have no information about the onset of the emission; however, it lasted significantly longer than the impulsive hard X-ray emission.

Details Plotted in Figure B2. C3.7 class flare at E22 lasting ∼35 minutes.; ∼1000 km s^{-1} CME with CDAW projected onset at ∼07:43 UT consistent with measurements of *SDO*/AIA movies, and a sharp peak in soft X-ray emission; only DH (decameter-hectometric) Type II emission; barely detectable flux of solar energetic protons observed up to 35 MeV; GBM did not observe the flare and *RHESSI* only observed the flare up until 07:36 UT and thus missed the peak of the soft X-ray emission and time of CME onset. This is confirmed by plotting the derivative of the soft X-ray emission that is a proxy for the hard X-ray emission. The derivative shows two peaks, one from about 07:20–

07:33 UT and another one from 07:33–07:48 UT. The latter one peaks at about 07:43 UT, the time of the CME onset. It is likely then that any high-energy impulsive hard X-ray emission occurred during the second peak, where there were no available *RHESSI* observations. This is a weak LAT event only identified at just over 3σ significance in the Pass8 Source class data, but not in our earlier search of Pass7 data. It was also listed as an event in Ackermann et al. (2014). Weak >100 MeV emission was only observed in the first LAT exposure from 09:40 to 10:25 UT, two hours after the impulsive phase. There is no evidence for time variability and thus no information on when the LPGRE began. The flare would not have been identified as having the potential for >100 MeV emission because no hard X-ray measurements were available during most of the flare. Our estimate of the number of >500 MeV protons at the Sun in Table 3 was made by assuming that the emission began just after the impulsive phase , peaked at 10 UT, and fell to zero by 12 UT. We could not estimate the number of protons in the impulsive phase.

C.3. *SOL2011-06-07T06:16*

Distinct nature of the LPGRE >100 MeV γ-rays were only observed during one ∼30-minute exposure one hour after the impulsive hard X-ray emission; there was no evidence for flux variability. The upper limit on the number of protons in the impulsive phase was a factor of five smaller than observed in the LPGRE. Therefore, it is unlikely that the LPGRE was the tail of the impulsive emission.

Details Plotted in Figure C7 (additional details in Ackermann et al. (2014)). M2.5 class flare at W54 lasting ∼40 minutes; ∼1200 km s^{-1} CME with onset ∼7 minutes before the 100-300 keV X-ray onset; M (metric) and DH (decameter-hectometric) Type II emissions observed with the M onset ∼9 minutes after the CME launch; moderate solar energetic proton event with emission observed >100 MeV; impulsive hard X-ray emission up to 300–800 keV observed by both GBM (100–300 keV time history plotted in inset) and *RHESSI* with no evidence for the 2.223 MeV neutron-capture line (limit on line flux is used to estimate a limit on number of >500 MeV protons during the impulsive phase of the flare). There was no LAT solar exposure during the impulsive phase ; the first good LAT solar exposure flare was 07:48–08:22 UT, an hour after the flare. There is a significant flux of >100 MeV emission during this interval with no evidence for temporal variability; the peak flux in Table 3 is consistent with that reported by Ackermann et al. (2014) in their Table 2. During this time interval prominence material was observed to fall back to the solar surface. There was no evidence for >100 MeV during the next LAT exposure three hours later. The best fitting pion-decay spectra suggest that the >300 MeV proton followed a power law with an index of ∼4.5 (Table 3); this is consistent with that measured by Ackermann et al. (2014). As LAT had no exposure to the impulsive phase , we used upper limits on the 2.223 neutron-capture line observed in the front *RHESSI* detectors to estimate the number of impulsive protons. The number of protons >500 MeV in the LPGRE exceeded the number in the impulsive phase by at least a factor of five but it is only ∼4% of the number of >500 MeV protons observed in space (Table 3). The LPGRE lasted no more than about three hours; in contrast, the >100 MeV proton event at Earth lasted close to two days.

C.4. *SOL2011-08-04T03:41*

Distinct nature of the LPGRE The LAT detected >100 MeV emission one hour after the impulsive phase and there was no clear temporal variation; no emission was observed in the next exposure three hours later. The estimated upper limit on the number of protons in the impulsive phase was a factor of ten smaller than observed in the late phase. Therefore, it is unlikely that the γ-ray emission was the tail of the impulsive phase.

Details Plotted in Figure C8. M9.3 class flare at W46 lasting ∼25 minutes.; ∼1300 km s^{-1} CME with estimated onset ∼4 minutes before the 100–300 keV X-ray onset observed by GBM and plotted in inset; M (metric) and DH (decameter-hectometric) Type II emissions observed with the M onset ∼8 minutes after the CME launch; moderate solar energetic proton event with emission observed >100 MeV; impulsive hard X-ray emission observed up to ∼400 keV by GBM with no evidence for the 2.223 MeV neutron-capture line. LAT solar exposure between 03:30–03:50 UT during the impulsive phase was poor and Ackermann et al. (2014) only classify this as a LPGRE event with no impulsive component observable using their LLE data. The recently released Pass8 solar-impulsive class data had only marginal exposure to the rising phase of the hard X-ray emission between 03:43 and 03:49 UT and only upper limits on the >100 MeV could be estimated during that interval. The first good LAT solar exposure was between 04:56–05:38 UT, about 90 minutes after the flare. The measured >100 MeV flux during this interval (see Table 3 is consistent with Ackermann et al. (2014) with no evidence for temporal variability. There was no evidence for >100 MeV during the next good LAT exposure three hours later. We estimated a limit on the number of >500 MeV protons during the impulsive phase in two ways. First we obtained an upper limit using the limit on >100 MeV emission observed between 03:43–03:49 UT scaled to the entirety of the observed hard X-ray time history. This gave a limit of 0.4×10^{28} protons >500 MeV. From a limit on the neutron capture line obtained by GBM we obtained a proton limit about four

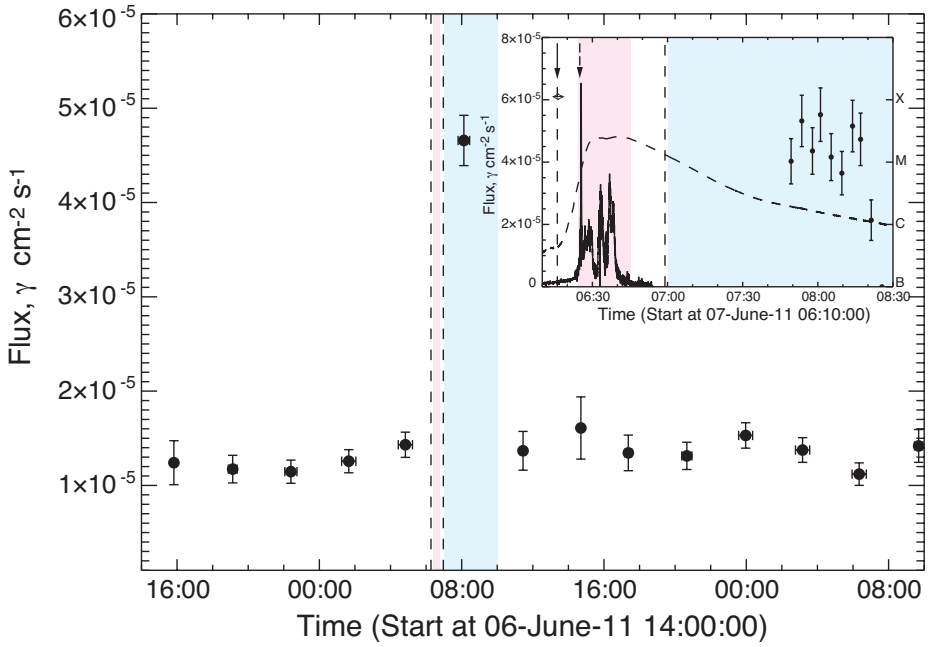

Figure C7. Time history of the 2011 June 7 LPGRE event observed by LAT observed about an hour after the flare. The inset shows 4-minute accumulation LAT >100 MeV fluxes with $\pm 1\sigma$ statistical errors derived from Source class data. The solid line plots the arbitrarily scaled 100-300 keV count rates observed by GBM during the impulsive phase. See caption for Figure C5 for more details.

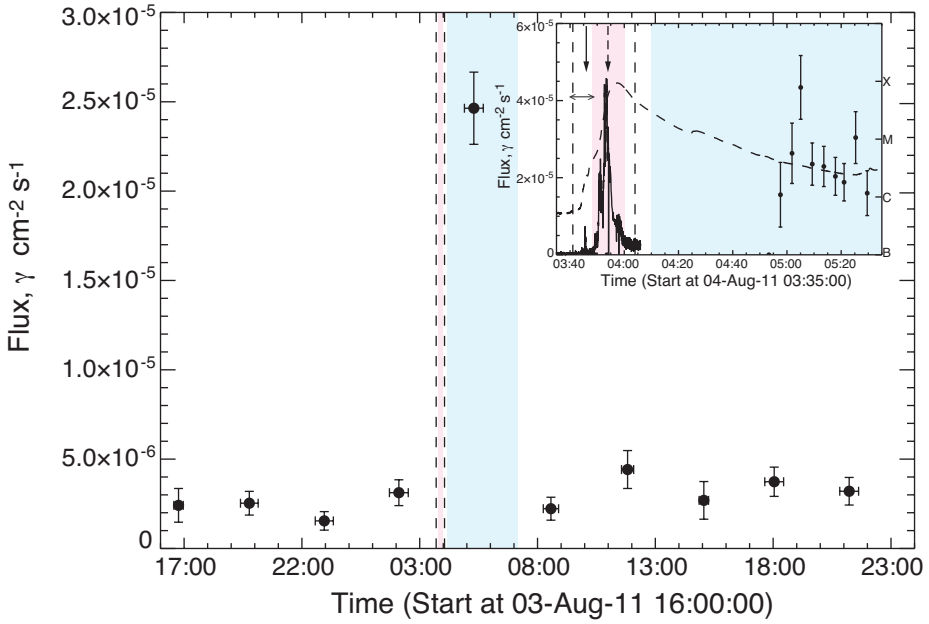

Figure C8. Time history of the 2011 August 4 LPGRE event observed by LAT about an hour after the flare, plotted at 4-minute resolution in the inset. Arbitrarily scaled GBM 100-300 keV rates are plotted during the flare. See caption for Figure C5 for more details.

times lower with 95% confidence. We find that the number of protons >500 MeV in the LPGRE exceeds the number in the impulsive phase by at least a factor of ten but it is only ∼2% of the number of >500 MeV protons observed in space (Table 3). The event at the Sun lasted no more than about four hours; in contrast the >100 MeV proton event at Earth lasted close to 20 hours.

C.5. *SOL2011-08-09T07:48*

Distinct nature of the LPGRE The event had an impulsive phase dominated by two hard X-ray peaks, with

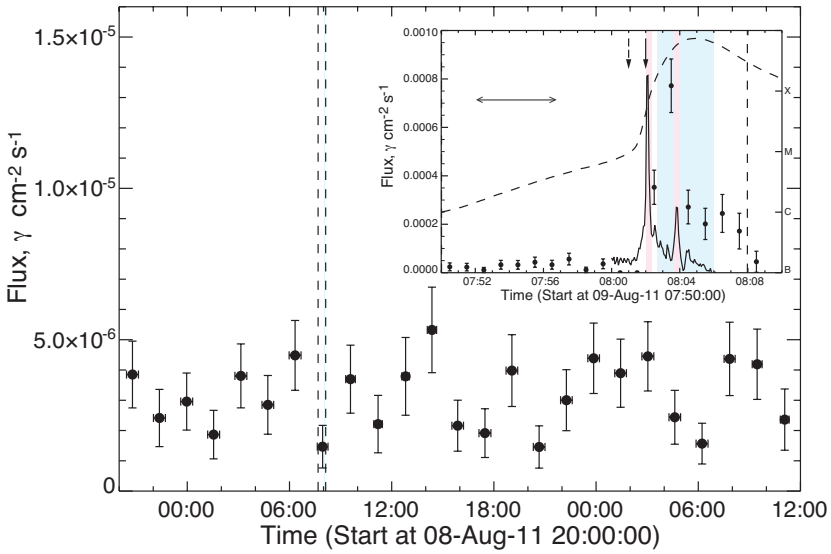

Figure C9. Time profile of the 2011 August 9 LPGRE event observed by LAT. Source class data in the main plot were compromised by high rates in the ACD during the flare resulting in a low flux. Solar Flare Transient class data were used to plot the >100 MeV time history at 1-minute resolution with $\pm 1\sigma$ errors in the inset. The solid trace shows the arbitrarily scaled GBM 100-300 keV rates that differ significantly from the LPGRE time history. See caption for Figure C5 for more details.

nuclear-line emission detected by GBM and *RHESSI*, and >100 MeV γ-ray emission observed by the LAT in both LLE and Solar Flare Transient class data. As >100 MeV emission was detected within a minute of the hard X-ray peaks, the event was classified by Ackermann et al. (2014) as impulsive. On closer inspection of the time history, we believe that there are two distinct phases of emission. This is seen in the inset of Figure C9 where the >100 MeV flux measured in the Solar Flare Transient class data appears to rise just after the hard X-ray peak and reaches a maximum about one minute later. The ∼1-minute high-energy delay from the first hard X-ray peaks contrasts with the shorter ∼10-second delays observed in the nuclear and >100 MeV emission observed in the impulsive 2010 June 12 flare (Event 3 in Table B1) (Ackermann et al. 2012c,b). The distinct components of the 2011 August 9 flare are revealed in Figure C10 where the impulsive component is reflected in the two peaks at about 08:02:10 and 08:03:50 UT visible in a few hundred keV hard X-rays and in the nuclear emission. The two peaks appear to be of comparable strength, with higher-energy electrons producing the bremsstrahlung (panel b) and tens of MeV protons producing the γ-ray lines (panel c). There is an additional temporal component in the γ-ray line time profile that rose just after the first peak and lasted for about two minutes. This rise and duration is similar to that observed in the >100 MeV flux plotted in panel d), obtained from spectral fits to the LLE data. It is interesting to note that the CME and Type II radio emission onsets occurred within about one minute of each other and near the time of the first hard X-ray peak, suggesting the formation of a shock deep in the corona that could be responsible for this distinct component of tens to hundreds of MeV protons. Even though this event lasts only a few minutes, we include this event in our list of LPGRE events because of its distinct temporal history. There is no evidence for LPGRE in the two good LAT exposures at 09:20–09:45 and 10:58–11:20 UT following the flare.

Details Plotted in Figure C9. X6.9 class flare at W70 lasting ∼20 minutes; ∼1600 km s^{-1} CME with onset coincident with the rise of the 100–300 keV X-ray emission; M (metric) and DH (decameter-hectometric) Type II emissions observed with the M onset within a minute of the CME launch; small solar energetic proton event with emission observed >100 MeV; >100 MeV γ-ray emission was observed in LAT Solar Flare Transient class data plotted at 1-minute resolution in the inset of the figure beginning just after the prominent hard X-ray peak; GBM spectrum showed clear evidence for the 2.223 MeV neutron-capture line and nuclear de-excitation lines between 08:00–08:08 UT. The event was classified by Ackermann et al. (2014) as impulsive but on closer inspection there are two distinct phase s of emission as can be seen in the inset of Figure C9) where the >100 MeV flux appears to rise just after the hard X-ray peak and reaches a maximum about one minute later. This behavior is different than observed in the impulsive 2010 June 12 flare (Event 3 in Table B1) (Ackermann et al. 2012c,b), where the hard X-ray and γ-ray time histories follow one another closely.

Comparing the flux observed in nuclear lines with that observed in pion-decay emission from 08:02:40–08:06:00 UT

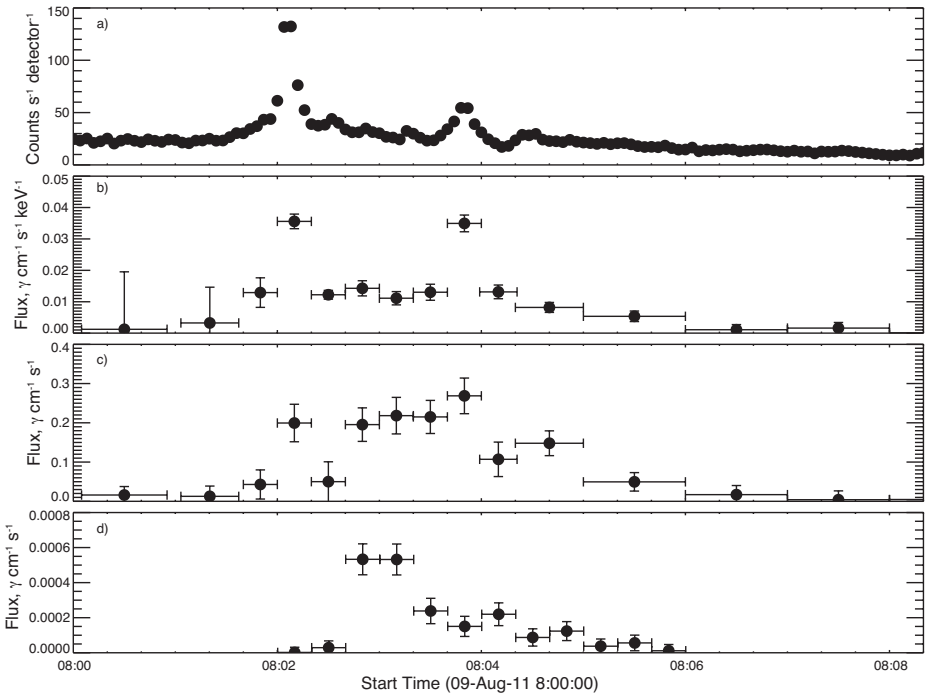

Figure C10. Time histories of various hard X-ray and γ-ray components during the impulsive emission from the 2011 August 9 flare. a) 100–300 keV X rays observed by *RHESSI*, b) flux at 200 keV from power-law electron bremsstrahlung fit to GBM spectrum >200 keV, c) fitted flux of nuclear de-excitation lines in GBM >200 keV, and d) flux of >100 MeV γ rays from fits to LLE data.

(after removing the contribution from the second impulsive peak), we estimate that the proton spectrum between 5 and 300 MeV was consistent with a power law having an index of 4.3 ± 0.3. This compares with a much steeper proton spectrum above 300 MeV, power-law index of 5.8 ± 0.9 that we measured from LLE spectral fits. Thus the proton spectrum of the LPGRE steepened significantly above a few hundred MeV. There is no evidence for LPGRE in the two good LAT exposures between 09:20–09:45 and 10:58–11:20 UT following the flare. We have also compared the upper limit on >100 MeV emission with that observed in nuclear lines during the impulsive phase peaks and conclude that the proton spectrum between 5 and 300 MeV during the flare was steeper than a power law with index of 4.2. It is interesting that the peak SEP flux is about a factor of 10 smaller than what we might expect for such a fast CME which was preceded by a broad CME a few hours earlier (Gopalswamy et al. 2004).

C.6. *SOL2011-09-06T22:12*

Distinct nature of the LPGRE The >100 MeV emission was only observed in one ∼30-minute exposure during and just after the associated impulsive phase. Because of possible saturation effects, we used LLE data to obtain the 1-minute >100 MeV time history shown in the upper inset of the figure up until 22:34 UT; after this time we used Pass7 Source class data. The >100 MeV time history plotted in the insets reveals two peaks: one delayed by about eight seconds from the peak in 100–300 keV hard X rays, and a second peak with onset within one minute following the >100 MeV impulsive peak that reached a maximum at about 22:27 UT and then gradually fell until the end of the LAT solar exposure. Thus both impulsive and late phase >100 MeV γ-rays were observed in this event.

Details Plotted in Figure C11. X2.1 class flare at W18 lasting ∼12 minutes; ∼575 km s^{-1} CME in CDAW catalog but listed as ∼1000 km s^{-1} for both *STEREO A and B* in the CACTUS catalog with onset coincident with rise of 100-300 keV X-rays; only M (metric) Type II emission with onset time within about one minute of CME onset; small solar energetic proton event but emission observed >100 MeV; both *RHESSI* and GBM (100–300 keV time history plotted in top inset) observed the impulsive phase of the flare up to energies in excess of 1 MeV with evidence for nuclear-line emission between about 22:18 and 22:20 UT.

LAT had good solar exposure between 22:12–22:46 UT, covering the entire impulsive phase ; there is clear evidence for >100 MeV emission in the Source class data, but the measured flux was compromised because of the high rates in the ACD. We fit the publicly available LLE data for this flare to obtain the 1-minute >100 MeV time history plotted in the upper inset up until 22:34 UT; after this time we fit the Source class data. The LLE time history plotted in the top inset reveals a sharp peak during the latter part of the impulsive phase. Studying the LLE emission >80 MeV

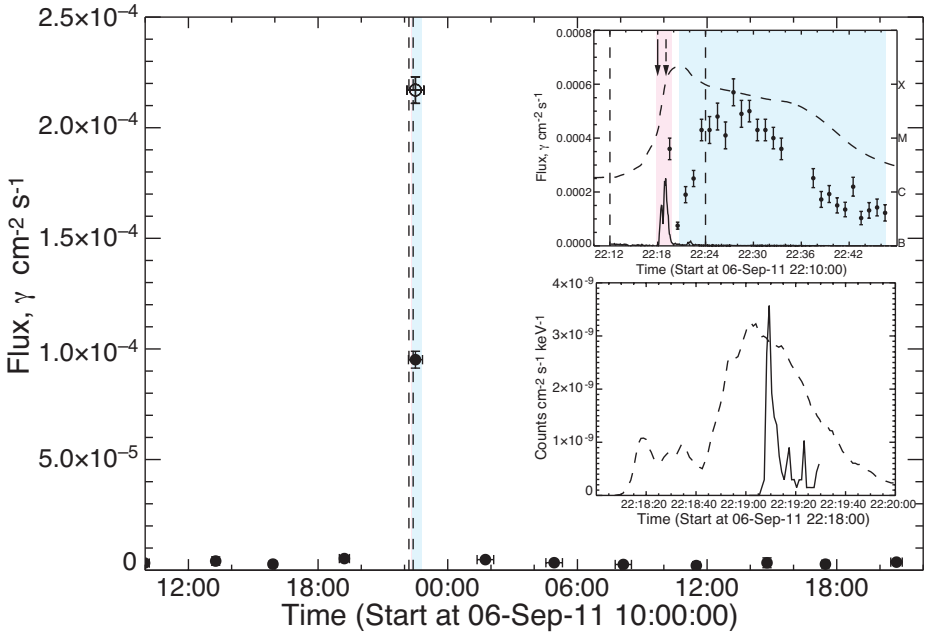

Figure C11. Time profile of the 2011 September 6 LPGRE event observed by LAT. Top inset shows the 100–300 keV GBM count rate during the flare along with 1-minute resolution >100 MeV γ-ray fluxes derived from fits to LLE data until 22:33 UT and from Source class data after 22:37 UT. The bottom inset shows a blowup of the flare region comparing the 100-300 keV rates observed by GBM (dashed trace) with >80 MeV fluxes derived from LLE data (solid trace). The open circle in the main plot is the weighted mean of the >100 MeV fluxes plotted in the top inset and derived from Solar Flare Transient class data; it is larger than the the Source class data flux, plotted as a filled circle, because of dead time effects in those data. See caption for Figure C5 for more details.

at higher time resolution we find that the peak lasts about 10 seconds is about eight seconds after the peak in the broader 100–300 keV X-ray time history (see bottom inset). The >100 MeV LPGRE flux plotted in the top inset of Figure C11 rose after 20:20 UT, peaking about 22:27 UT, and then falling until the end of the exposure. We have also studied the time history of this event using the recently available Solar Flare Transient class data. The time history of the extended-phase emission agrees well LLE data plotted in the Figure. There is no evidence for >100 MeV emission during the next good solar exposure beginning on September 7 at 01:23 UT. We have fit LAT/LLE LPGRE photon spectra after 22:21UT during the rise to and the fall from the peak (Table 3). The fitted proton spectrum before the peak is significantly softer (power-law index 5.3) than the spectrum after the peak (power-law index 3.5). Our fits to the Source class data after 22:37 UT indicate that the proton spectrum also followed a power-law with index of about 3.5. We've obtained information on the LPGRE proton spectrum below 300 MeV by searching for the neutron-capture line in GBM spectrum accumulated between 22:21 and 22:47 UT. Comparing the 95% confidence upper limit 2.223 MeV flux with the average flux observed >100 MeV by LAT enables us to determine that the proton spectrum from 20–300 MeV was harder than a power-law with index ∼4.0 during the rising portion of the emission. As the measured spectral index above 300 MeV was 5.3 ± 0.4, the proton spectrum steepened above 300 MeV.

We also obtained spectral information during the impulsive phase of the flare, 22:18–22:20 UT using both GBM and LLE data. Nuclear line emission was distributed over this full time interval while >100 MeV emission was mostly concentrated between 22:19:00 and 22:19:30 UT, as seen by the solid trace plotted in the lower inset with a sharp peak delayed from about eight seconds from a peak in the 100–300 keV X-rays (dashed trace). Our spectral fit to the >100 MeV LLE data yields a very soft accelerated proton spectrum >300 MeV with power law index steeper than ∼6, much softer than observed in the LPGRE. Our fits also rule out a power-law bremsstrahlung origin for the impulsive emission with a confidence of 95%. We have fit GBM spectra over the same 22:18–22:20 UT time interval and detected nuclear de-excitation lines and the neutron-capture line. By comparing the measured pion-decay, neutron-capture line, and de-excitation line fluxes we estimate proton power-law spectral indices from ∼4.0 between 5 and 40 MeV and ∼4.2 between 40 and 300 MeV assuming a downward isotropic distribution for the protons. Thus the impulsive phase proton spectrum steepened rapidly above 300 MeV.

We have estimated the numbers of protons >500 MeV during the impulsive and time-extended phase s of the event. We see from Table 3 that the number of impulsive phase protons >500 MeV was less than 10% of the number in the

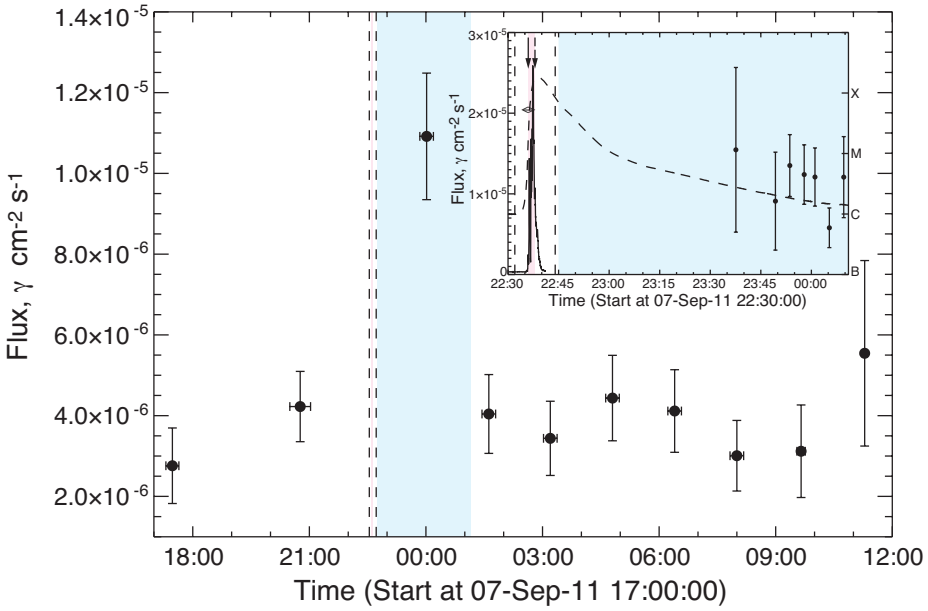

Figure C12. Time profile of the 2011 September 7 LPGRE event observed by LAT. The solid trace in the inset is the arbitrarily scaled GBM 100–300 keV rate and the data points with uncertainties are LAT >100 MeV fluxes. See caption for Figure C5 for more details.

time-extended phase. This fact, along with the vastly different spectra of protons >300 MeV indicates that impulsive phase could not have been the major energy source for the LPGRE. There is only an upper limit of the number of >500 MeV protons in space; it is thirty times larger than the number in the LPGRE.

C.7. *SOL2011-09-07T22:32*

Distinct nature of the LPGRE >100 MeV γ-rays were observed in only one LAT exposure about an hour after the impulsive phase and there is no evidence for flux variability during that time interval, suggesting that the measurement may have been made at the peak of the emission. Thus, the onset of the LPGRE was within one hour of the impulsive phase of the associated flare and the emission lasted at least 1.5 hours after the hard X-rays. As discussed below, the upper limit on the number of protons in the impulsive phase was within a factor two of the number in the LPGRE. Therefore, it is not possible on energetic grounds to rule out the tail of the impulsive phase as the source LPGRE.

Details Plotted in Figure C12. X1.8 class flare at W32 lasting ∼12 minutes; ∼800 km s^{-1} CME with estimated onset coincident with the 100–300 keV hard X-ray rise; only M (metric) Type II emission observed ∼2 minutes after the CME launch; no evidence for solar energetic protons; impulsive hard X-ray emission up to at least 1 MeV observed by GBM (100–300 keV time history plotted in inset). No LAT solar exposure during the impulsive phase ; first good LAT solar exposures at 23:36 (1 minute duration) and 23:52–00:10 UT (4-minute resolution) during a target of opportunity, an hour after the flare. >100 MeV flux consistent with Ackermann et al. (2014) with no evidence for temporal variability. There was no evidence for >100 MeV during the next LAT exposure 90 minutes later. There is weak evidence for both nuclear de-excitation and 2.223 MeV line emission observed by GBM during the impulsive phase of the flare. We obtained a limit on the number of >500 MeV protons at the Sun during the flare from the 95% confidence limit on the 2.223 MeV flux, assuming a proton spectra >40 MeV that follows an unbroken power law with an index of 4.5. The limit on the number of protons during the flare is a factor of two smaller than the number of LPGRE protons (Table 3).

C.8. *SOL2011-09-24T09:21*

Distinct nature of the LPGRE LAT had good solar exposure between 09:18–09:45 UT, covering the entire flare. Weak γ-ray emission >100 MeV appears to have began about six minutes after the 100–300 keV impulsive hard X-ray peak and lasted about four minutes.

Details Plotted in Figure C13. X1.9 class flare at E61 lasting ∼27 minutes; the CME speed is uncertain although the CDAW catalog lists it as ∼1936 km s^{-1} (both CACTUS and DONKI list lower speeds) with onset ∼1 minute before the 100–300 keV X-ray narrow peak; questionable M (metric) Type II emission with onset ∼1 minute after the CME

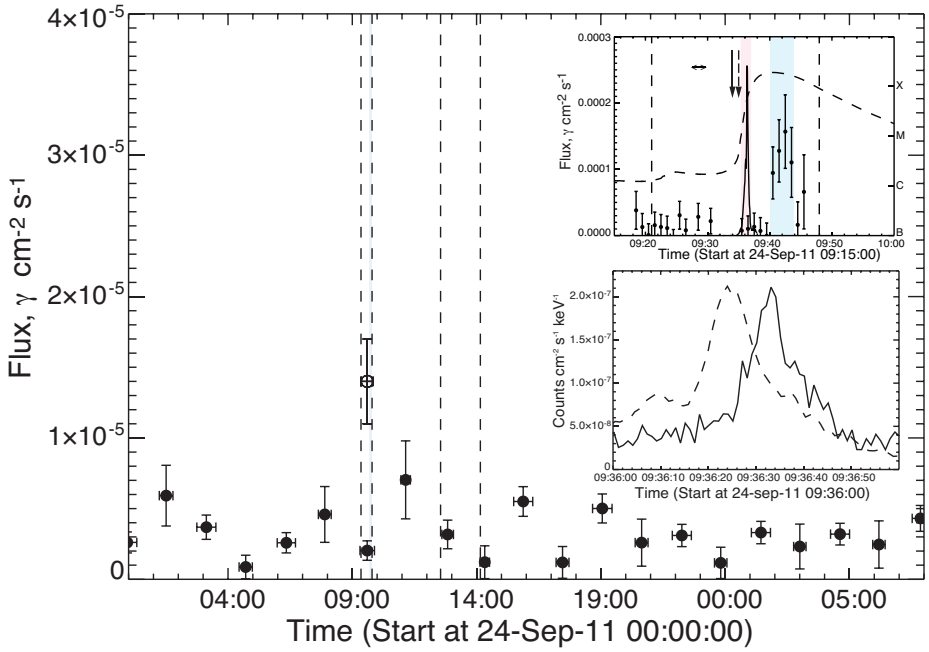

Figure C13. Time profile of the LPGRE event during the first flare at 09:20 UT on 2011 September 24. The filled circles in the main plot denote the >100 MeV fluxes and uncertainties derived from Source class data. The open circle shows the flux obtained from Solar Flare Transient class data revealing LPGRE during the flare when the Source class data were compromised. The upper inset plots the GBM 100-300 keV count rates on the same scale as the Solar Flare Transient class >100 MeV fluxes. The short LPGRE event began about six minutes after the impulsive hard X-ray peak. The impulsive phase 10–60 MeV count rates in LLE data (solid trace) and arbitrarily scaled GBM 100-300 keV rates (dashed trace) are plotted in the lower inset at higher time resolution. Otherwise the same caption as Figure B1

launch; only an upper limit on the SEP proton flux was obtained because of the large particle event on September 22. Both *RHESSI* and GBM observed emission up to about 10 MeV during the impulsive phase with evidence for nuclear de-excitation and neutron-capture lines. LAT had good solar exposure between 09:18–09:45 UT, covering the entire impulsive phase. The GBM 100–300 keV time history is plotted in the top inset along with the >100 MeV flux derived Solar Flare Transient class data. The >100 MeV fluxes derived from source class data were affected by the high ACD rates during the flare. This can be seen by the difference between the open-circle (Solar Flare Transient class data) and filled-circle (Source class data) fluxes. There is no clear evidence for >100 MeV emission during the impulsive X-ray peak. The LPGRE began about six minutes later and lasted only about five minutes. LAT had poor solar exposure between 10:58–11:18 UT and good exposure between 12:37–13:00 UT and no LPGRE was observed during those time intervals. The spectrum of the LPGRE is consistent with emission from pion-decays produced by protons following a power-law index of 3.4 ± 1.4. The 95% confidence upper limit on the number of >500 MeV protons during the impulsive peak is less than 25% of the number observed in the LPGRE.

As shown in the bottom inset, LAT/LLE data reveal a striking peak in ∼10–60 MeV γ-ray emission delayed by about eight seconds from the 100-300 keV hard X-ray peak in the impulsive phase. This delay is similar to that observed by LAT in the impulsive event on 2010 June 12 (event A3, Ackermann et al. (2012c,b)), but in this case the emission is clearly dominated by electron bremsstrahlung; thus the delay measures the time to accelerate electrons to energies >10 MeV and is not due to delays associated with accelerating ions to hundreds of MeV as may have been the case for the 2010 June 12 flare. Ackermann et al. (2014) also report this event as impulsive. LAT LLE photon spectrum appears to follow a power-law in energy visible up to just above 100 MeV with index ∼4.8; there is only marginal evidence for pion decay emission at the 67% confidence level. If this steep bremsstrahlung spectrum extended to energies below 10 MeV it should have been detectable by GBM; but our studies indicate that it was not detected. GBM measured 2.223 MeV and de-excitation line fluxes indicating that the 4–40 MeV proton spectrum in the impulsive phase had an index of about 4.5. If this proton spectrum extended without steepening to energies of 300 MeV, the >100 MeV pion-decay flux would have been about a factor of two higher than the limits on emission that we set. This indicates that the impulsive proton spectrum steepened above ∼40 MeV.

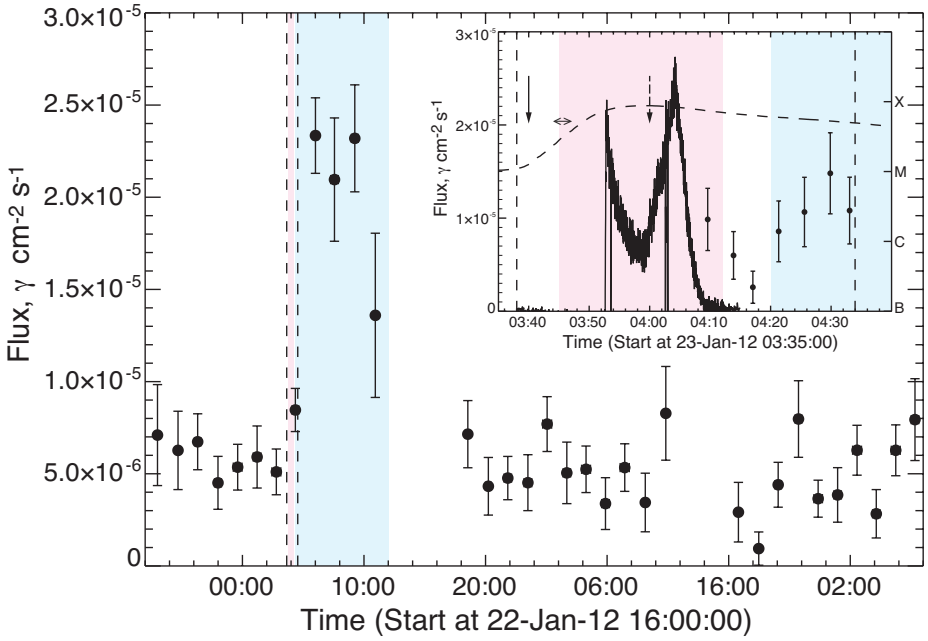

Figure C14. Time profile of the 2012 January 23 LPGRE event observed by LAT. The solid trace in the inset shows the arbitrarily scaled GBM 100–300 keV hard X-ray time history compared with >100 MeV fluxes and uncertainties plotted at 4-minute resolution. GBM missed most of the hard X-ray emission that began at 3:40 UT and peaked at 03:50 UT from a plot of the derivative of the *GOES* soft X-ray flux. Plotted by the dashed downward arrow is the DH Type II onset time; there were no metric Type II observations. See caption for Figure C5 for more details.

C.9. *SOL2012-01-23T03:38*

Distinct nature of the LPGRE LAT began observing the Sun late in the flare and may have detected a weak decreasing impulsive >100 MeV flux and the onset of late phase emission 15 minutes after the impulsive hard X-ray peak. The flux in the next orbit is at least five times higher and the emission lasted for eight hours.

Details Plotted in Figure C14. M8.7 class flare at W21 lasting ∼55 minutes; ∼2000 km s^{-1} CME with onset about the time of soft X-ray event, before *Fermi* entered sunlight at 03:53 UT; only DH (decameter-hectometric) Type II emission; intense solar energetic proton event with emission observed >100 MeV; impulsive hard X-ray emission up to 100–300 keV observed by GBM (time history plotted in inset) with no evidence for the 2.223 MeV neutron-capture line. LAT had good Source class data exposures to the Sun ∼04:08–04:36 and 05:46–06:10 UT in response to an autonomous repoint to the Sun, and at 07:18–07:48, 08:58–09:28, and 10:48–11:00 UT (truncated by the SAA). >100 MeV emission was observed in each of these intervals. The Source class data plotted at 4-minute resolution in the inset suggests that there were >100 MeV γ-rays associated with the impulsive hard X-rays and that the LPGRE began ∼04:20 UT, ∼15 minutes after the observed hard X-ray peak. This variation is due to the solar flux and not to modulation (<20%) of the weaker celestial background by the varying solar exposure. We reach the same conclusion using the Solar Flare Transient class data. Ackermann et al. (2014) report a >100 MeV flux of $(0.8 \pm 0.1) \times 10^{-5}\gamma$ cm^{-2} s^{-1} that is consistent with our measurement between 04:08 and 04:34 UT. We have fit the background-subtracted γ-ray spectra between 05:46 and 09:29 UT assuming that the emission is due to pion-decay radiation. The results of these fits are given in Table 3. Our best fitting >100 MeV γ-ray fluxes are consistent with those listed by Ackermann et al. (2014) with the possible exception of the 07:18–07:48 UT interval that had relatively poor solar exposure and large flux uncertainty. The data between 05:46 and 06:10 UT were good enough to provide an estimate of the accelerated proton power-law spectral index, 5.1. Power-law spectra with indices of ∼5 also fit the weaker fluxes in the next two intervals reasonably well and were used in our determination of the numbers of protons. Based on these spectral fits we estimate that there were 3×10^{28} >500 MeV protons accelerated at the Sun during the six-hour period of the LPGRE. As *RHESSI* was not operating at the time and GBM missed the most intense portion of the flare, we have no information on the number of protons in the impulsive phase of the flare from neutron capture line observations.

C.10. *SOL2012-01-27T17:37*

Distinct nature of the LPGRE There is evidence for a rising >100 MeV γ-ray flux about an hour after the impulsive phase. Much of the impulsive phase was not observed because *Fermi* was in the SAA. The LPGRE event

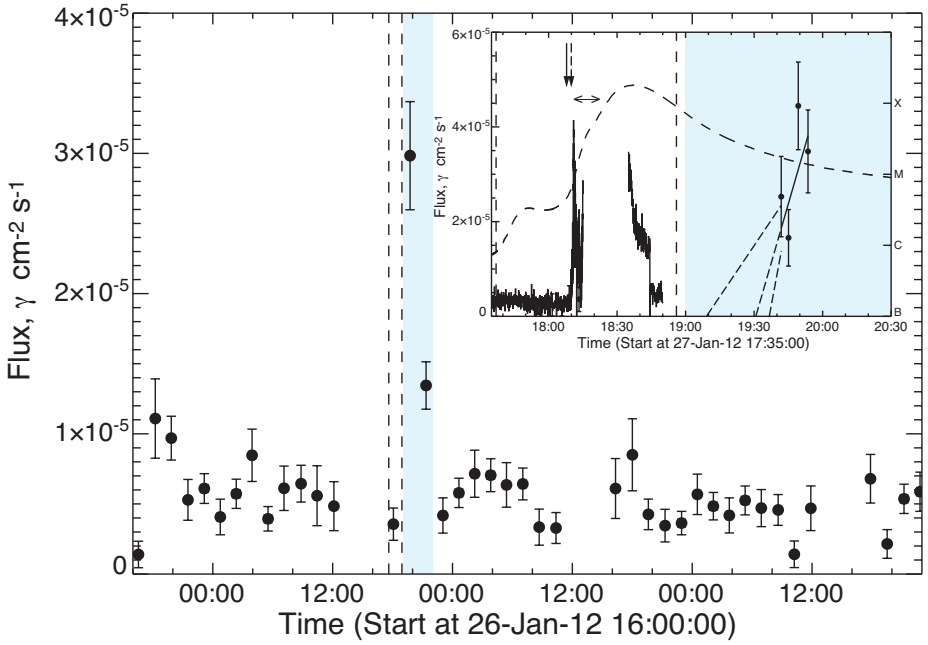

Figure C15. Time profile of the 2012 January 27 LPGRE event observed by LAT. The solid trace in the inset shows the arbitrarily scaled GBM 100-300 keV rates during the flare; missing data are due to an SAA passage. The best fit to an increasing >100 MeV flux after 19:40 UT is shown by the solid line. Extrapolations to determine γ-ray onset and $\pm 1\sigma$ deviations are shown by the dashed lines. See caption for Figure C5 for more details.

appears to have lasted about three hours.

Details Plotted in Figure C15 using Pass8 data. X1.7 class flare at about W81(using *STEREO A* observations because *RHESSI* was being annealed at the time) lasting 79 minutes; ∼2500 km s^{-1} CME with estimated onset coincident with the 100-300 keV X-ray rise; M (metric) and DH (decameter-hectometric) Type II emissions observed with the M onset ∼5 minutes after the CME launch; strong SEP event with proton energies not exceeding 100 MeV; *Fermi* was in SAA between 18:15–18:34 UT; 100–300 keV hard X-rays observed by GBM at beginning and end of impulsive phase (see time history plotted in inset). Poor GBM exposure and large background after SAA prevents estimate of the neutron capture line flux during the impulsive phase , although any line emission would have been strongly attenuated because the flare was near the limb. Using Solar Flare Transient class data, we found no evidence for >100 MeV emission during the first part of the flare from 18:10–18:15 UT. Because the flare was at a heliocentric angle of ∼ 81°, the >100 MeV flux at that location would have been attenuated by about 40% relative to disk center.

LPGRE was observed during the next two exposures 19:36–19:56 and 21:06–21:37 UT. Within the large uncertainties the γ-ray fluxes, determined using Pass8 data and listed in Table 3 are consistent with those reported by Ackermann et al. (2014). The increasing fluxes with time 98% confidence), plotted in the inset of Figure C15, suggest that the onset of the LPGRE occurred about an hour after the impulsive phase. The derived LPGRE proton spectrum during the first exposure followed a power law with index 4.2 ± 0.7 while the spectrum taken 90 minutes later appears to be much harder power-law index 2.8 ± 0.6. We have estimated the number of >500 protons producing the LPGRE assuming that they interact at the location of the flare (Table 3). The number of >500 MeV protons in space was about two orders of magnitude larger those producing the LPGRE event (Table 3). Due to the limited exposure of GBM and LAT, we have no information on the number of >500 MeV protons at the Sun during the flare.

C.11. *SOL2012-03-05T02:30*

Distinct nature of the LPGRE The latter part of the impulsive phase of this event was well observed by LAT. Spectral fits to background-subtracted Solar Flare Transient class data were used to obtain the 1-minute resolution time history plotted in the right inset of Figure C16. There is no evidence for impulsive >100 MeV emission associated with the hard X-ray peak that followed the main phase of the flare. The late phase γ-ray emission appears to have begun within about five minutes of the hard X-ray peak and was observed for about five hours.

Details Plotted in Figure C16. X1.1 class flare at E54 lasting ∼210 minutes.; ∼1500 km s^{-1} CME with onset an hour after the *GOES* start time and ∼17 minutes before GBM hard X-ray data become available (note that this was the last of series of three CMEs occurring over a 3-hour period (Colaninno & Vourlidas 2015)) ; only DH (decameter-

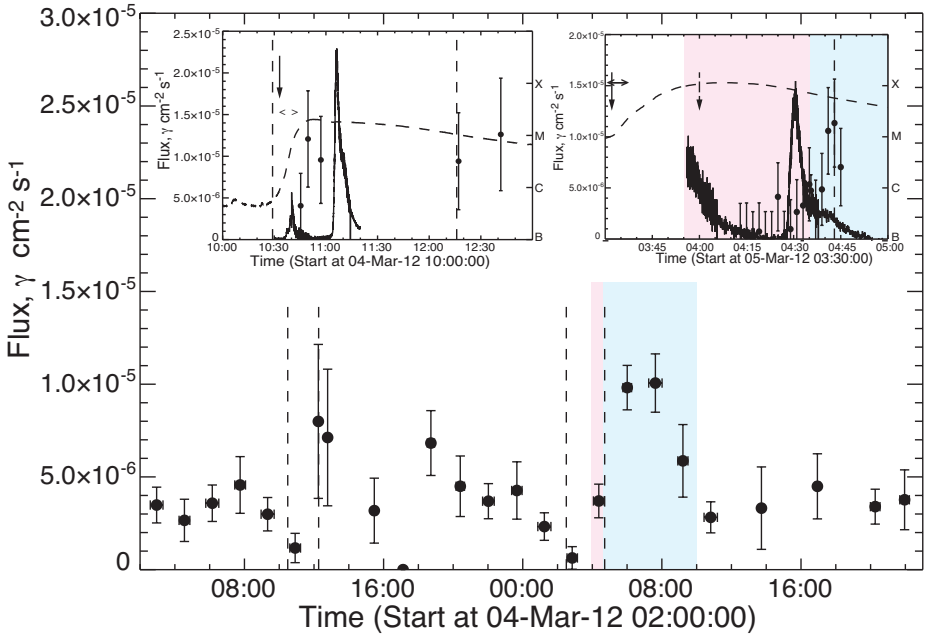

Figure C16. Time histories of the 2012 March 4 event with no significant LPGRE detected by LAT and the 2012 March 5 event for which late phase emission was observed in three exposures after the flare. The left inset shows a blowup of the March 4 flare with GBM 50–100 keV rates scaled to the >100 MeV flux derived from fits to Solar Flare Transient class data. There is no evidence >100 MeV γ rays during the flare. The solid trace in the right inset shows the GBM 100–300 keV rates for the March 5 flare plotted on the same scale as the >100 MeV background subtracted fluxes and $\pm 1\sigma$ uncertainties obtained from fits to the Solar Flare Transient class data. GBM missed the most intense hard X-ray emission between 03:30 and 04:00 UT. Plotted by the dashed downward arrow is the DH Type II onset time; there were no metric Type II observations. See caption for Figure C5 for more details.

hectometric) Type II emission; only upper limit on solar energetic proton flux due to preceding March 4 SEP event; impulsive hard X-ray emission observed up to 100–300 keV by GBM (see time history in right inset) after 03:55 UT when *Fermi* moved into daylight; this initiated an autonomous repoint to the Sun that lasted until 06:15 UT; no evidence for the 2.223 MeV neutron-capture line in GBM spectra. LAT solar exposures in Pass7 source class data: 02:35–03:04, 04:06–04:38, 05:46–06:12, 07:18–07:56, 08:56–09:26 UT. There is clear evidence in Figure C16 for LPGRE in the two orbits following the flare, begining at 05:46 UT. The >100 MeV fluxes that we derived for these these two orbits are consistent with those reported by Ackermann et al. (2014). Our fits also suggest that the proton spectrum may have hardened with time, although the uncertainties are large. Ackermann et al. (2014) report a >100 MeV flux of 5 $\times 10^{-6}\gamma$ cm^{-2} s^{-1} in the flare exposure between 04:12 and 05:01 having both impulsive and LPGRE components.

The right inset shows time history of >100 MeV emission around the time of the late hard X-ray peak near 04:30 UT that we derive using spectral fits to the Solar Flare Transient class data. There is no evidence for >100 MeV γ-rays during the hard X-ray peak between 04:28 and 04:35 UT with a upper limit of 1.5 $\times 10^{-5}\gamma$ cm^{-2} s^{-1}. There is evidence for an increase (85% confidence) in flux after that time, with a peak of $\sim$ 5 $\times 10^{-6}\gamma$ cm^{-2} s^{-1}, that is likely the onset of the LPGRE. As the solar exposure was increasing during this time period the increase was not due modulation of the celestial background. Because GBM missed the most intense portion of hard X-ray emission between 03:30 and 04:00 UT, we have no information on the number of >500 MeV protons at the Sun during the impulsive phase. We have no estimate of the number in space because of a preceding SEP event.

C.12. *SOL2012-03-07T00:02/T01:05*

Distinct nature of the LPGRE There are two intense late phase emission events associated with two flares within about one hour of each other. LLE data (Ajello et al. 2014) reveal >100 emission about 20 minutes after the first flare, a *GOES*-class X5.4 that lasted for at least one hour. Our study of Pass8 Solar Flare Transient class data plotted in the upper right inset reveals that this is a short LPGRE event similar to the one observed on 2011 September 6. The longer LPGRE event shown in the lower-left inset began about 02 UT, 45 minutes after an M7 flare, and lasted about 16 hours.

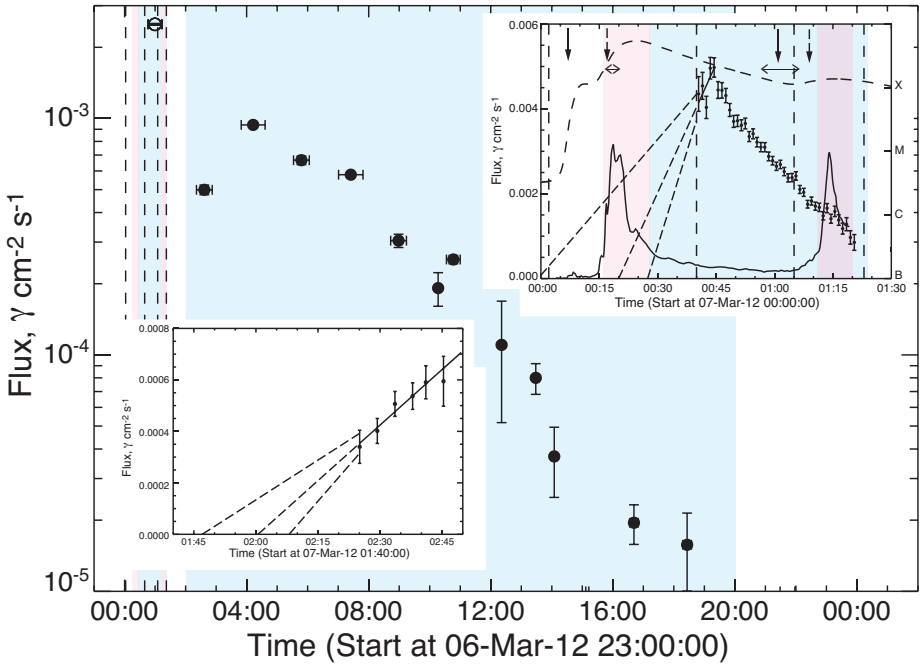

Figure C17. Time history 2012 March 7 event when two episodes of LPGRE were detected by LAT. Inset on upper right shows the >100 keV time histories (solid trace) derived from the *INTEGRAL*/SPI ACD plotted on the same scale as >100 MeV fluxes and $\pm 1\sigma$ uncertainties derived from fits to one-minute Solar Flare Transient class data. The observed rise to a peak indicates that the >100 MeV emission is distinct from the X5.4 impulsive phase. The open circle on the main plot is the weighted mean of the >100 MeV Solar Flare Transient class fluxes plotted in the top inset. The solid line is a fit to the rise in >100 MeV flux and the dashed lines are its extrapolation and $\pm 1\sigma$ deviations used to estimate the LPGRE onset. The inset on lower left shows four-minute resolution >100 MeV fluxes derived from source class data showing the onset of 18-hour duration LPGRE. The solid line is a fit to the rise in >100 MeV flux and the dashed lines are its extrapolation and $\pm 1\sigma$ deviations used to estimate the LPGRE onset. See caption for Figure C5 for more details.

Details Plotted in Figure C17. X5.4 and M7[20] class flares at E27 lasting ∼38 and 18 minutes, respectively; ∼2700 and 1800 km s^{-1} CMEs with onsets several minutes before hard X-ray peaks; M (metric) and DH (decameter-hectometric) Type II emissions observed with M onsets delayed by ∼17 and eight minutes after the respective CME launches; intense solar energetic proton event with emission >100 MeV; impulsive hard X-ray and γ-ray emission from both flares observed to MeV energies (Zhang et al. 2012). Detailed temporal, spectroscopic, and location studies of this event are discussed by Ajello et al. (2014). The >100 keV time history in the upper right inset was derived from the *INTEGRAL*/SPI anticoincidence detector (Zhang et al. 2012) and covers the entire period of the two flares. LPGRE from both events was observed for up to 18 hours. Because the fluxes from this event were so large it was possible to make LAT observations every orbit, even when the peak solar exposure was about 20% of the maximum. *Fermi* came into sunlight at 00:30 UT and GBM observed the decay of the X5.4 and most of the M7 flare. Due to the high hard X-ray rates there were no Source class data during the flares but there were LLE data from 00:35–01:25 UT analyzed by Ajello et al. (2014). We have analyzed data from the new Solar Flare Transient class data and plot >100 MeV flux histories in the upper right inset at 1-minute resolution. The plot shows that the flux peaked at 00:44 UT, suggesting that this emission was not from the impulsive phase but from a short LPGRE event similar to that observed on 2011 September 6 (event 6). Good LAT Source class exposures were obtained between: 02:18–02:48, 04:06–04:34, 05:34–06:01, 07:02–07:46, 08:42–09:12,10:33–10:58, 13:23–13:33, 16:35–16:49, and 19:46–20:14 UT. The fluxes for these observations were derived from Pass8 Source class data. The rising flux between 02:18–02:45 UT, plotted along with an extrapolation to earlier times, suggests that the onset of the 16-hour long LPGRE began about 02:00 UT, about 45 minutes after the peak of the M7 flare.

Table 3 presents the results of our spectroscopic analysis of the LAT data. As discussed above, there were two discrete LPGRE events: LPGRE (A) began ∼20 minutes after the hard X-ray peak associated with the X5.4 flare and lasted through M7-class flare, and LPGRE (B) began about 45 minutes after the M7-class flare. Assuming that LPGRE (A) began at 00:28 UT we estimate that there 4.0 $\times 10^{29}$ >500 MeV protons producing the emission. In

[20] The flare is listed as an X1.3 class flare because of the high X-ray background from the X5.4 flare

contrast there were $1.3{\times}10^{30}$ protons >500 MeV responsible for producing LPGRE (B). These numbers were obtained assuming that the proton angular distribution is isotropic. For a downward isotropic distribution the number should be about two times larger. We confirm the finding of Ajello et al. (2014) that the spectrum of protons producing the pion-decay γ rays appeared to be variable from 00:39 to 01:21 UT. The spectrum initially softened from an index, $s_p \simeq 3.6$ to $\simeq 3.9$ at about 01:00 UT and then hardened to an index $s_p \simeq 3.3$ about the time of the M7 flare. This hardening might have been caused by protons from the M7 flare. The γ-ray fluxes and proton spectral indices derived for LPGRE (B) are consistent with those reported by Ajello et al. (2014). The >300 MeV proton spectrum exhibited spectral softening through at least the first eight hours of the event.

We estimated the numbers of protons >500 MeV during X5.4 and M7 flares flares using the neutron-capture line fluences of 85 and 65 γ cm^{-2}, respectively, measured by the *INTEGRAL* high-resolution gamma-ray spectrometer Zhang et al. (2012). We estimate that both flares accelerated less that 1% of the number of >500 MeV protons produced in LPGRE (A) and LPGRE (B) (Table 3) for a downward isotropic distribution. We can also estimate the number of >500 MeV protons accelerated during the M7 flare by estimating the excess >100 MeV γ-ray flux over the decay emission from LPGRE (A). The excess is only significant at the 1-σ level. The 95% confidence limit in the number of protons for a a downward isotropic flux, 0.9, is about the same as that inferred from neutron-capture line measurement. The number of >500 MeV protons in space was about ten times the number producing the two LPGRE events.

When the LPGRE fluxes exceed $\sim 1.0 \times 10^{-4}\gamma$ cm^{-2} s^{-1} it is possible to use measurements of the 2.223 MeV neutron-capture line to constrain the proton spectrum below 300 MeV during these exposures. We were able to use *RHESSI* rear detector observations of the neutron-capture line because the flare occurred just after an anneal of the detectors when the spectral resolution was about 20 keV FWHM at 2.223 MeV. We obtained background-corrected spectra on orbital time-frames using background ±15 orbits when the environmental conditions were comparable to that during the observing period. We found no evidence for a significant flux in the neutron-capture line in any exposure. We then estimated limits on the index of the power-law proton spectrum between about 40 and 300 MeV using our 95% confidence limits on the 2.223 MeV line flux from *RHESSI* compared with the *Fermi*/LAT measured >100 MeV γ-ray flux. The upper limits on the power indices between 40 and 300 MeV are shown in Table 3 in the row below the indices measured above 300 MeV. All of the limits on the 40–300 MeV index are smaller than those measured above 300 MeV indicating that the proton spectrum producing the LPGRE events steepened above about 300 MeV.

C.13. *SOL2012-03-09T03:22*

Distinct nature of the LPGRE The γ-ray emission has a clear onset within an hour of the flare; it peaked about four hours later, and had a relatively short decay phase. As shown in the inset, there is no evidence for impulsive >100 MeV emission and the number of protons in the LPGRE is at least an order of magnitude higher than in the impulsive phase.

Details Plotted in Figure C18. M6.3 class flare at W02 lasting ∼56 minutes; ∼850 km s^{-1} CME with onset ∼8 minutes after start of 100-300 keV emission; M (metric) and DH (decameter-hectometric) Type II emissions observed with the M onset ∼3 minutes after the CME launch; only an upper limit on solar energetic proton flux due to continuing March 7 event; impulsive hard X-ray emission weakly observed up to >100 keV by GBM (we plot GBM 50-100 keV time history in the inset); no evidence for the 2.223 MeV neutron-capture line in GBM spectra. There are good LAT exposures each orbit due ToO in response to the March 7 SEP event. A LAT solar exposure occurred during the impulsive phase of the flare but there were no Source class data due to high ACD rates; no LLE data are publicly available, but Ackermann et al. (2014) indicate that no >100 MeV emission was detected. We have analyzed the Solar Flare Transient class data to study >100 MeV time history during the impulsive phase. Because of the higher background in the impulsive class of data we have normalized the fluxes to the LAT Source class background rate. This time history is plotted in the inset. There is no evidence for impulsive >100 MeV emission associated with the hard X-ray peaks. There is also no evidence for modulation of the celestial background caused by the factor of two increase in the solar exposure function during this time period. Other LAT exposures were at 05:10–05:58, 06:46–07:32, and 08:22–09:08 UT. LPGRE commenced about 04:00 UT, after the impulsive phase and consistent with the delayed nature of the event reported by Ackermann et al. (2014), and lasted until about 10:30 UT. LPGRE fluxes in the three exposures are consistent with Ackermann et al. (2014) (Table 3); the spectra of the protons producing pion-decay radiation in the exposures appear to be steep with power-law indices ≥6. We estimate that 1.5 $\times 10^{28}$ >500 MeV produced the LPGRE and that there were fewer than 10% of this number during the impulsive phase. Due to large SEP event on March 7 we have no estimate of the number of protons in space.

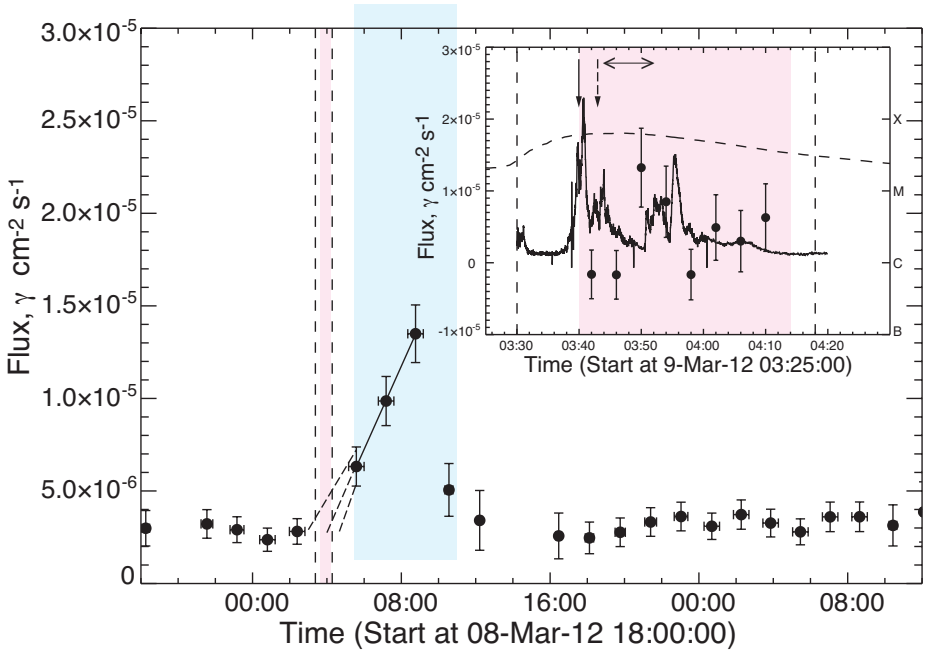

Figure C18. Time profile of the 2012 March 9 LPGRE event observed by LAT. The best fit to an increasing >100 MeV flux after 05:00 UT is shown by the solid line. Extrapolations to determine γ-ray onset and $\pm 1\sigma$ deviations are shown by the dashed lines. Inset shows GBM 50–100 keV rates plotted on the same scale as >100 MeV fluxes derived from fits to Solar Flare Transient class data after normalization to the LAT background rate observed in Source class data. See caption for Figure C5 for more details.

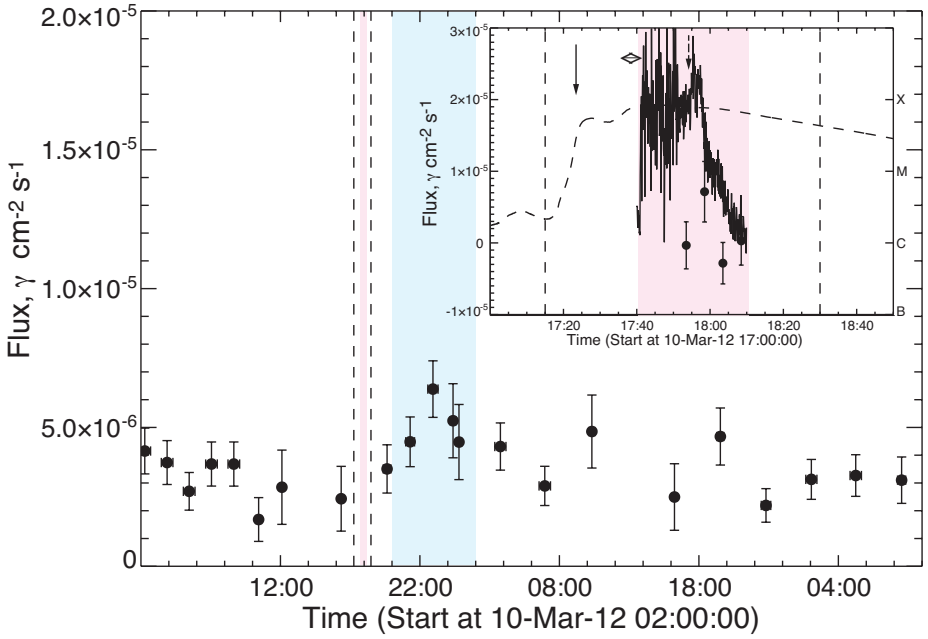

Figure C19. Time profile of the 2012 March 10 LPGRE event observed by LAT. Inset shows GBM 50–100 keV rates plotted on the same scale as >100 MeV fluxes derived from fits to Solar Flare Transient class data after normalization to the LAT background rate observed in Source class data. Plotted by the dashed downward arrow is the DH Type II onset time; no metric Type II emission was detected. See caption for Figure C5 for more details.

C.14. *SOL2012-03-10T17:15*

Distinct nature of the LPGRE The γ-ray onset occurred within about two hours of the associated flare and emission lasted about six hours. The time profile was similar to that observed in the LPGRE event on March 9, but the flux was weaker.

Details Plotted in Figure C19; M8.4 class flare at W26 lasting ∼75 minutes; ∼1300 km s^{-1} CME with onset ∼8 minutes after the *GOES* start time and 15 minutes before GBM hard X-ray data became available; only DH (decameter-hectometric) Type II emission detected; only upper limit on solar energetic proton flux due to background from earlier events; impulsive hard X-ray emission observed up to 100–300 keV by GBM after entering daylight (see time history in inset); no evidence for the 2.223 MeV neutron-capture line in GBM spectra. There are good LAT exposures each orbit due the continuing ToO in response to the March 7 event. A LAT exposure occurred during the impulsive phase of the flare but there were no Source class data due to high ACD rates. No LLE data are publicly available but Ackermann et al. (2014) indicate that no >100 MeV emission was detected during the flare. We analyzed the Solar Flare Transient class data to study the >100 MeV time history during the impulsive phase. Because of the higher background in the Solar Flare Transient class data we have normalized the fluxes to the LAT Source class background rate. We plot the time history in the inset. There is no evidence for >100 MeV emission associated with the hard X-ray peaks. There is also no evidence for modulation of the celestial background caused by an increase in the solar exposure function during this time period. Other LAT exposures: 19:24–19:52, 21:02–21:34, 22:34–23:14, 00:10–00:55 (with data gap) UT. The LPGRE was weak, had an uncertain onset time, and lasted about six hours. Our spectral fits suggest weak 2 σ detections in each of three orbits with >300 MeV proton spectra having power-law indices steeper than 6 (Table 3). We estimate that ∼0.5 $\times 10^{28}$ >500 MeV protons were responsible for the LPGRE. We obtained a limit on the number of protons during the impulsive phase from a limit on the number of 2.223 MeV photons observed by *RHESSI* at the end of the impulsive phase. This limit is less than the number observed in the LPGRE. We have also searched for impulsive >100 MeV γ-ray emission using the Solar Flare Transient class data in four 5-minute intervals starting at 17:51 UT (see inset of figure). There is no evidence for emission and we set a limit of 0.03 $\times 10^{28}$ >500 MeV protons. As this observation only covers about 60% of the impulsive phase we list the upper limit as 0.1 $\times 10^{28}$ in the Table. Due to the large SEP event on March 7, we only obtained an upper limit on the number of >500 MeV protons.

C.15. *SOL2012-05-17T01:25*

Distinct nature of the LPGRE There is no clear evidence for temporal variability >100 MeV in the first exposure taken about 30 min after the last hard X-ray peak. As the flux in the next exposure was not significantly lower, it is likely that the *gamma*-ray emission peaked between the two exposures suggesting that the LPGRE began less than 30 minutes after the last impulsive phase peak. The event lasted about four hours. As discussed below, the upper limit on the number of protons in the impulsive phase was a factor of four larger than the observed number of protons responsible for the observed emission after the flare. Therefore, it is not possible on energetic grounds to rule out the tail of the flare as the source of the >100 MeV γ rays.

Details Plotted in Figure C20. M5.1 class flare at W77 lasting ∼50 minutes; ∼1600 km s^{-1} CME with onset ∼2 minutes after the *GOES* start time and 10 minutes before *RHESSI* hard X-ray data became available; M (metric) and DH (decameter-hectometric) Type II emissions observed with the M onset ∼4 minutes after the CME launch; strong SEP event with proton emission >100 MeV and observed as the first ground level event of Cycle 24; impulsive hard X-rays observed by *RHESSI* up to 100–300 keV after entering daylight (see 50-100 keV time history plotted in inset); no evidence for 2.223 MeV line in the *RHESSI* spectrum during the flare.

There were good LAT solar exposures every orbit including one just before the flare at 00:34–01:10 and at 02:10–02:48, 03:46–04:22, and 05:22-05:56 UT. There was significant LPGRE in the first two exposures after the flare. The measured flux (Table 3 in the first exposure is consistent with that reported by Ackermann et al. (2014). It is not clear why they classify this event as being both impulsive and sustained as there are no >100 MeV observations during the flare. The γ-ray flux just after the flare is plotted at 4-minute resolution in the inset of the Figure and shows no clear evidence for variation in time. Therefore, there is no clear evidence for an onset of the LPGRE but assuming the >100 MeV came from a distinct late phase the onset had to be <30 minutes after the hard X-ray peak. It is also possible that the falling flux observed in the two orbits after the flare could be due the decay of the impulsive phase. The proton spectrum producing the π-decay emission was one of the hardest observed in any LPGRE. The number of >500 MeV protons producing the LPGRE is less than the upper limit on the number during the impulsive phase derived from the limit on the solar 2.223 MeV line. What is surprising is that the >100 MeV flux is so weak that the inferred number of protons in the LPGRE is about 1000 times less than observed in SEPs in space. These comparisons of proton numbers suggests that a significant fraction of the LPGRE may have been radiated behind the west limb of the Sun.

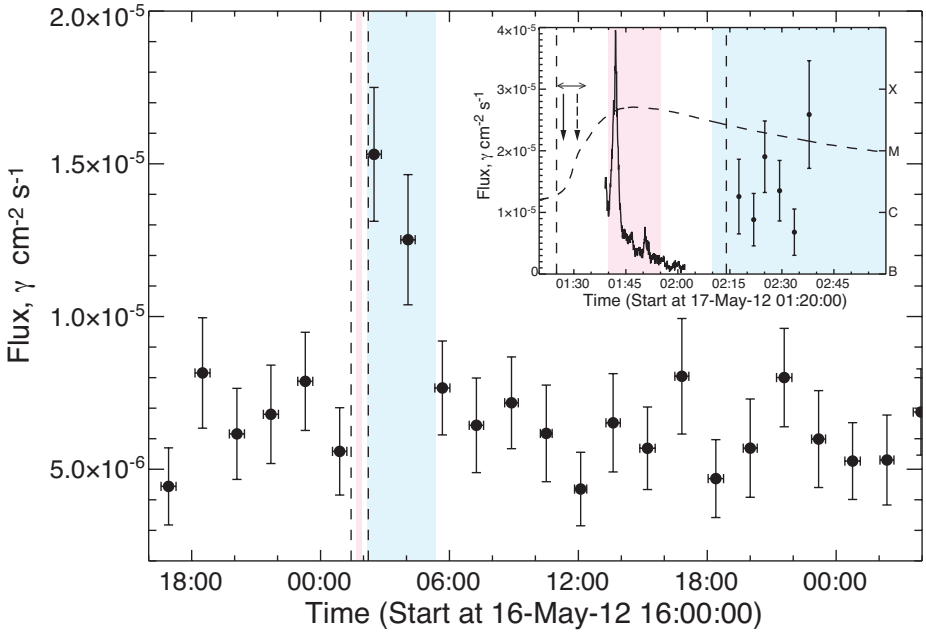

Figure C20. Time profile of the 2012 May 17 LPGRE event observed by LAT. The solid trace shows the *RHESSI* 50-100 keV rates plotted on the same scale as the >100 MeV fluxes. See caption for Figure C5 for more details.

C.16. *SOL2012-06-03T17:48*

Distinct nature of the LPGRE Solar Flare Transient class data, plotted in the inset, reveal a one-minute >100 MeV peak flux coincident with the impulsive hard X-ray peak near 17:53:30 UT and emission following the peak until the end of the exposure at 18:02 UT. The >100 MeV spectrum during the one-minute impulsive phase is steep and can be fit by pion-decay produced by protons following a power-law spectrum with index 6.5 ± 1.0 (see Table 3). In contrast the protons producing what appears to be the eight-minute late phase emission following the peak has an average power-law index of 4.3 ±0.7. There is evidence that the proton spectrum softened during this eight-minute period because the power-law index was 3.6 ± 0.9 between 17:54–17:55 UT, just after flare peak. The significant spectral difference between the protons producing the flare and those producing the time-extended emission suggests an additional acceleration process.

Details Plotted in Figure C21. M3.3 class flare at E38 lasting ∼9 minutes; ∼605 km s^{-1} CME with estimated onset coincident with the 100–300 keV X-ray rise; only M (metric) Type II emission observed with onset ∼6 minutes after the CME launch; weak SEP event; impulsive hard X-rays observed up to 300-800 keV by *RHESSI* and GBM (100–300 keV time history plotted in inset). This event would not have been included in 4-yr study because of the low CDAW CME speed, but this may have been due to its viewing angle as CACTUS reported a maximum speed of 892 km s^{-1} observed from *STEREO B*. Gamma-ray emission was detected in our automated search of Source class data during a single solar exposure (17:38–18:03 UT) and listed by Ackermann et al. (2014) as both an impulsive and sustained event; our 1-minute resolution plot of Solar Flare Transient class >100 MeV fluxes in the inset of the figure clearly shows both characteristics. We note that the time profile derived from Source class data is similar, although the fluxes are lower due to ACD live-time effects from the high rate of impulsive hard X-rays. The solar exposure was relatively constant during the observation, varying by at most 25%, thus background modulation is not significant. There is no evidence for >100 MeV γ-ray emission during the next LAT exposure between 20:50 and 21:26 UT.

There is weak evidence for enhanced >100 MeV emission between 17:51 and 17:53 UT in both source and Solar Flare Transient class data, suggesting that the LPGRE may have began as early as two minutes before the impulsive hard X-rays peak. We fit the flare (17:53-17:54 UT) and post flare (17:54-18:02 UT) Solar Flare Transient class data using pion-decay templates. The proton spectrum during the flare is significantly softer that during the LPGRE , power law index of 6.5 vs 4.3, respectively. The average flux from this study from 17:50–18:02 UT is 30% higher than reported by Ackermann et al. (2014). We estimated the number of protons in the LPGRE by assuming that the emission lasted until 19:00 UT. If this is the case, then the LPGRE was produced by about four-times the number of >500 MeV protons as those in the impulsive phase. We have no information on the number of protons in space. There is no evidence for the neutron-capture line or for nuclear-deexcitation lines in the GBM spectrum during the

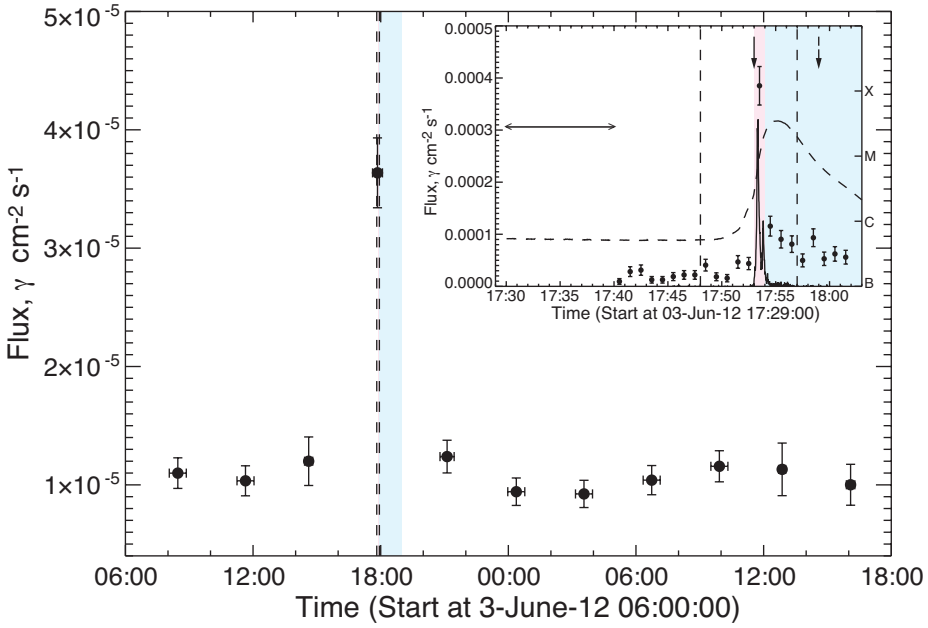

Figure C21. Time profile of the 2012 June 03 LPGRE event observed by LAT. Source class data fluxes are plotted in the main section; the average flux at 18 UT is smaller but consistent with that derived from Solar Flare Transient class data plotted in the inset. Inset compares 100–300 keV rates observed by GBM plotted on the same scale as >100 MeV fluxes derived from Solar Flare Transient class data. See caption for Figure C5 for more details.

one-minute impulsive phase of the flare. Comparing these limits with the observed >100 MeV flux we estimate that the spectrum of flare accelerated protons between about 10 MeV and 300 MeV is consistent with a power law with index of 4 or harder. This indicates that the flare proton spectrum steepened significantly above a few hundred MeV.

In Figure C22 we compare the GBM 100-300 keV and >80 MeV LLE rates during the flare. There are two peaks visible >80 MeV. The first peak is coincident with the hard X-ray peak. The γ-ray emission is not delayed by about 10 seconds from the hard X-ray emission as has been found in other studies of impulsive flares on 2010 June 12 (Ackermann et al. 2012c,b), 2011 September 6 (Appendix C.6, and 2011 September 24 (Appendix C.8. The second γ-ray peak is delayed by about 20 seconds, but with no accompanying hard X-ray emission.

C.17. *SOL2012-07-06T23:01*

Distinct nature of the LPGRE Neither *RHESSI* nor GBM observed the Sun during the impulsive phase, although burst data are available from the Konus instrument on *Wind* (Aptekar et al. 1995) which revealed the presence of >500 keV emission. There is only one LAT exposure in which >100 MeV emission was observed; this began about 15 minutes after the impulsive phase and our 4-minute resolution plot in the inset indicates that the flux was falling during this time period. Thus, we cannot tell whether the emission came from a separate delayed phase beginning in the 15 minutes after the hard X-ray peak or whether it was the tail of the impulsive phase emission. As there were no γ-ray observations during the flare, we have no comparison of the relative numbers of protons in the impulsive and late phase emission.

Details Plotted in Figure C23. X1.1 class flare at W52 lasting ∼13 minutes; ∼1800 km s^{-1} CME with onset coincident with the rise of the *GOES* 0.5–4Å power plotted in the inset; there were no hard X-ray observations during the peak of the flare as both *RHESSI* and *Fermi* were in nighttime (in lieu of a 100-300 keV X-ray time history, we plot the *GOES* 0.5-4Å time history); hard X-ray emission >500 keV was observed by Konus during the rise of the impulsive emission; M (metric) and DH (decameter-hectometric) Type II emissions observed with the M onset ∼5 minutes after the CME launch; moderate SEP event with emission >100 MeV. Listed by Ackermann et al. (2014) as both an impulsive and LPGRE event but there were no >100 MeV observations during the impulsive phase. Good LAT solar exposures each orbit due to Crab Nebula ToO. >100 MeV γ rays observed during the 23:27–23:54 UT solar exposure with a flux (Table 3) that is consistent with that listed by Ackermann et al. (2014). The inset of the Figure shows the >100 MeV emission accumulated in 4-minute intervals over this time period; the flux appears to be falling. This suggests that the emission may be the decay phase of the impulsive flare, but it could also be a separate component with onset time in the 15 minutes after the impulsive peak. The best fitting pion-decay spectrum over

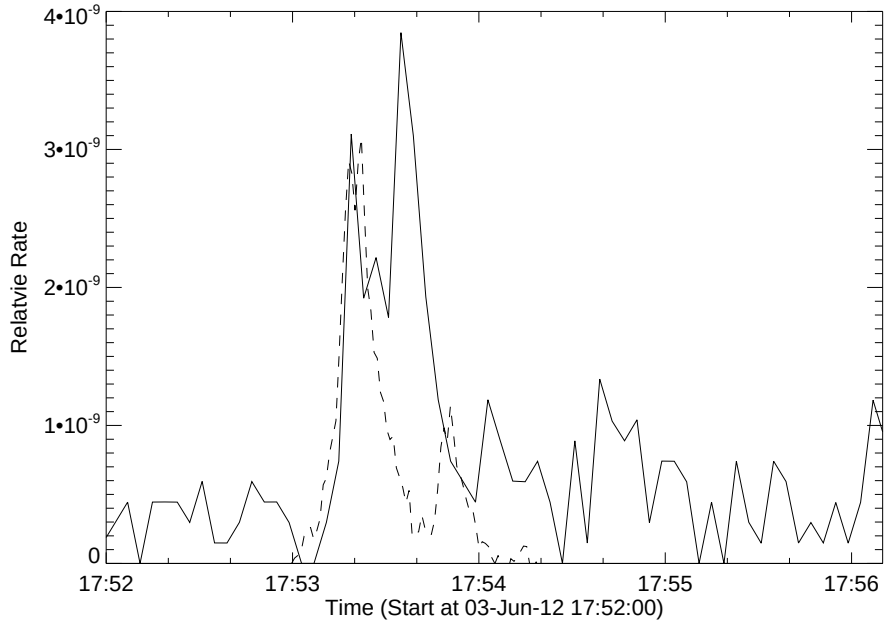

Figure C22. Comparison of 100–300 keV rates observed by GBM (dashed trace) and >80 MeV rates observed in LLE data (solid trace) during the peak of 2012 June 3 flare.

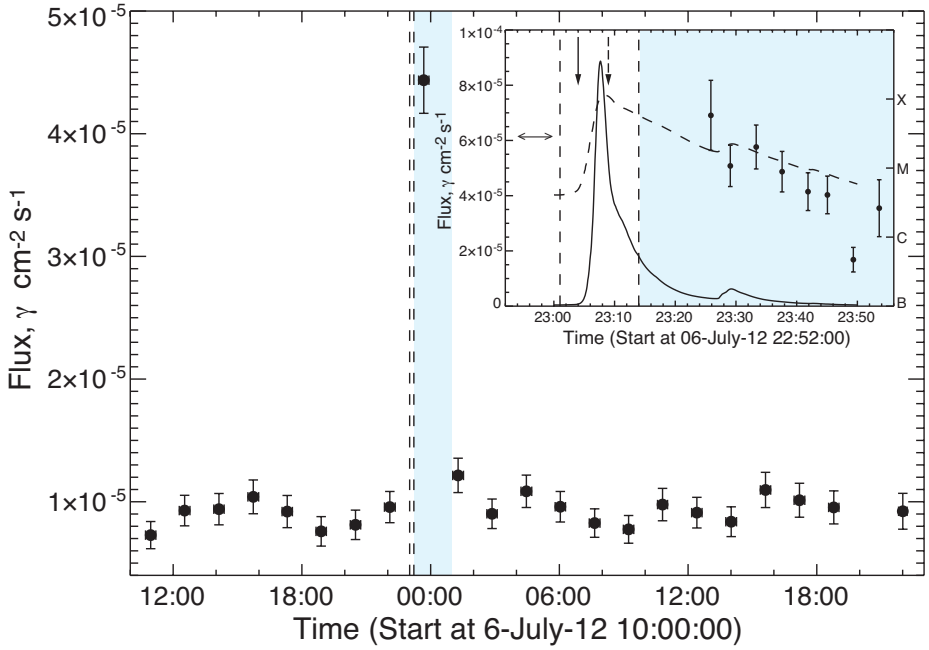

Figure C23. Time profile of the 2012 July 6 LPGRE event observed by LAT. As both *RHESSI* and GBM were in nighttime during the flare, we plot the *GOES* 0.5–4Å time history in the inset. See caption for Figure C5 for more details.

the full 27-minute exposure is consistent with a proton spectrum with index 5.1, but the spectrum appears to have softened in time: 4.7 ± 0.8 from 23:27–23:40 UT, and was steeper than 6.0 from 23:40–23:54 UT. There were $\sim 1 \times 10^{28}$ associated with LPGRE assuming an onset just after the impulsive phase ; we only have an upper limit on the number of protons in the SEP event (Table 3).

C.18. *SOL2012-10-23T0313*

Distinct nature of the LPGRE LAT observed γ-ray emission during a single 30 minute exposure about 50 minutes after the 5-minute duration impulsive phase on 2012 October 23. There is no evidence for variability in the

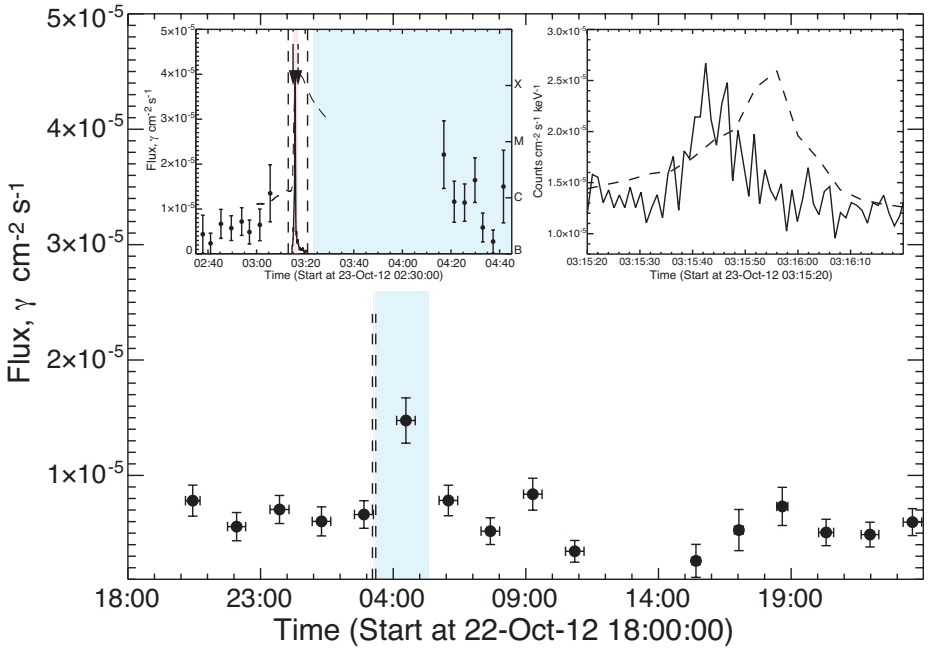

Figure C24. Time profile of the 2012 October 23 LPGRE event observed by LAT. Left inset shows GBM 100-300 keV rates plotted on the same scale as >100 MeV fluxes derived from source class data. Right inset compares GBM 100-300 keV (dashed trace) and >9 MeV (solid trace) rates. See caption for Figure C5 for more details.

flux during the exposure (we note that solar exposure for the first and last points was about 30% of the peak and that there may be some contribution from background modulation effects for those two fluxes). We only know that the emission began before this time. The flare itself was observed by both *RHESSI* and GBM and the right inset of the Figure C24 a shows a high-time resolution plot of the impulsive phase in two GBM energy channels, 100–300 keV (dashed) and >9 MeV (solid) revealing two peaks separated by ∼15s. The spectrum of the first peak can be fit by bremsstrahlung from the sum of two power-law electron spectra, one having a steep index 5.1 and the second a hard index of 3; only bremsstrahlung from a steep electron spectrum could fit the second peak. Although the Sun had just left the LAT aperture, γ rays from the first peak scattered in the spacecraft were in LLE data up to ∼50 MeV and had a relatively steep spectrum. This suggests that the impulsive phase was dominated by electron bremsstrahlung and that it was not the source of the delayed emission. Thus it is not likely that the there were a sufficient number of impulsive phase protons to account for the emission. This event differed from all of the previous events in that it was not accompanied by a CME. As discussed below, the upper limit on the number of protons in the impulsive phase was smaller than the number in the LPGRE. Therefore, it is not likely that the tail of the flare was the source of the >100 MeV γ rays.

Details Plotted in C24. X1.8 class flare at E57 lasting eight minutes; no CME or SEP event detected but Metric Type II radio emission was observed; impulsive hard X-ray and γ-ray emission observed to >9 MeV (see 100–300 keV time history in the left inset). There is evidence for the eruption of a magnetic loop in AIA 94Å and 131Å images at 03:15 UT (time denoted by the downward arrow in the left inset) along with material moving away from the flare region suggesting that this might have been a failed CME (Ji et al. 2003). The LPGRE event was only revealed in the Pass8 source class data; it only appeared at 2σ significance in the Pass7 Source class data. LAT had good solar exposures each orbit: 02:34–03:12 (just before the impulsive peak), 04:10–04:40, and 05:45–06:22 UT. LPGRE was only observed between 04:10–04:40 UT and there is no clear evidence for variability during 4-minute integrations. The onset delay of the >100 MeV emission was estimated from the time of the erupting magnetic loop. The right inset shows a high-time resolution plot of the impulsive phase in two GBM energy channels, 100-300 keV (dashed) and >9 MeV (solid) that reveals two peaks separated by ∼15s. The first peak can be fit by the sum of an electron spectra made up of two power-law components, one having a steep spectral index, ∼5, and the second a harder spectral index, ∼3; only the steep spectral component of electrons was observed in the second peak and there is no evidence for emission >9 MeV. Although the Sun had just left the aperture of LAT, scattered radiation from the hard first flare peak was observed in LLE data up to about 50 MeV. Thus, the emission in the impulsive phase was dominated by electron bremsstrahlung. We estimated the number of >500 MeV protons in the LPGRE assuming that is began just after

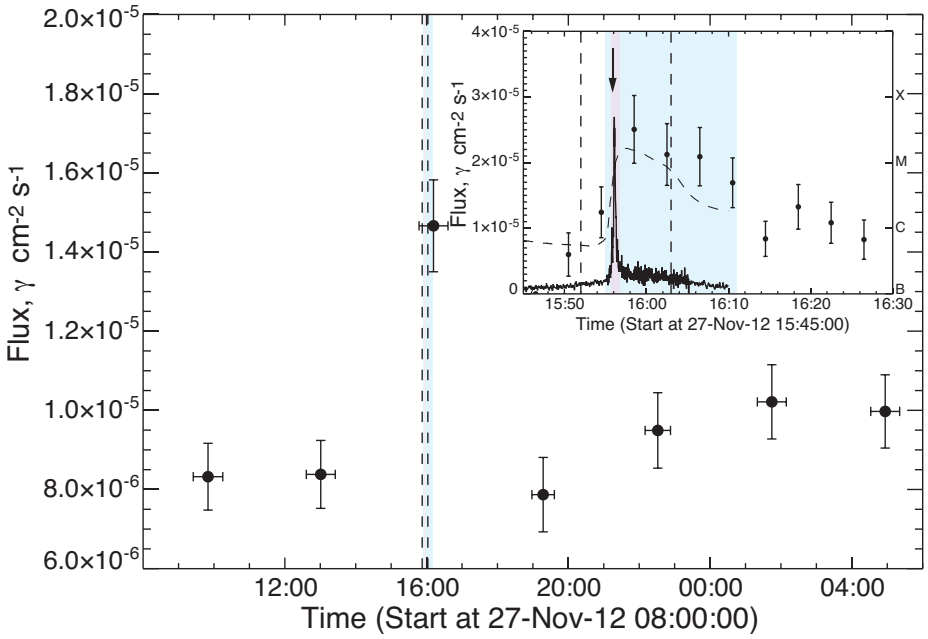

Figure C25. Time profile of the 2012 November 27 LPGRE event observed by LAT. Inset displays the expanded flare region with GBM 100–300 keV rates plotted on the same scale as the >100 MeV Source class fluxes and $\pm 1\sigma$ uncertainties plotted at 4-minute resolution. See caption for Figure C5 for more details.

the impulsive phase and peaked in intensity between 04:10 and 04:40 UT. We estimated the number of protons in the impulsive phase by using the upper limit on the 2.223 MeV capture line. The results of this study are presented in Table 3 and indicate that the number of >500 MeV protons in the flare was only about 20% of the number producing the LPGRE , but the uncertainties are large.

C.19. *SOL2012-11-27T1552*

Distinct nature of the LPGRE LAT had good exposure throughout the impulsive phase, which was not accompanied by a CME. >100 MeV emission was observed only during this exposure and the fluxes are plotted at 4-minute resolution in the inset along with GBM 100-300 keV rates. Plots at higher resolution indicate that the late phase emission began within a minute of the the narrow impulsive peak observed in hard X-rays. It lasted for at least 16 minutes, suggesting that it was produced by a distinctly different acceleration process than the flare. The flare spectrum can be fit with bremsstrahlung from a power-law electron spectrum with a break near 1 MeV. The upper limit on the number of protons in the flare was more than a factor of ten less than the number in the LPGRE based on pion-decay fits to the LAT spectrum. Therefore, it is not likely that protons accelerated in the flare was the source of the >100 MeV γ rays.

Details Plotted in Figure C25; M1.6 class flare at W73 lasting ∼35 minutes; no CME, Type II emission, or SEP event observed; one-minute long impulsive hard X-ray peak reaching energies >300 keV observed by GBM; 100–300 keV rates plotted in inset. There is evidence for the eruption (time denoted by downward arrow in the inset) of a magnetic loop in AIA 171Å at 15:55:50 UT, along with material moving away from the flare region, suggesting that this was a failed CME (Ji et al. 2003). The Sun was in LAT's field of view during the impulsive phase of the flare. The solar exposure varied by less than 25% from 15:55 to 16:30 UT. Source class data could be used for the study because the rates in the ACD from hard X-rays were not too high. The LPGRE flux between 04:10 and 04:40 UT measured using the Solar Flare Transient class data is consistent with the flux derived using the Source class data. We plot the >100 MeV γ rays at four-minute resolution in the inset to improve the statistical significance of each point. Plots at one and two minute resolution indicate that the LPGRE began within a minute of the X-ray peak and that there no peak in >100 MeV γ-rays coincident with the X-rays. The LPGRE lasted about 16 minutes with marginal evidence for more rapid time variations when plotted at one- and two-minute resolution. The >100 MeV emission appears to have been produced by an acceleration process distinctly different from the flare. Our fits to the spectra indicate that the protons producing the LPGRE followed a power-law with index ∼3 that was constant over the observation period. In contrast, the spectrum of electrons producing the flare bremsstrahlung, observed up to 800 keV, followed a power law with index of ∼3.7. There is no evidence for either nuclear de-excitation or 2.223 MeV neutron-capture γ-rays

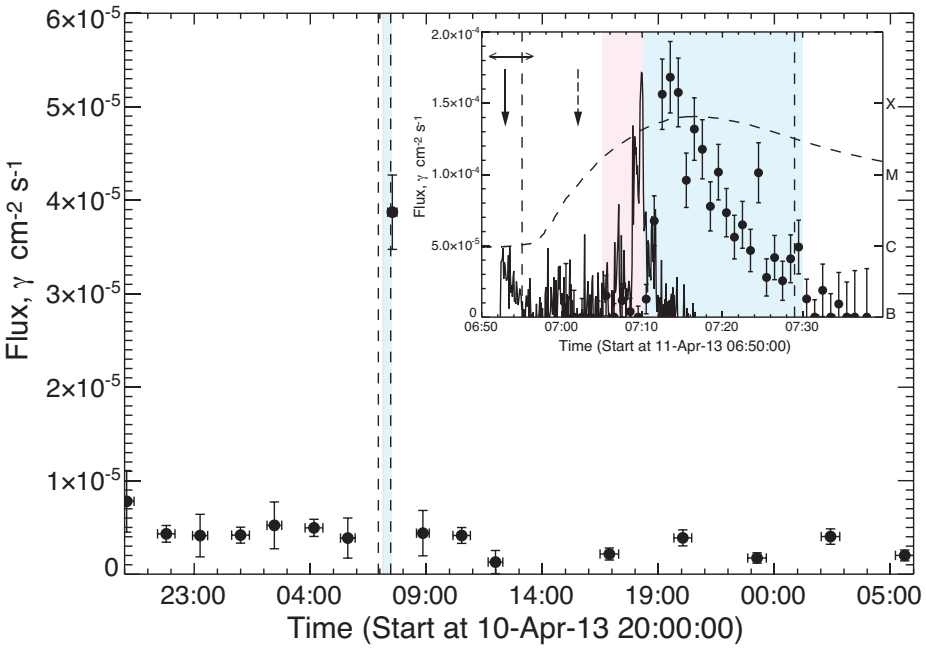

Figure C26. Time profile of the 2013 April 11 LPGRE event observed by LAT. Inset shows blowup of flare region with GBM 100-300 keV rates plotted on the same scale as >100 MeV fluxes and $\pm 1\sigma$ uncertainties derived from fits to Solar Flare Transient class data. See caption for Figure C5 for more details.

during the flare in the GBM data. The number of protons >500 MeV in the LPGRE was the smallest observed by LAT, but still exceeded the upper limit on the number of protons in the impulsive phase by at least a factor of ten. The onset delay of the >100 MeV emission for this event is estimated from the time of the erupting magnetic loop.

C.20. *SOL2013-04-11T06:55*

Distinct nature of the LPGRE LAT had a good exposure to most of the impulsive phase. There is no evidence for >100 MeV γ-ray emission during the four-minute long impulsive X-ray peak. The onset of the LPGRE was clearly observed at 07:10 UT, about one minute after this peak. It reached a maximum about three minutes later, and lasted only about 20 minutes. The estimated number of >500 MeV protons in the LPGRE is at least 25 times more than in the impulsive phase.

Details Plotted in Figure C26. M6.5 class flare at W13 lasting ∼34 minutes; ∼850 km s^{-1} CME with onset ∼15 minutes before the main peak in 100–300 keV flux observed by GBM (plotted in inset); M (metric) and DH (decameter-hectometric) Type II emissions observed with the M onset ∼9 minutes after the CME launch; strong SEP event with emission >60 MeV. The Sun was in LAT's field of view during most of the flare but Source class data are only available between 07:21–07:40 UT due to high rates in the ACD. However, Solar Flare Transient class data are available beginning at 07:00 UT. The >100 MeV fluxes derived from fits to background-subtracted spectra at 1-minute resolution, show no detectable γ-ray emission during the prominent X-ray peak. The LPGRE began about one-minute later, peaked three minutes after onset, and lasted ∼20 minutes. From fits to spectra in three time intervals during the event, we estimate that $\sim 0.7 \times 10^{28}$ >500 MeV protons produced the LPGRE. The proton spectrum >300 MeV had an average power-law index of ∼5.5 and may have hardened during the event (see Table 3). Comparing the 0.05 γ cm^{-2} s^{-1} upper limit on the flux in the 2.223 MeV line from 07:10–07:30 UT with the observed flux >100 MeV, we estimate that the 40–300 MeV LPGRE protons followed a power-law with index harder than 4.5. This suggests that the LPGRE proton spectrum steepened above 300 MeV. An upper limit on the flux of 2.223 MeV γ rays during the impulsive phase of the flare provided a limit on the number of >500 MeV protons that is a factor of ten below the number in the LPGRE. An even more constraining limit comes from the upper limit on the >100 MeV flux during the hard X-ray peak listed in Table 3. The number of >500 MeV protons in the SEP event was at 2 to 3 orders of magnitude larger than the number the Sun.

C.21. *SOL2013-05-13T01:53*

Distinct nature of the LPGRE LAT had no exposure to the impulsive phase and it only observed >100 MeV emission during its first solar exposure two hours later. We found no evidence for time variation in the flux during

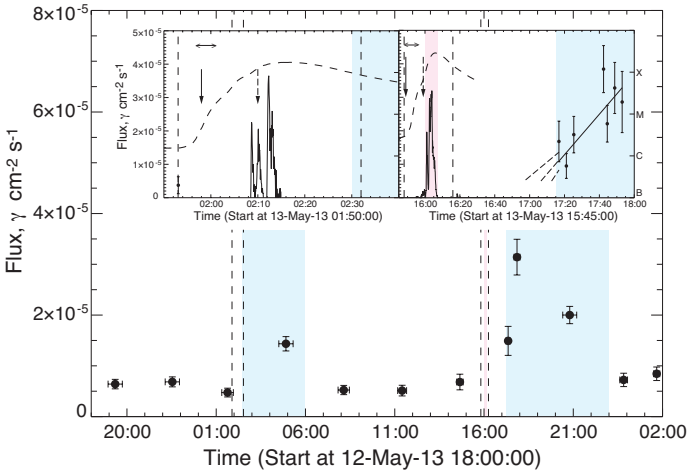

Figure C27. Time profiles of two LPGRE events on 2013 May 13 observed by LAT. Blowups of the regions around both flares are shown in the two insets with *RHESSI* 100–300 keV time histories scaled to the >100 Mev γ-ray fluxes and $\pm1\sigma$ uncertainties. The best fit to an increasing >100 MeV flux after 17:20 UT is shown by the solid line in the right inset. Extrapolations to determine γ-ray onset and $\pm1\sigma$ deviations are shown by the dashed lines. See caption for Figure C5 for more details.

this exposure suggesting that the observation may have been made near the peak of the emission. We note that if the γ rays came from the footpoints of the flare at 89E, the flux would have been attenuated by about a factor of 6. Due to the flare's location near the solar limb, we could not use the 2.223 MeV line to estimate the number of protons in the impulsive phase that could be compared with the number producing the LPGRE.

Details Plotted in Figure C27. X1.7 class flare at E89 lasting ∼39 minutes; ∼1300 km s^{-1} CME with onset ∼ coincident with the 50-100 keV X-ray rise and 10 minutes before the 100–300 keV X-ray rise observed by *RHESSI* and GBM; M (metric) and DH (decameter-hectometric) Type II emissions observed with the M onset ∼12 minutes after the CME launch; small SEP event with emission >60 MeV; 100–300 keV hard X-ray emission observed by *RHESSI* (left inset of the figure). A good LAT exposure ended about the start time of the X-class flare; the next exposure was 04:30–05:15 UT, two hours after the flare and weak >100 MeV flux was observed with a flux of $\sim 1 \times 10^{-5}$ cm^{-2} s^{-1} produced by a proton spectrum with power-law index ∼5.5 (Table 3). There was no observable flux variability during the exposure. If the emission came from the active region it would have been attenuated by about a factor of 6. There was no significant hard X-ray emission above 300 keV. Due to the extreme attenuation of the neutron-capture line at E89, we cannot obtain a limit on the numbers of protons at the Sun during the impulsive phase of the flare.

C.22. *SOL2013-05-13T15:48*

Distinct nature of the LPGRE LAT had no exposure to the impulsive phase but it did observe >100 MeV emission in its first solar exposure after the flare. The clearly increasing flux in this exposure measured at 4-minute resolution and plotted in the right inset indicates that the LPGRE began about an hour after the impulsive phase. The emission lasted for up to six hours.

Details Plotted in Figure C27. X2.8 class flare at E80 lasting ∼28 minutes; ∼1500 km s^{-1} CME with estimated onset ∼10 minutes before the 100–300 keV X-ray peaks; M (metric) and DH (decameter-hectometric) Type II emissions observed with the M onset ∼12 minutes after the CME launch; strong SEP event with emission >60 MeV; hard X-ray and γ-ray emission observed >1 MeV by *RHESSI* (*RHESSI* 100–300 keV time history plotted in right inset). Good LAT solar exposures were obtained every other orbit with >100 MeV γ-ray emission observed during the first orbit after the impulsive phase, between 17:15–17:28 and 17:41–17:59 UT (with comparable solar exposures broken by an SAA passage), and during the third orbit between 20:25–21:10 UT. The emission appears to be rising during the first exposure (see right inset of Figure) with an apparent onset time near 17:00 UT, about one hour after the impulsive phase. The emission lasted at most five hours. Fits to the LAT spectra with pion-decay models indicate that the proton spectrum softened between 17:50 and 20:30 UT. About 3.3 $\times 10^{29}$ >500 MeV protons would have been needed to produce the γ rays if the interactions took place at a heliocentric angle of 80°. *RHESSI* had the best exposure to the impulsive phase while GBM began observations in the middle of the flare when its MeV spectrum was dominated by SAA-produced radioactivity. Only the *RHESSI* front detectors could be used to search for line radiation (below 2.4 MeV) because of radiation damage in its rear detectors; the front detector spectral resolution was ∼ 30 keV FWHM at 2 MeV. The impulsive bremsstrahlung spectrum had a spectral index of 2.8 and extended to above 1 MeV; there

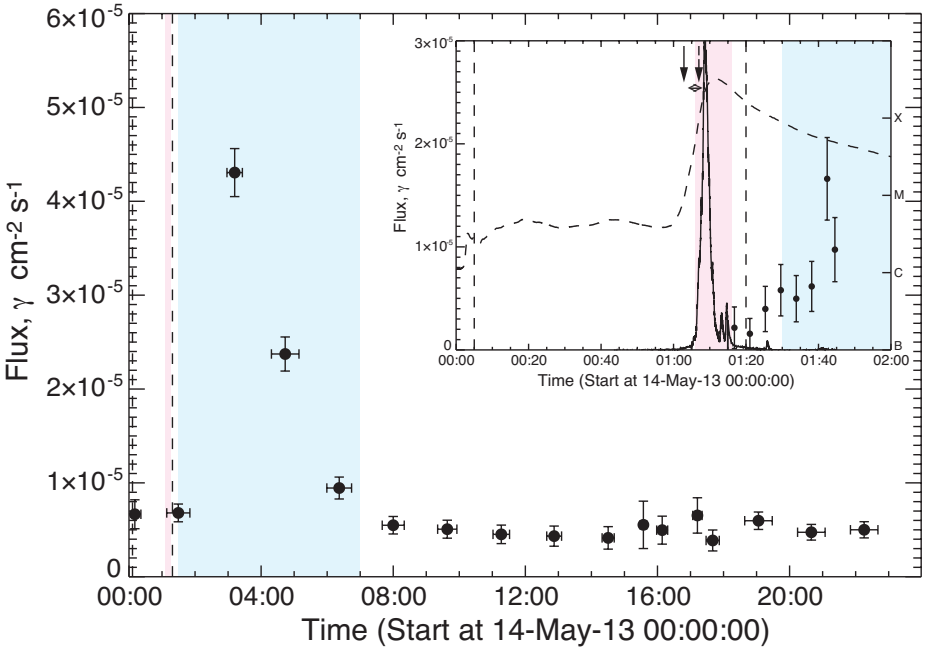

Figure C28. Time profile of the 2013 May 14 LPGRE event observed by LAT. Inset shows blowup of flare region with GBM 100–300 keV rates plotted on the same scale as >100 MeV fluxes and $\pm 1\sigma$ uncertainties derived from Source class data after the flare. See caption for Figure C5 for more details.

was also evidence for nuclear de-excitation line emission with 6 σ significance, but no evidence for the neutron capture line with a 95% confidence upper limit on the flux of 0.035 γ cm^{-2} s^{-1}. From this 2.223 MeV line limit the number of protons were at least a factor of five below the number observed during the LPGRE assuming they all interacted at a heliocentric angle of 80° (Table 3). This also assumed that the proton spectrum followed a power law with index 4.5 >40 MeV. However, the proton spectrum was likely to be steeper than that because the power-law index between 4 and 40 MeV, determined by comparing the nuclear de-excitation and 2.223 MeV line, was steeper than 5.

C.23. *SOL2013-05-14T00:00*

Distinct nature of the LPGRE The >100 MeV LPGRE clearly began about five minutes after the impulsive 100–300 keV X-ray peak. The LPGRE peaked in about one hour and had a gradual four to five hour decay. The estimated number of >500 MeV protons in the LPGRE exceeded the number in the impulsive phase by more than a factor of ten.

Details Plotted in Figure C28. X3.2-class flare at E77 lasting ∼80 minutes (strongest emission began after 01:00 UT and lasted 20 minutes); ∼2600 km s^{-1} CME with estimated onset about one minute before the hard X-ray peak observed by GBM; M (metric) and DH (decameter-hectometric) Type II emissions observed with the M onset ∼3 minutes after the CME launch; strong SEP event with emission >60 MeV; hard X-ray emission >1000 keV observed by GBM; the inset shows the 100–300 keV time history (weak impulsive emission barely visible in the plot continued until 02:00 UT). There were good LAT solar exposures each orbit in response to a ToO on May 13 and even better exposure for two orbits due to an ARR solar pointing in response to the flare. Pass7 Source class data were originally available from 01:10 – 01:47 UT, but later versions of it and Pass8 data only began after 01:30 due to concerns about ACD rates. However, these rates do not appear to be high enough to have seriously affected LAT time histories after 01:15 UT. The >100 MeV flux in the Pass 7 data appears to be rising after 01:15 UT (95% confidence). The >100 MeV fluxes in the Pass8 source class data after 01:30 UT show the same increase. Solar Flare Transient class data are available after 01:11 UT. We found no evidence for >100 MeV emission between 01:11–01:16 UT just after the large X-ray peak. Other solar exposures were made 02:58–03:23, 04:20–05:06, and 06:01–06:41 UT. The LPGRE peaked in the exposure from 02:58 to 03:23 UT as evidenced by the relatively constant 4-minute resolution fluxes in that exposure. Our 4-minute resolution plots clearly show that the flux was falling in the next exposure between 04:40–05:06 UT. From the weak flux observed between 06:01–06:41 UT, we infer that the emission lasted until about 07:00 UT. Fits to the background subtracted spectra suggest that the spectrum of protons producing the LPGRE had a steep power-law spectrum (Table 3). For an interaction site at 77° it required about 5 $\times 10^{28}$ >500 MeV protons to

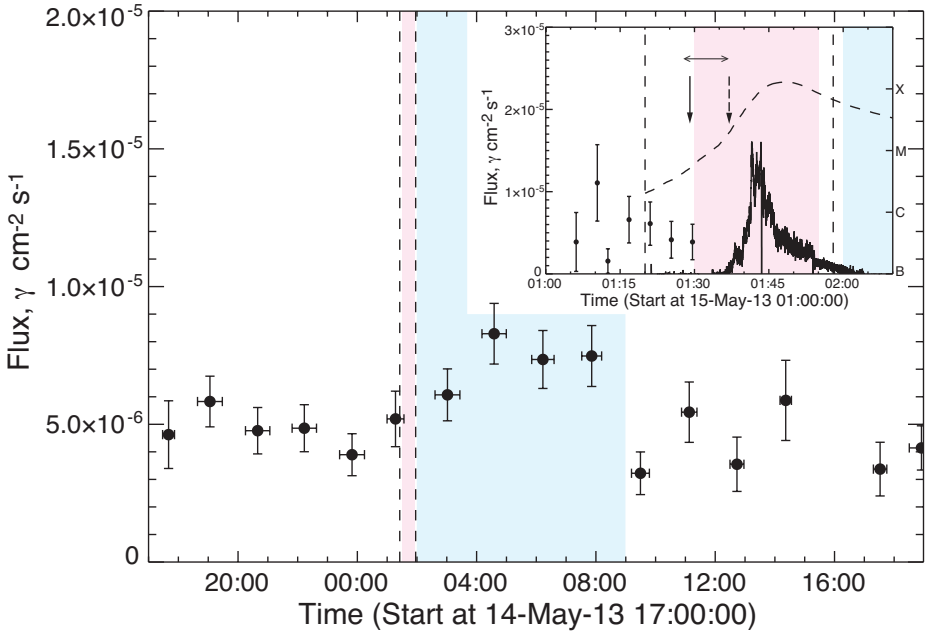

Figure C29. Time profile of the 2013 May 15 LPGRE event observed by LAT. Inset shows blowup of flare region with GBM 100–300 keV rates plotted on the same scale as >100 MeV fluxes and $\pm 1\sigma$ uncertainties derived from Source class data before the flare. See caption for Figure C5 for more details.

produce the LPGRE. The impulsive phase spectrum measured by GBM can be fit by a power-law with index ∼2.5 and a weak contribution from nuclear lines. There is only an upper limit on the neutron-capture line flux of 0.01 γ cm^{-2} s^{-1}; this value suggests that the number of >500 MeV protons at the Sun during the impulsive phase was at most a few percent of the number in the LPGRE.

C.24. *SOL2013-05-15T01:25*

Distinct nature of the LPGRE The LPGRE was relatively weak and below the 4.2 σ threshold in our light-bucket analysis; it was identified in the LAT Team's more sensitive Maximum Likelihood study and lasted up to seven hours. The time history in the main plot suggests that the LPGRE began no more than an hour after the hard X-ray peak. The estimated number of >500 MeV protons in the LPGRE exceeded the number in the impulsive phase by more than a factor of ten.

Details Plotted in Figure C29. X1.2 class flare at E65 lasting ∼33 minutes; ∼1350 km s^{-1} CME with estimated onset ∼15 minutes before the hard X-ray peak; M (metric) and DH (decameter-hectometric) Type II emissions observed with the M onset ∼8 minutes after the CME launch; upper limit on SEP protons due to ongoing event from previous eruption; hard X-ray emission reached 100–300 keV in *RHESSI* and GBM (time history in the inset). Good LAT solar exposures each orbit due to ongoing ToO; Source class solar exposure 01:01–01:33 UT truncated before flare due to high ACD rate. Good Source class exposures 02:37–03:23, 04:13–04:58, 05:52–06:34, 07:33–08:09 UT. This marginal event was noted in the LAT Team's Maximum Likelihood study plotted in the RHESSI browser and was not significant enough to be noted in the light- bucket study even using the PASS8 Source class data. As plotted in Figure C29 the LPGRE was relatively weak and appears to last about six hours. >100 MeV emission appears to have begun before 02:40 UT and there is no evidence for temporal variability during that observing period. Fit to background-subtracted spectra for the four observations spanning 02:37 to 08:09 UT with pion-decay spectral templates (Table 3) indicate significant flux levels above 3 σ in three time intervals; the proton spectra are typically harder than power laws with indices of –5. The total number of protons producing the LPGRE was $\sim 5 \times 10^{27}$. The upper limit on the number of protons during the impulsive phase derived from the limit on the neutron-capture line is comparable to this. With Solar Flare Transient class data we obtained an upper limit on the >100 MeV flux covering the impulsive phase from 01:36–01:46 UT and a limit on the number of protons >500 MeV fewer than 5% of that producing the LPGRE.

C.25. *SOL2013-10-11T07:01*

Distinct nature of the LPGRE This was the first LPGRE event detected from a flare behind the solar limb (Pesce-Rollins et al. 2015a; Ackermann et al. 2017). The hard X-rays from the flare at E103 peaked about three

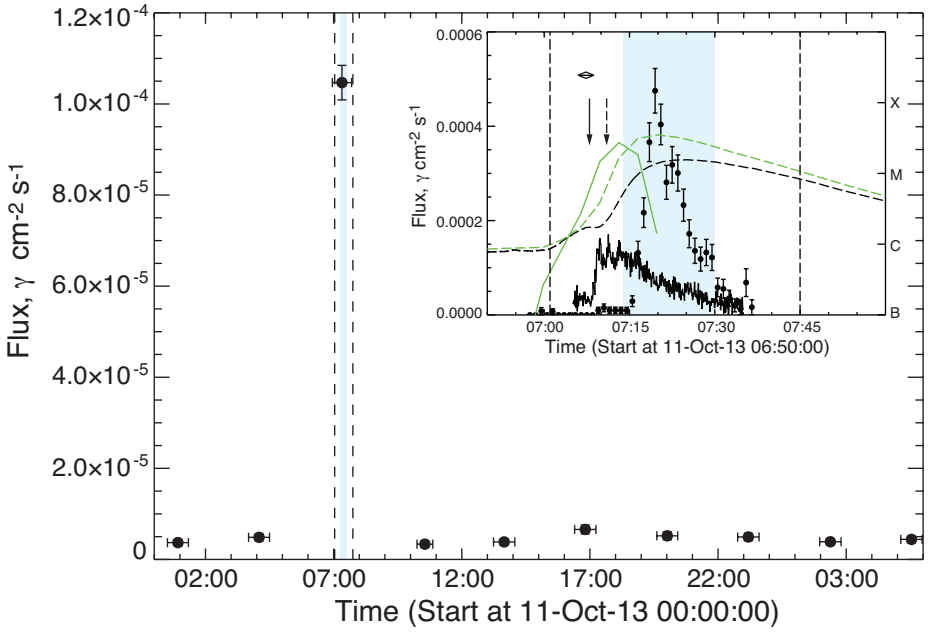

Figure C30. Time profile of the 2013 October 11 LPGRE event observed by LAT. The inset shows GBM 100-300 keV rates plotted on the same scale as >100 MeV γ-ray fluxes $\pm 1\sigma$ uncertainties derived from Source class data. In addition to the *GOES* X-ray plot we also plot the soft X-ray rates from the *MESSENGER* SAX instrument that observed the flare region as the dashed green trace. The time derivative of this flux is a good representation of the flare hard X-ray emission that we plot as solid green trace. See caption for Figure C5 for more details.

minutes before the onset of the LPGRE. This can be seen in Figure C30 by comparing hard X-ray time profile (green solid trace) estimated from the derivative of the soft X-ray rates observed by *MESSENGER* (green dashed trace) and the >100 MeV flux observed by LAT (data points with uncertainties). There is no evidence for an increase in the 100-300 keV rates observed by the GBM NaI detector at the time of >100 MeV onset.

Details Plotted in Figure C30. Estimated (Pesce-Rollins et al. 2015a,b) M4.9 class flare beyond the limb at E106 lasting ∼44 minutes; ∼1200 km s^{-1} CME with onset within two minutes of the rise of hard X-rays observed by GBM; M (metric) and DH (decameter-hectometric) Type II emissions observed with the M onset ∼3 minutes after the CME launch; strong SEP event extending to energies >60 MeV; hard X-ray emission only observed to 50–100 keV. Good LAT solar exposures every other orbit: 06:58–0740, 10:16–10:50 UT. Emission >100 MeV was only observed during the first orbit. The 50–100 keV GBM time history (also observed by RHESSI) plotted in the inset of the figure shows an abrupt increase at about 07:08 UT followed by a slower decay lasting until about 07:35 UT. The dashed green trace plotted at 3.5-minute resolution follows the 1–4 keV time history observed by the Solar Assembly for X-rays (SAX) instrument on *MESSENGER* (Schlemm et al. 2007) that directly observed the flare site. This emission preceded the occulted soft X-ray emission observed by *GOES* (dashed black trace) by ∼2–3 minutes. The derivative of the SAX 1–4 keV emission (shown by the solid green trace) reflects the hard X-ray time history of the flare and has an onset near 07:00 UT. The sharp rise in hard X-rays observed by GBM at 07:08 UT may be due to the emission region rising above the solar limb. *RHESSI* hard X-ray images up to 50 keV indicate that the source of the emission was above the Sun's limb (Pesce-Rollins et al. 2015a; Ackermann et al. 2017). The background-subtracted hard X-ray spectrum observed by GBM from 38 to 200 keV between 07:09 and 07:12 UT, before the start of the LPGRE , can be fit acceptably (probability 10%) by an electron spectrum with power-law index 5.0 ± 0.1 interacting in a thick-target or by an electron spectrum with index 3.3 ± 0.06 interacting in a thin target. We note that there is an artifact in GBM NaI spectrum that prevents us from fitting <38 keV.

The time profile of the >100 MeV γ-ray flux, plotted at 1-minute resolution, reveals an increase beginning at 07:15 UT that peaks in five minutes and falls back to background by about 07:35 UT. The γ-ray onset occurred about 15 minutes after the inferred onset of hard X-ray emission observed by *MESSENGER* SAX. There is no evidence for this onset in the 100-300 keV rates. This difference in temporal structure suggests that the protons producing the >100 MeV emission were accelerated by a second process. Plotnikov et al. (2017) studied the timing in detail and concluded that the γ-ray onset occurred just after protons accelerated by the CME shock reached magnetic field lines that reached the visible disk of the Sun. The centroid of the >100 MeV emission by LAT is consistent with a

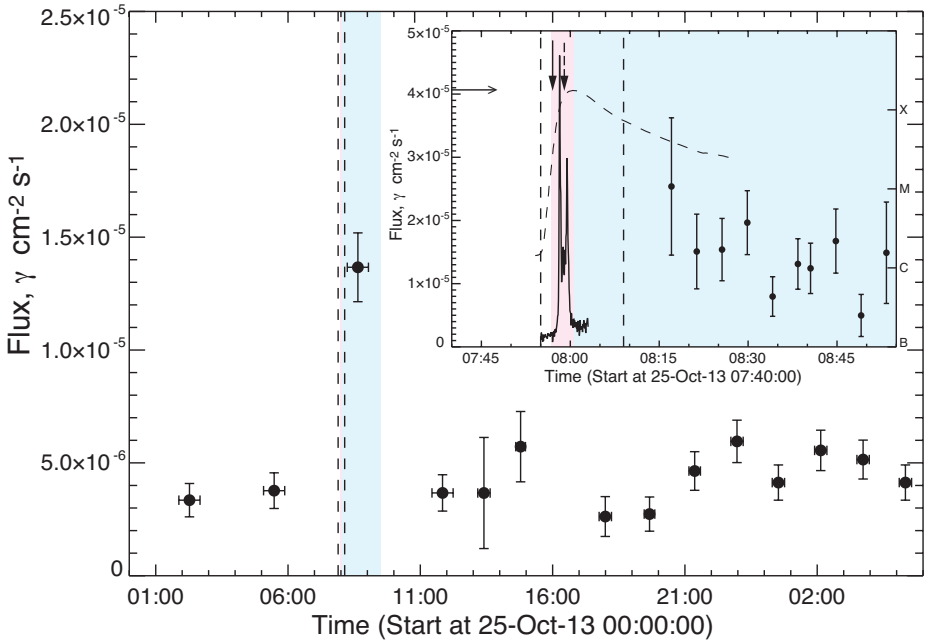

Figure C31. Time profile of the 2013 October 25 LPGRE event observed by LAT. The inset shows *RHESSI* 100-300 keV rates plotted on the same scale as >100 MeV γ-ray fluxes and $\pm 1\sigma$ uncertainties after the flare, derived from Source class data. See caption for Figure C5 for more details.

location near the East limb of the Sun at N03E62 with a 1σ range in longitude from E39 to just above the Eastern limb (Pesce-Rollins et al. 2015a). The background-subtracted γ-ray spectrum from 07:14–07:30 UT can be fit with a pion-decay template for a power-law proton spectrum with an index of ~ 3.8 (Table 3) with no evidence for spectral variation during the rising and falling phases. There is evidence that a better fit would be achieved with a proton spectrum rolling over at energies above 500 MeV. Assuming that the protons impacted at E85, we estimate that the their total number was $\sim 3.5 \times 10^{28}$; because we do not know the true interaction location, this number is probably uncertain by a factor of 5. As the flare site was beyond the limb we have no estimate of the number of protons during the impulsive phase. There is also no evidence for the presence of a solar 2.223 MeV neutron capture line in GBM spectra between 07:15– 07:30 UT. Because the γ rays in this line would be highly attenuated near the solar limb, we could not obtain information on the proton spectrum below 300 MeV.

C.26. *SOL2013-10-25T07:53*

Distinct nature of the LPGRE LAT had good solar exposure beginning about 15 minutes after the impulsive hard X-ray peak and significant >100 MeV emission was detected. There is a suggestion (90% confidence) that the >100 MeV flux, plotted at 4-minute resolution, was decreasing during that time interval, and there is no evidence for emission in the next good exposure three hours later. We are, therefore, not able to determine whether the observed emission comes from the tail of the impulsive phase or from LPGRE beginning after the flare. The 95% confidence limit on the number of impulsive phase protons >500 MeV is comparable to the number protons in the LPGRE. Therefore, there is no significant constraint on whether the impulsive phase was the primary source of the LPGRE.

Details Plotted in Figure C31. X1.7 class flare at E71 lasting ~16 minutes; a relatively slow ~590 km s^{-1} halo CME with onset coincident with the rise in 100–300 keV X-rays; M (metric) and DH (decameter-hectometric) Type II emissions observed with the M onset ~2 minutes after the CME launch; moderate SEP event extending to energies >60 MeV; hard X-ray emission observed up to in excess of 800 keV by *RHESSI* (100–300 keV time history plotted in inset). Good LAT solar exposures every other orbit: 08:14–08.59. 11:26–12:10 UT with a weak <20% exposure 10:00–10:24 UT. Emission >100 MeV was only observed during the first solar exposure, beginning ~15 minutes after the hard X-ray peak; 4-minute accumulations of LAT Source class data suggest (95% confidence) that the >100 MeV emission was decreasing during the 08:14–08.59 UT exposure; therefore, it is not clear whether the emission is just the tail of flare or an associated event beginning after the impulsive hard X-rays. Modulation of the celestial background flux by the solar exposure is not a significant fraction of the observed variation. The spectrum of protons producing the pion-decay γ rays was relatively steep with a power-law index between 4 and 7 (Table 3). We estimate that $\sim 3 \times 10^{27}$ >500 MeV protons were required to produce the LPGRE , assuming that it began just after the impulsive

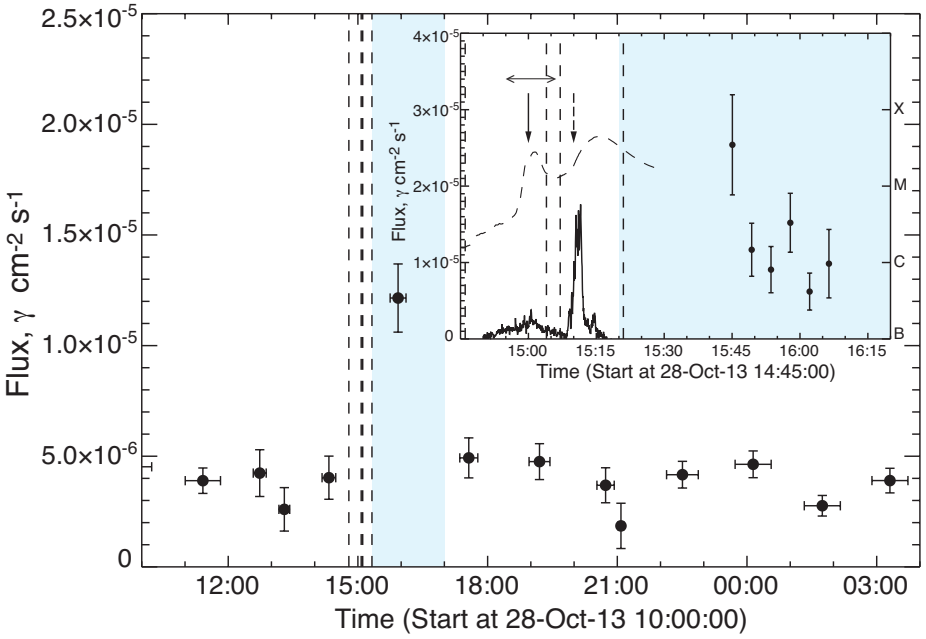

Figure C32. Time profile of the 2013 October 28 LPGRE event observed by LAT. The inset shows *RHESSI* 100-300 keV rates plotted on the same scale as >100 MeV γ-ray fluxes and $\pm 1\sigma$ uncertainties after the flare, derived from Source class data. See caption for Figure C5 for more details.

phase and lasted until 09:30 UT. *RHESSI* front detectors were used to study the impulsive phase (note that due to radiation damage the spectral resolution was ∼20 keV at 511 keV); emission was observed up to about 1500 keV. There is a hint of nuclear-line emission in the spectrum with about 70% confidence and only an upper limit on the neutron-capture line flux. This 95% limit was used to set an upper limit on the number of >500 MeV protons that is comparable to the number observed in the LPGRE.

C.27. *SOL2013-10-28T15:07*

Distinct nature of the LPGRE LAT had good exposure about 30 minutes after the impulsive phase and significant >100 MeV emission was detected. There is a weak suggestion (80% confidence) that the >100 MeV flux, plotted at 4-minute resolution, was decreasing during that time interval, and there is no evidence for emission in the next good exposure 90 minutes later. We are therefore not able to determine whether the observed emission is just the tail of impulsive phase radiation or a distinct late phase component. We have no information on the number of flare-produced protons that could constrain the flare contribution to the LPGRE proton numbers.

Details Plotted in Figure C32. M4.4 class flare at E28 lasting ∼14 minutes preceded by a weaker flare; ∼800 km s^{-1} CME with onset ∼7 minutes before rise of prominent 50-100 keV X-ray peak observed by *RHESSI* and GBM; M (metric) and DH (decameter-hectometric) Type II emissions observed with the M onset ∼10 minutes after the CME launch; weak SEP radiation; hard X-ray emission observed up to just above 100 keV by *RHESSI* (*RHESSI* 50–100 keV time history plotted in inset). *Fermi* was performing a solar ToO but the exposures were shortened by SAA passages; good solar exposures between 15:46 and 16:06 UT and between 17:21 and 17:40 UT. Emission >100 MeV was only observed during the first exposure, beginning ∼35 minutes after the hard X-ray peak associated with the second M-class flare; inset shows 4-minute >100 MeV accumulations with evidence that the flux was falling (80% confidence). Fit to time-integrated γ-ray spectrum indicates that accelerated proton spectrum was hard (Table 3). We estimated the number of >500 MeV protons at the Sun by assuming that the LPGRE flux peaked at the time of the observation and decreased after that time. *RHESSI* hard X-ray spectrum follows a power law up to about 140 keV. The poor quality of the γ-ray spectrum due to radiation damage prevented measurement of the neutron-capture line flux and ability to place a constraint on the number of protons during the impulsive phase. Therefore, we have no information on the number of flare-produced protons that could constrain the flare contribution to the LPGRE proton numbers. We note that there was an impulsive flare on the same day beginning at 01:41 UT with hard X-ray emission extending up to about 1 MeV, but not associated with any LPGRE.

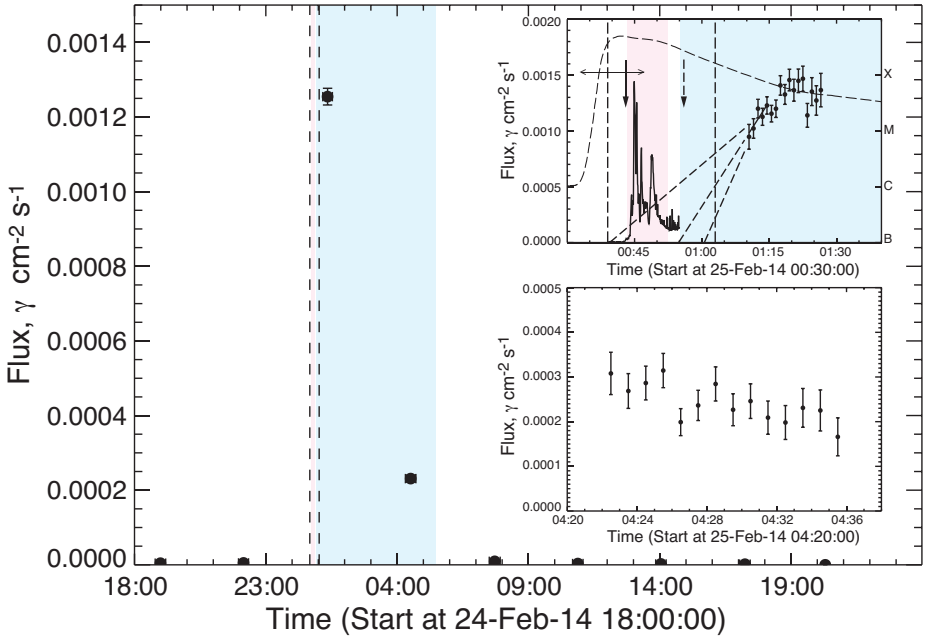

Figure C33. Time profile of the 2014 February 25 LPGRE event observed by LAT. Top inset shows a blowup of the flare region with *RHESSI* 100-300 keV rates plotted on the same scale as >100 MeV γ-ray fluxes derived from Source class data. The best fit to an increasing >100 MeV flux after 01:10 UT is shown by the solid line in the right inset. Extrapolations to determine γ-ray onset and $\pm1\sigma$ deviations are shown by the dashed lines. Bottom inset is a blowup of the 2^{nd} LAT solar exposure showing a falling γ-ray flux. See caption for Figure C5 for more details.

C.28. *SOL2014-02-25T00:39*

Distinct nature of the LPGRE LAT began observing intense >100 MeV solar γ-ray emission ~20 minutes after the impulsive phase. The emission had an onset before 01:00 UT and increased to a maximum near 01:22 UT, after which time it began to fall. The fluxes during the next exposure three hours later continued to decrease. There were 25 time more >500 MeV protons in the LPGRE than in the impulsive phase.

Details Plotted in Figure C33. X4.9 class flare at E78 lasting ~24 minutes; ~2150 km s^{-1} halo CME with onset coincident with the rise of 100-300 keV X-ray emission; M (metric) and DH (decameter-hectometric) Type II emissions observed with the M onset ~13 minutes after the CME launch; strong SEP event extending to energies >700 MeV; hard X-ray/γ-ray line emission observed into the MeV range by both *RHESSI* (100–300 keV time history plotted in inset) and GBM. *Fermi* came into daylight at about 00:39 UT. Both GBM and *RHESSI* observed the entire impulsive phase of the flare. LAT was observing the Galactic Center at the time of the flare but had a good solar exposure from 01:11–01:30 UT. It also had a good exposure three hours later from 04:21–04:40 UT. LAT observed emission >100 MeV during both these exposures, but not three hours later. For both the 01:25 and 04:36 UT observations the exposure rapidly increased as Fermi slewed from the Galactic Center to its normal rocking position, peaked for about two minutes and then decreased over the next 10-15 minutes as the Sun left the FoV. The upper inset shows the 100-300 keV time history observed by *RHESSI* and 1-minute resolution time history observed by LAT. The >100 MeV emission rose to a peak near 01:25 UT. The lower inset shows the falling >100 MeV intensity during the exposure beginning 04:20 UT. In §4.1 we discussed fits to the background-subtracted spectrum >100 MeV at the peak of the LAT exposure from 01:13:30–01:17:30 where instrumental effects are minimum. We showed that the data require a pion-decay spectrum produced by a power-law proton spectrum with a break at about 1.3 GeV. We used this fit and a single power-law fit to data between the peak exposure between 04:24–04:30 UT to estimate the numbers of >500 MeV protons at the Sun (Table 3). The spectrum softened significantly in the three hours between the observations.

GBM observed clear γ-ray lines above 2 MeV, including the neutron capture, carbon, and oxygen lines. The nuclear spectrum dropped precipitously above 7.5 MeV and there was no evidence for any emission above 10 MeV. We fit the background-subtracted GBM spectrum with a power-law and exponentiated power law, along with 2.2 and 0.511 MeV lines, narrow and broad nuclear line and pion-decay templates. It concerns us that the fitted width of the solar 2.2 MeV line is ~85 keV. From the measured 2.2 MeV flux of 0.14 γ cm^{-2} s^{-1} we estimate that there were 3 $\times10^{28}$ protons >500 MeV protons at the Sun during the impulsive phase assuming the proton spectrum followed a power law with index 4.5 above 50 MeV. This value is less than 10% of the number in the LPGRE.

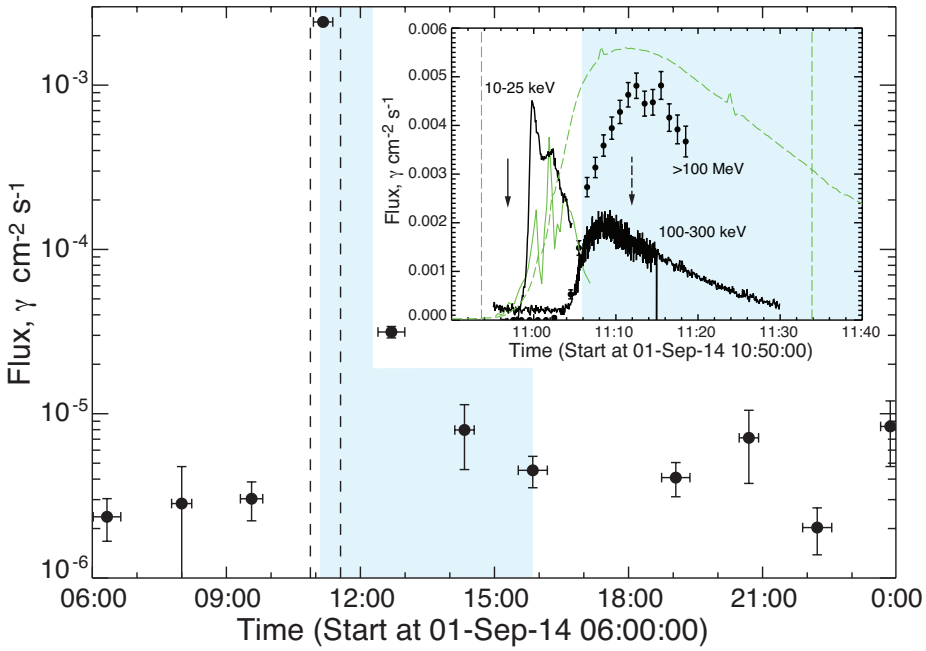

Figure C34. Time profile of the 2014 September 1 LPGRE event observed by LAT. The inset shows GBM 100-300 keV rates plotted on the same scale as >100 MeV γ-ray fluxes derived from Source class data. The dashed green curve shows the soft X-ray rates from the *MESSENGER* SAX instrument that observed the flare region. The dashed green vertical lines are our estimate of the equivalent *GOES* start and stop time of this behind-the-limb flare. The solid green trace is a representation of the flare hard X-ray time history estimated by taking the time derivative of the soft X-ray rates. The GBM observed 10-25 keV emission coincident with the flare hard X-ray emission. See caption for Figure C5 for more details.

C.29. *SOL2014-09-01T10:54*

Distinct nature of the LPGRE >100 MeV emission began about seven minutes after the onset of hard X-rays from the flare located nearly 40° beyond the East Limb of the Sun (Pesce-Rollins et al. 2015b). The emission continued for about six hours.

Details Plotted in Figure C34. Estimated X2.1 *GOES* soft X-ray class flare (Ackermann et al. 2017) at E126 that was observed by the Solar Assembly for X-rays (SAX) instrument on *MESSENGER* (Schlemm et al. 2007) and lasted ∼40 minutes (dashed green curve in inset of figure); ∼1500 km s^{-1} CME with estimated onset time of 10:57 UT, from *SDO* 193Å, 211Å images, just at the rise of the inferred flare hard X-ray emission plotted as the solid green trace in the inset (estimated by taking the derivative of the SAX soft X-ray time history); M (metric) and DH (decameter-hectometric) Type II emissions observed with the late M onset at 11:13 UT likely the time when the shock was first visible from Earth; very intense SEP event with comparable peak fluxes of 0.7–4.0 MeV electrons and >13 MeV protons consistent with what has been observed in other CME/shock gradual SEP events.

LAT had good solar exposures every other orbit on September 1 and had exposures four-times smaller in the intervening orbits. Such a 25% exposure occurred between 11:06 and 11:20 UT during the behind-the-limb flare when the Sun was at a large angle with respect the LAT telescope axis. Source class data could be used to study >100 MeV γ-ray emission because the intense hard X-ray emission from the flare did not reach *Fermi*. At these large solar viewing angles the detector response is small and not as accurately determined. There were also two good exposures between 12:26–12:58 and 15:36–16:08 UT during which LAT had significantly higher sensitivity to search for late high-energy emission. The >100 MeV flux just after the flare was the largest observed by LAT with the exception of the first peak observed on 2012 March 7 just after the X5.6 flare. The hourly fluxes are plotted logarithmically in the figure in order to reveal the large range in intensity of LPGRE that lasted up to six hours, In the inset we plot >100 MeV fluxes at 1-minute resolution along with 100–300 keV rates observed by GBM. Both the γ-ray and 100–300 keV X-ray emissions, as viewed from Earth, appear to rise at ∼11:04 UT, about seven minutes after the onset of the hard X-ray emission observed from the flare as viewed by *MESSENGER*. The hard X-rays observed by GBM peaked by 11:08 UT while the >100 MeV γ-ray flux peaked about five minutes later.

We have fit the background-subtracted >100 MeV γ-ray spectrum with a pion-decay spectrum produced by >300 MeV protons following a differential power-law spectrum and interacting in a thick target. Our fits indicate that the spectrum hardened over the duration of the event with spectral indices of 4.25 ± 0.15, 3.85 ± 0.1, and 3.45 ± 0.35, at

11:06–11:12, 11:12–11:20, 12:26–12:58 UT, respectively.

The NaI detectors on GBM observed an increase in 10-25 keV flux (solid black trace) about two minutes after the hard X-ray onset detected by SAX on *MESSENGER*. This may be due to the appearance of the flare's coronal hard X-ray source 2 $\times 10^5$ km above the solar limb. Higher energy emission observed into the MeV range began as the 10-25 keV X-ray emission from the flare decreased in intensity. Our fit to the GBM NaI detector spectrum with the best view of the Sun between 42 and 900 keV from 11:06 to 11:15 UT was acceptable (27% probability) for thick target bremsstrahlung model from electrons following a power law spectrum with index 3.2 $\pm$ 0.1 and having low-energy cutoff of ∼130 keV. There is no evidence for spectral variability. The spectral index of the electrons interacting in a thin target is 1.90 $\pm$ 0.02, significantly harder than that for a thick target. However, our fit to the spectrum with thin target bremsstrahlung was not acceptable ($< 10^{-6}$ probability) suggesting that the electrons interacted deep in the solar atmosphere. This is confirmed by our fit to GBM BGO data up to 40 MeV which was also consistent with thick target bremsstrahlung from electrons following a power-law with index 3.2 $\pm$ 0.1. Observation of such an energetic population of electrons at the same time as the LPGRE suggests that they were accelerated by the same process responsible for the >300 MeV protons (see §5.5).

There is no evidence for the presence of a 2.23 MeV line in the background-subtracted GBM spectrum from 11:04 to 11:30 UT with a 95% confidence upper limit of 0.016 γ cm^{-2} s^{-1}. Three of the rear *RHESSI* detectors had moderate spectral resolution at that time, due to a recent anneal, allowing us to search for solar nuclear de-excitation and neutron-capture lines. Because of contamination from a preceding SAA passage, we could not perform a sensitive search for the de-excitation lines, but we were able to set a 95% confidence upper limit of 0.028 cm^{-2} s^{-1} from 11:11 to 11:31 UT on the flux in the neutron-capture line, consistent with the GBM result. Comparing the >100 MeV γ-ray fluence with the upper limit on the 2.223 MeV line fluence we estimate with 95% confidence that the proton power-law spectral index between 40 and 300 MeV was harder than 3.4, assuming that the protons interacted at a heliocentric angle of 85°. For smaller heliocentric angles the index would be even harder. Because the spectral index for protons >300 MeV was ∼4 at the same time interval we conclude that the LPGRE proton spectrum steepened above a few hundred MeV. Our estimate of the number of >500 MeV protons was also made assuming that the interactions occurred at 85°. As there are no measurements of γ-rays during the flare, we cannot compare this number with number of protons at the flare site.

C.30. *SOL2015-06-21T02:03*

Distinct nature of the LPGRE LPGRE began after the most intense portion of the impulsive phase and lasted 10 hours. There were at least five time more >500 MeV protons in the LPGRE than in the impulsive phase.

Details Plotted in Figure C35. M2.6 class flare at E16 lasting ∼72 minutes; ∼1500 km s^{-1} halo CME with estimated onset time 02:10 UT based on SDO 211Å images coincident with the peak in 100-300 keV X-rays; M (metric) Type II emission observed with onset ∼14 minutes after the CME launch but no data on DH (decameter-hectometric) emission; slowly rising SEP event not observable above 50 MeV by *GOES*. LAT had a good exposure to the Sun between 02:11–02:41 UT, overlapping much of the impulsive phase. The main plot shows Pass 8 Source class data. As the Sun was near the Crab Nebula in mid-June the celestial background is high. LPGRE was detected during the next good LAT solar exposures between 05:22–05:52, 08:32–09:03, and 11:42–12:14 UT. LAT Source class data during the impulsive phase were compromised by the hard X-ray flux in the ACD at that time. We have fit the Solar Flare Transient class spectra accumulated in 3-minute intervals to obtain the time history of the >100 MeV emission during the flare. This is shown in the inset of the figure and reveals an increase near the end of the impulsive HXR peaks in the 50-100 keV time history from GBM (solid trace). The >100 MeV spectral data between 02:20 and 02:41 UT were not sufficient to determine a proton power-law index. We estimated the number of >500 MeV protons at the Sun in the LPGRE using the four exposures. We also obtained upper limits on the number of >500 MeV protons in the impulsive phase using two different methods. We first obtained an upper limit on the neutron-capture line flux in the *RHESSI* front detectors (15 keV FWHM resolution at 1275 keV at that time in the Mission) after 02:08 UT. From this limit we estimated that there were no more than half the number of protons founds in the LPGRE. Integrating the LAT flux observed in the Solar Flare Transient class data after 02:11 UT, including what appears to be LPGRE , we obtained a more constraining upper limit 20% of the number in the LPGRE.

D. ESTIMATE OF NUMBER OF SEP PROTONS

For comparison with the number of protons interacting in the solar atmosphere in LPGRE events, we made an estimate of the number of >500 MeV SEP protons emitted from the vicinity of the Sun and escaping to at least 1 AU using fluences from the High-Energy Proton and Alpha Detectors (HEPAD) (Sauer 1993) on GOES-13 and GOES-

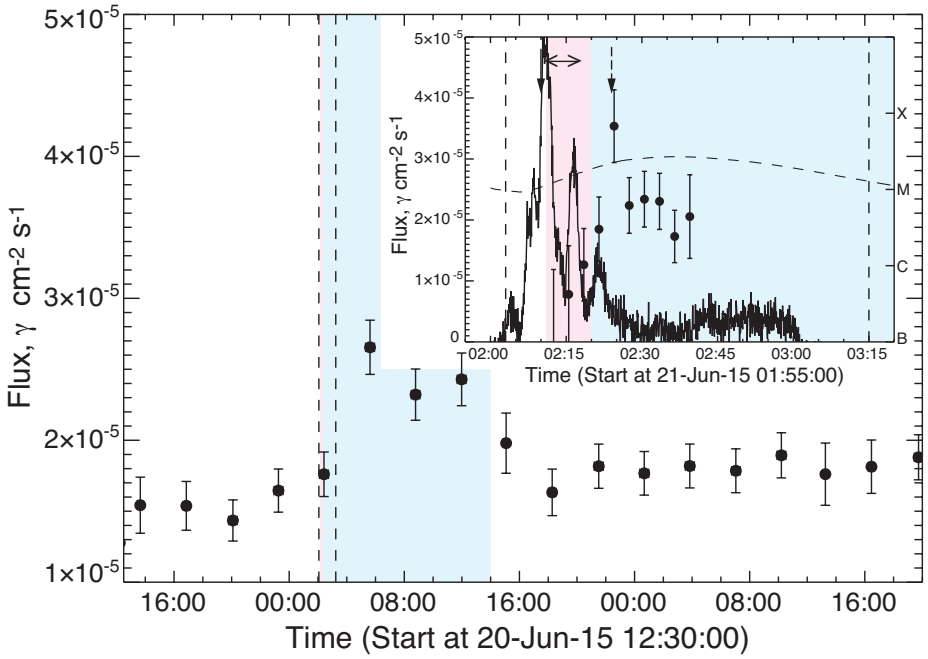

Figure C35. Time profile of the 2015 June 21 LPGRE event observed by LAT. The inset shows GBM 50–100 keV rates plotted on the same scale as >100 MeV fluxes and $\pm 1\sigma$ uncertainties derived from fits to Solar Flare Transient class data. These impulsive-class fluxes are not affected by ACD rates that affect the Source class flux plotted in the main figure. See caption for Figure C5 for more details.

15[21]. HEPAD records the proton flux in three differential energy bins covering the range from ∼330–700 MeV and one integral bin above about 700 MeV in a 34° conical field of view radially away from Earth. Tylka et al. (2014)[22] corrected the observed fluxes in each channel for both background and geometry factors in seven events based on the work of H. Sauer (private communication, 2007). Because the fluxes in the study were integrated over the ∼1–2-day duration of the particle event, they treated the derived fluences, J_{Earth}, as omnidirectional. Tylka & Dietrich (2009) validated this technique by comparing 400–700 MeV HEPAD proton fluences with those measured in 25 Ground Level Enhancements (GLEs) from 1989–2006. Tylka et al. (2014) estimated the >500 MeV HEPAD proton fluences by fitting the time integrated spectra above 300 MeV. Recently, Bruno (2017) used PAMELA data to calibrate the HEPAD sensors and provided fluence spectra for three SEP events studied by Tylka et al. (2014). Using the Bruno (2017) spectra we estimate that the >500 MeV fluences were about 2700, 4300, 1700 p cm^{-2} sr^{-1} for the 2012 January 27, 2012 May 17, and 2014 February 25 events, respectively. Tylka et al. (2014) estimated fluences of 3400, 5400, and 1200 p cm^{-2} sr^{-1} for these three events, respectively. The estimated fluences agree to within 50%. In our ensuing discussion, we will use the fluences derived by Tylka et al. (2014) and assume that they are accurate to ±50%. The resulting >500 MeV SEP proton fluences for seven LPGRE events are listed in column (3) of Table D3.

To estimate the number of >500 MeV protons, N_{IP}, in interplanetary space from the HEPAD fluence, J_{Earth}, we used the heuristic method outlined by Mewaldt et al. (2005) in an analogous study at lower energies. This method requires the estimation of two correction factors, one related to interplanetary transport, $C_{transport}$, and a second related to the large scale distribution of the protons in interplanetary space, $C_{spatial}$. The total number of SEP protons in interplanetary space is then given by

$$N_{IP} = 2\pi R_0^2 J_{Earth} C_{spatial} C_{transport}^{-1} \quad \text{(D1)}$$

where R_0 is 1 AU and we assume that the protons are emitted from a point source near the Sun.

The transport factor is also called the crossing-correction factor because it takes into account the fact that some protons may cross back and forth across the 1-AU boundary multiple times during the event. We estimated the crossing factor for these >500 MeV protons by using the time-dependent front-back asymmetries observed by the world-wide neutron monitor network in the GLE of 2012 May 17 and in the particularly well-observed and modeled GLE of 2001

[21] https://ngdc.noaa.gov/stp/satellite/goes/datanotes.html

[22] https://hesperia.gsfc.nasa.gov/fermi_solar/EGU_Spring_2014_16847_Tylka_Thursday_1330.pdf

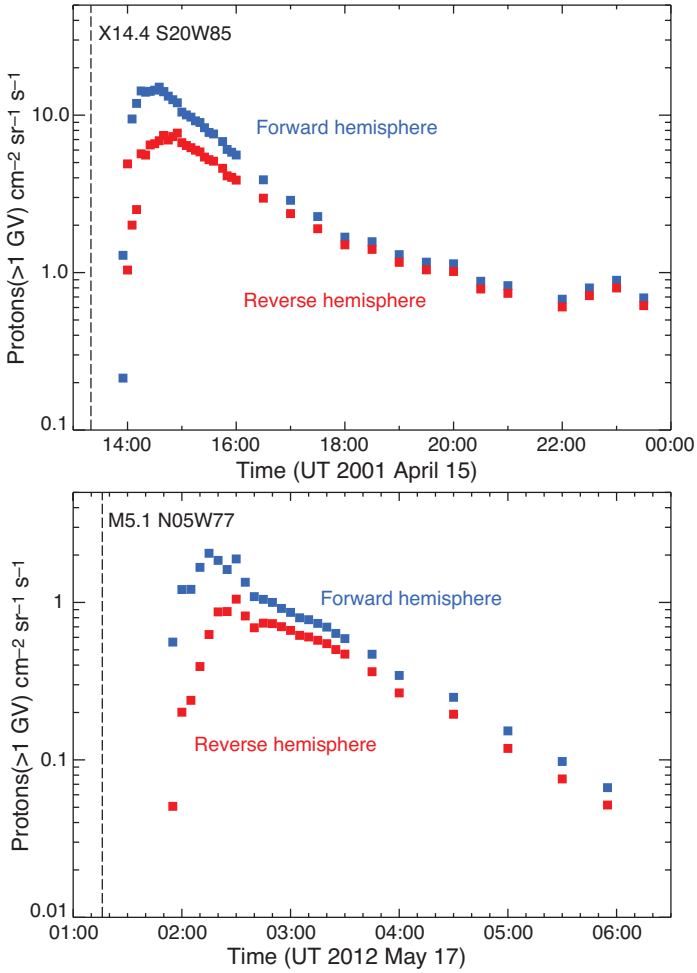

Figure D36. >1 GV fluxes in the sunward and anti-sunward directions observed by neutron monitors for the 2001 April 15 and 2012 May 17 GLEs as a function of time. The *GOES* class and heliographic coordinates of the associated flare are given.

April 15. We plot the forward and reverse fluxes for the two events in Figure D36. The crossing factor for the events is $C_{transport} = J_{Earth}/(J_{forward} - J_{reverse})$, where $J_{forward}$ and $J_{reverse}$ are the forward and reverse fluences and where the omnidirectional fluence at Earth is $J_{Earth} = 0.5(J_{forward} + J_{reverse})$. We obtained $C_{transport}$ values of 2.3 ± 0.1 and 1.9 ± 0.3 for the 2001 April and 2012 May events, respectively. These values may be considered upper limits on the crossing factor because we have assumed that none of the protons are lost back at the Sun and therefore $J_{forward} - J_{reverse}$ is a lower limit. Chollet et al. (2010) describe a Monte Carlo method for determining the crossing factor at energies below 100 MeV using a non-relativistic calculation. They obtain values for $C_{transport}$ that range from about two to eight at 100 MeV, for plausible interplanetary scattering lengths. Based on the more definitive empirical GLE analysis, we use a crossing-factor of two, with an uncertainly of ±30%, for >500 MeV protons observed over about a one-day period.

There are three factors that contribute to the spatial correction factor, $C_{spatial}$ used to determine the number of >500 MeV SEP protons in equation (D1): 1) a factor that corrects for the HEPAD fluence measurement on an interplanetary magnetic field line that is not optimally connected to the active region on the Sun; 2) a factor that corrects for the spatial distribution of SEP protons since these protons do not uniformly fill the hemisphere around the radial vector at the active region; and 3) a factor that corrects for the assumed r^{-2} radial dependence implicit in equation (1). In this discussion we assume that the correction factor for the radial dependence is unity. In order to estimate the first two factors, we need to estimate the large-scale spatial distribution of the particles as a function of longitude. Lario et al. (2013) studied the longitude distribution of 25–53 MeV protons by comparing *GOES*, *STEREO A*, and *STEREO B* measurements. They found that the distribution can be fit by a Gaussian with a 1σ value of about 45°. We would expect the distribution to be narrower at higher energies. Tylka et al. (2014) studied the longitude distribution of SEP protons for the 2012 May 17 event recorded by both *STEREO* spacecraft and *GOES*. Because

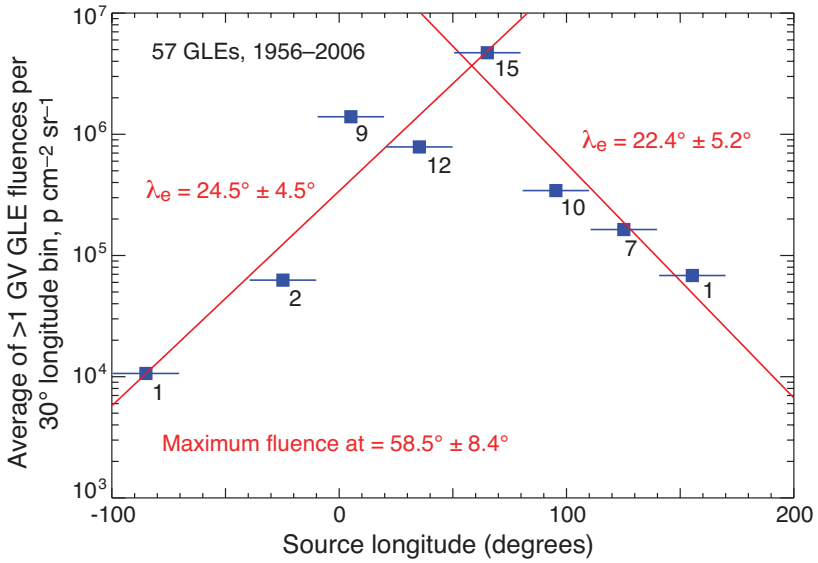

Figure D37. Mean fluences of 57 GLE events observed in eight 30° wide bins of longitude. The number of events in each bin is shown below the data point. The distribution on either side of the maximum was fit by an exponential distribution, $exp^{-|longitude-58|/23}$.

the *STEREO* HED instrument records protons only up to 100 MeV, Tylka et al. (2014) used a power-law fit to the measurements in the two highest-energy bins (30–60 and 60–100 MeV) to estimate the event-integrated fluence at >100 MeV. Given these two measurements and that of *GOES*, they fit the longitude distribution with a Gaussian that peaked at 82° and had a width (1σ) value of about 36°. The only available data above 100 MeV come from neutron monitor observations of GLEs. Tylka et al. (2014) also studied neutron monitor fluences and their associated source-region solar longitudes for 57 GLEs between 1956 and 2006. They summed up fluences in 30°-wide bins of longitude to produce the average fluence distribution versus longitude that we plot in Figure D37. In principle this method is only valid for large numbers of events, but it is the best that can be done. The distribution peaks at the nominal best-connected longitude of 58° and falls off exponentially in both directions with an e-folding width of ∼ 23°. We used both this exponential distribution and a Gaussian distribution peaked at 58° with a width of 40° to determine a range in values for factors 1) and 2). For factor 1), we corrected the observed fluence for offset of the emission site from the optimum 58° longitude for an observer at Earth. For factor 2), we integrated the numbers of protons in spherical rings around the radial vector in the ecliptic projecting away from the emission site, using the two longitude distributions to approximate the zenith angle distribution of the protons.

We summarize the results of this study in Table D3 for eight SEP events, with proton emission that can be studied above 100 MeV, that are associated with LPGRE events. For each event we list the date, heliographic longitude of the solar active region, estimated >500 MeV HEPAD proton fluence and uncertainty at Earth, the transport correction $C_{transport}$ and uncertainty, the spatial correction $C_{spatial}$ and uncertainty, and our estimate of the number of SEP protons in interplanetary space and uncertainty. The spatial correction is the mean of the corrections determined using the two spatial distributions discussed above; its uncertainty is just the difference between the two spatial corrections divided by two. The total number of SEP protons is derived from equation (1); its uncertainty is determined by multiplying the number of protons by the root mean square of the percentage uncertainties in the fluence, transport correction, and spatial correction. Due to an error in their spatial corrections, Tylka et al. (2014) reported >500 MeV proton numbers from three to sixteen times higher than those listed in Table D3.

Table D3. Number of >500 MeV SEP Protons

Date	Longitude	HEPAD >500 MeV Fluence	Transport Correction	Spatial Correction	Number of Protons
yyyy/mm/dd	degrees	J_{Earth}, p cm^{-2} sr^{-1}	$C_{transport}$	$C_{spatial}$	10^{28}
(1)	(2)	(3)	(4)	(5)	(6)
2011/06/07	54	240 ± 120	2.0 ± 0.7	0.28 ± 0.12	4.3 ± 3.2

Table D3 continued on next page

Table D3 *(continued)*

Date yyyy/mm/dd (1)	Longitude degrees (2)	HEPAD >500 MeV Fluence J_{Earth}, p cm^{-2} sr^{-1} (3)	Transport Correction $C_{transport}$ (4)	Spatial Correction $C_{spatial}$ (5)	Number of Protons 10^{28} (6)
2011/08/04	46	320 ± 160	2.0 ± 0.7	0.32 ± 0.10	7.3 ± 5.0
2012/01/23	21	830 ± 415	2.0 ± 0.7	0.64 ± 0.03	37 ± 23
2012/01/27	81	3400 ± 1700	2.0 ± 0.7	0.42 ± 0.04	100 ±62
2012/03/07	-27	12900 ± 6450	2.0 ± 0.7	4.5 ± 0.8	4075 ± 2590
2012/05/17	77	5430 ± 2715	2.0 ± 0.7	0.38 ± 0.08	143 ± 92
2013/04/11	13	680 ± 340	2.0 ± 0.7	0.84 ± 0.09	41 ± 25
2014/02/25	-78	5250 ± 2625	2.0 ± 0.7	83 ± 35	30600 ± 22700

E. SOLAR RADIO BURSTS

Solar radio bursts provide valuable diagnostics of flare and eruptive phenomena in the solar corona. We focus on two particular types of radio burst commonly seen at metric and longer wavelengths (e.g. Wild et al. (1963); McLean & Labrum (1985)):

- Type III bursts, which are attributed to beams of energetic electrons propagating on field lines that extend into the outer corona. The durations of individual beams are short, of order seconds or less, although the waves they generate can last longer, and on a frequency-time plot they are seen to drift very rapidly from high to low frequency. They have to drift over a significant frequency range in order to be identified as Type IIIs. In most cases, the electrons in the beams are thought to have typical energies of order 10 keV (e.g. Lin (1985)).
- Type II bursts have slower frequency-time drift rates (also from high to low frequency), with instantaneously narrow bandwidth and usually striking fundamental-harmonic structure (at least at higher frequencies). They are attributed to electrons accelerated at a shock and radiating in its vicinity as it moves through the corona: the speed of a coronal shock is of order of (but larger than) the Alfvén speed, v_A (typically 500 km s^{-1}), which is much slower than the velocity of an electron in a Type III-producing beam.

Both burst types are believed to radiate at the local plasma frequency, $f_p = 9000\sqrt{n_e}$ Hz, where n_e is the ambient electron density (cm^{-3}). The high-to-low frequency drift corresponds to the motion of the radiating source outwards through a decreasing density gradient. There is therefore a mapping between the frequency of emission and height in the solar atmosphere: thus, emission at 100 MHz (metric wavelengths) occurs around 0.5 $R_\odot$ above the photosphere, 10 MHz (decametric wavelengths) is several $R_\odot$ above the photosphere, and 1 MHz (hectometric wavelengths) is 10-20 $R_\odot$ out (these heights are crude estimates, varying greatly from one atmospheric density model to another).

The diagnostic value of Type III bursts is that they indicate that electrons accelerated low in the corona have access to magnetic field lines that carry them far out into the solar wind, if they are seen to emit down to low frequency ($\sim$1 MHz). Type III bursts often occur early in the impulsive phase of solar flares, but they can also occur for extended periods at low frequencies later in an event (e.g. Cane et al. (2002)).

Type II bursts require the presence of a shock that can accelerate electrons, and CMEs provide a natural driver for this process. Shock formation in a magnetized plasma such as the solar corona requires that the driver exceed the local MHD fast-mode speed, which is close to the Alfvén speed, v_A. v_A varies with density and magnetic field strength in the solar corona. High values of the Alfvén speed occur in strong magnetic-field regions low in the atmosphere, generally decreasing initially outwards with height, with values of order 100-200 km s^{-1}, before increasing again to a local peak in the Alfvén speed at a height of order several $R_\odot$, with a value of order 500 km s^{-1}. Gopalswamy et al. (2001) suggest that metric Type II bursts form at heights below the local peak in v_A, while Type II bursts observed below 10 MHz may form at heights above the local peak in v_A. This picture is consistent with the finding of Cane & Erickson (2005) that there are in fact two classes of Type II burst: the coronal Type II bursts, typically observed at metric wavelengths below the height of the local peak in v_A and never observed to propagate to low frequencies characteristic of the interplanetary (IP) medium; and IP Type II bursts, which can occur at low frequencies at the same time as coronal Type IIs at higher frequencies, and are capable of drifting well out into the solar wind to frequencies below 1 MHz.

The significance of Type II bursts is that, if they are indeed a reliable indicator of shock formation, then no shock acceleration of protons or electrons can take place before the onset of Type II radio emission. Type II bursts occur in conjunction with an accompanying flare, and the emission can start at any time after the onset of the flare's impulsive phase. Mäkelä et al. (2015) find that at the onset of metric Type II burst radio emission, the average radial height of an associated CME is of order 1.7 $R_\odot$. The implicit assumption in this analysis is that the Type II burst occurs at the nose of the CME, i.e., the location on the CME with the greatest height above the solar surface. The complication in this scenario is that Type II radio emission might not occur at this location. The sources of Type II radio emission must be spatially localized, since a very large source would necessarily extend over a large range of electron densities and therefore have a large instantaneous frequency bandwidth, which, by definition, is not observed (i.e., such broadband emission would not have the usual characteristics of Type II bursts in dynamic spectra). When radio imaging observations of Type II bursts have been able to identify the location of Type II emission relative to a CME, they generally do not show that the Type II emission occurs at the nose of the CME, but rather is often located on the flanks of the CME (Chen et al. 2014; Feng et al. 2015) or is associated with some feature distinct from the CME (e.g. Gary et al. (1984); Magdalenić et al. (2012); Bain et al. (2012); Zimovets et al. (2012). This complication implies that conditions other than simple shock formation might be required in order to see Type II radio emission, and therefore the presence of a Type II may be *sufficient* but not *necessary* evidence for the presence of a shock. If this is the case, the onset time of Type II emission does not constrain the start of shock acceleration.

In addition, the possible distinction between coronal Type II bursts, occurring while CMEs are still below a radius of order 2 $R_\odot$, and IP Type IIs is a further complication, since acceleration of energetic particles can in principle occur at either shock. The onset time of an IP Type II can be difficult to determine from low-frequency radio spectra because of the presence of bright Type III emission in the same frequency and time range.

The following table indicates the presence or absence of Type II and Type III radio emission for each of the flares associated with the 30 LPGRE events. Radio dynamic spectra were available for all 30 events, both from ground-based observations of metric frequencies (25-180 MHz from the four stations of the US Air Force Radio Solar Telescope Network, as well as the radio spectrograph at Culgoora operated by the Australian Space Weather Services section), and from space-based observations of decametric-hectometric frequencies (DH, 1-10 MHz) provided by the WAVES receivers on the WIND and STEREO spacecraft. Identification of Type II bursts relied on the NOAA event reports provided by RSTN for the metric data and the WIND/WAVES burst list for the DH data. In cases where the authors are not entirely convinced that a Type II is present in the dynamic spectra, question-marks qualify the report.

For the Type III emission, we attempt to determine whether it is present in the impulsive phase (identified as the initial rise in soft X-rays) as well as in the later phase, at least several minutes later (see discussion in Duffin et al. 2015). These two phases generally have different interpretations: acceleration of electrons to high energies with resulting hard X-ray production is generally most prolific in the impulsive phase, while there may also be late-phase energy release which is typically more evident in heating and soft X-rays. In either case, the presence of Type III emission out to low frequencies implies that accelerated electrons have ready access to open field lines in the acceleration region.

Table E4. Radio Bursts from LPGRE Events

Number	Date, *GOES* class	Type II	Type III metric	Type III DH[a]
		Metric[b] — DH[a]	Impulsive — Late	Impulsive — Late
(1)	(2)	(3)	(4)	(5)
1	2011/03/07, M3.7	Y? — Y	N — Y	N — Y
2	2011/06/02, C3.7	N — Y	Y — N	Y — N
3	2011/06/07, M2.5	Y? — Y	Y — Y	Y — Y
4	2011/08/04, M9.3	Y — Y	Y — Y	Y — Y
5	2011/08/09, X6.9	Y? — Y	Y — Y	Y — Y
6	2011/09/06, X2.1	Y — Y	N — Y	N — Y
7	2011/09/07, X1.8	Y — N	Y — Y	Y? — Y
8	2011/09/24, X1.9	Y? — N	Y — Y	Y — Y
9	2012/01/23, M8.7	N — Y	Y — Y	Y — Y
10	2012/01/27, X1.7	Y — Y	N — N	Y — Y
11	2012/03/05, X1.1	N — Y	Y — Y	Y — Y

Table E4 continued on next page

Table E4 *(continued)*

Number	Date, *GOES* class	Type II Metric[b] — DH[a]	Type III metric Impulsive — Late	Type III DH[a] Impulsive — Late
(1)	(2)	(3)	(4)	(5)
12	2012/03/07, X5.4	Y? — Y	Y — Y	Y — Y
	2012/03/07, M3	Y? — Y	Y	Y
13	2012/03/09, M6.3	Y — Y	N — Y	N — Y
14	2012/03/10, M8.4	N — Y	N — Y	N — Y
15	2012/05/17, M5.1	Y — Y	Y — Y	Y — Y
16	2012/06/03, M3.3	Y — N	Y — N	Y — Y
17	2012/07/06, X1.1	Y — Y	Y — N	Y — N
18	2012/10/23, X1.8	Y — N	N — N	N — N
19	2012/11/27, M1.6	N — N	N — N	N — N
20	2013/04/11, M6.5	Y — Y	Y — Y	Y — Y
21	2013/05/13, X1.7	Y — Y	Y — Y	Y — Y
22	2013/05/13, X2.8	Y — Y	N — Y	Y — Y
23	2013/05/14, X3.2	Y — Y	N — Y	Y — Y
24	2013/05/15, X1.2	Y — Y	N — N	N — Y
25	2013/10/11, M4.9	Y — Y	N — Y	Y — Y
26	2013/10/25, X1.7	Y — Y	N — Y	N — Y
27	2013/10/28, M4.4	Y — Y	Y — Y	Y — Y
28	2014/02/25, X4.9	Y — Y	Y — Y	Y — Y
29	2014/09/01, X2.1	Y? — Y	Y — Y	Y — Y
30	2015/06/21, M2.6	Y — Y	N — N	Y — Y

[a] DH = decametric/hectometric: this refers to observations at frequencies below 10 MHz that can only be carried out from space due to the ionospheric cutoff. The WIND and both STEREO spacecraft carry WAVES receivers operating in this frequency range, and observations in the 1-10 MHz range were used for the identifications indicated here.

[b] Metric dynamic-spectra radio observations are obtained in the frequency range 25-180 MHz by the four stations of the US Air Force Radio Solar Telescope Network (RSTN), and by the radio spectrograph at Culgoora operated by Australia's Space Weather Services section.

In all 30 events except one, there is evidence for the presence of Type II emission at metric or DH wavelengths, or both. In all except two events, there is evidence for Type III emission at metric or DH wavelengths, and those are the two events (2012-10-23, 2012-11-27) without reported CMEs.

REFERENCES

Abdo, A. A., Ackermann, M., Ajello, M., Baldini, L., Ballet, J., Barbiellini, G., Bastieri, D., & et al. 2011, ApJ, 734, 116

Abdo, A. A. & et al. 2010, Physical Review Letters, 104, 101101

Ackermann, M., Ajello, M., Albert, A., Allafort, A., Baldini, L., Barbiellini, G., Bastieri, D., & et al. 2014, ApJ, 787, 15

Ackermann, M., Ajello, M., Allafort, A., Atwood, W. B., Baldini, L., Barbiellini, G., Bastieri, D., Bechtol, K., Bellazzini, R., Bhat, P. N., Blandford, R. D., Bonamente, E., Borgland, A. W., Bregeon, J., Briggs, M. S., Brigida, M., Bruel, P., Buehler, R., Burgess, J. M., Buson, S., Caliandro, G. A., Cameron, R. A., Casandjian, J. M., Cecchi, C., Charles, E., Chekhtman, A., Chiang, J., Ciprini, S., Claus, R., Cohen-Tanugi, J., Connaughton, V., Conrad, J., Cutini, S., Dennis, B. R., de Palma, F., Dermer, C. D., Digel, S. W., Silva, E. d. C. e., Drell, P. S., Drlica-Wagner, A., Dubois, R., Favuzzi, C., Fegan, S. J., Ferrara, E. C., Fortin, P., Fukazawa, Y., Fusco, P., Gargano, F., Germani, S., Giglietto, N., Giordano, F., Giroletti, M., Glanzman, T., Godfrey, G., Grillo, L., Grove, J. E., Gruber, D., Guiriec, S., Hadasch, D., Hayashida, M., Hays, E., Horan, D., Iafrate, G., Jóhannesson, G., Johnson, A. S., Johnson, W. N., Kamae, T., Kippen, R. M., Knödlseder, J., Kuss, M., Lande, J., Latronico, L., Longo, F., Loparco, F., Lott, B., Lovellette, M. N., Lubrano, P., Mazziotta, M. N., McEnery, J. E., Meegan, C., Mehault, J., Michelson, P. F., Mitthumsiri, W., Monte, C., Monzani, M. E., Morselli, A., Moskalenko, I. V., Murgia, S., Murphy, R., Naumann-Godo, M., Nuss, E., Nymark, T., Ohno, M., Ohsugi, T., Okumura, A., Omodei, N., Orlando, E., Paciesas, W. S., Panetta, J. H., Parent, D., Pesce-Rollins, M., Petrosian, V.,

Ackermann, M., Ajello, M., Allafort, A., Atwood, W. B., Baldini, L., Barbiellini, G., Bastieri, D., & et al. 2012b, ApJ, 748, 151
—. 2012c, ApJ, 745, 144
Ackermann, M., Allafort, A., Baldini, L., Barbiellini, G., Bastieri, D., Bellazzini, R., Bissaldi, E., & et al. 2017, ApJ, 835, 219
Adriani, O., Barbarino, G. C., Bazilevskaya, G. A., Bellotti, R., Boezio, M., Bogomolov, E. A., Bongi, M., & et al. 2015, ApJL, 801, L3
Aguilar, M., Alberti, G., Alpat, B., Alvino, A., Ambrosi, G., Andeen, K., Anderhub, H., & et al. 2013, Physical Review Letters, 110, 141102
Ajello, M., Albert, A., Allafort, A., Baldini, L., Barbiellini, G., Bastieri, D., Bellazzini, R., & et al. 2014, ApJ, 789, 20
Akimov, V. V., Ambrož, P., Belov, A. V., Berlicki, A., Chertok, I. M., Karlický, M., Kurt, V. G., Leikov, N. G., Litvinenko, Y. E., Magun, A., Minko-Wasiluk, A., Rompolt, B., & Somov, B. V. 1996, SoPh, 166, 107
Akimov, V. V., Leikov, N. G., Kurt, V. G., & Chertok, I. M. 1994, in American Institute of Physics Conference Series, Vol. 294, High-Energy Solar Phenomena - a New Era of Spacecraft Measurements, ed. J. Ryan & W. T. Vestrand, 130–133
Allafort, A., Giglietto, N., Omodei, N., & et al. 2011a, in International Cosmic Ray Conference, Vol. 10, International Cosmic Ray Conference, 113
Allafort, A., Tanaka, Y. T., Omodei, N., & et al. 2011b, The Astronomer's Telegram, 3214, 1
Aptekar, R. L., Frederiks, D. D., Golenetskii, S. V., Ilynskii, V. N., Mazets, E. P., Panov, V. N., Sokolova, Z. J., Terekhov, M. M., Sheshin, L. O., Cline, T. L., & Stilwell, D. E. 1995, SSRv, 71, 265
Aschwanden, M. J., Wülser, J.-P., Nitta, N. V., Lemen, J. R., Freeland, S., & Thompson, W. T. 2014, SoPh, 289, 919
Atwood, W. B., Abdo, A. A., Ackermann, M., Althouse, W., Anderson, B., Axelsson, M., Baldini, L., Ballet, J., Band, D. L., Barbiellini, G., & et al. 2009, ApJ, 697, 1071
Bain, H. M., Krucker, S., Glesener, L., & Lin, R. P. 2012, ApJ, 750, 44
Bruno, A. 2017, Space Weather, 15, 1191
Cane, H. V. & Erickson, W. C. 2005, ApJ, 623, 1180
Cane, H. V., Erickson, W. C., & Prestage, N. P. 2002, Journal of Geophysical Research (Space Physics), 107, 1315
Chen, Y., Du, G., Feng, L., Feng, S., Kong, X., Guo, F., Wang, B., & Li, G. 2014, ApJ, 787, 59
Chollet, E. E., Giacalone, J., & Mewaldt, R. A. 2010, Journal of Geophysical Research (Space Physics), 115, A06101
Chupp, E. L., Debrunner, H., Flueckiger, E., Forrest, D. J., Golliez, F., Kanbach, G., Vestrand, W. T., Cooper, J., & Share, G. 1987, ApJ, 318, 913
Chupp, E. L. & Ryan, J. M. 2009, Research in Astronomy and Astrophysics, 9, 11
Colaninno, R. C. & Vourlidas, A. 2015, ApJ, 815, 70
de Jager, C. 1969, in Solar Flares and Space Research, ed. C. de Jager & Z. Svestka, 1
DelSignore, K. W. 1995, PhD thesis, , Case Western Reserve Univ., (1995)
Dolan, J. F. & Fazio, G. G. 1965, Reviews of Geophysics and Space Physics, 3, 319
Duffin, R. T., White, S. M., Ray, P. S., & Kaiser, M. L. 2015, Journal of Physics Conference Series, 642, 012006
Dunphy, P. P. & Chupp, E. L. 1994, in American Institute of Physics Conference Series, Vol. 294, High-Energy Solar Phenomena - a New Era of Spacecraft Measurements, ed. J. Ryan & W. T. Vestrand, 112–117
Ellison, D. C. & Ramaty, R. 1985, ApJ, 298, 400
Emslie, A. G., Dennis, B. R., Shih, A. Y., Chamberlin, P. C., Mewaldt, R. A., Moore, C. S., Share, G. H., Vourlidas, A., & Welsch, B. T. 2012, ApJ, 759, 71
Feng, S. W., Du, G. H., Chen, Y., Kong, X. L., Li, G., & Guo, F. 2015, SoPh, 290, 1195
Fleishman, G. D., Nita, G. M., & Gary, D. E. 2017, ApJ, 845, 135
Forrest, D. J., Vestrand, W. T., Chupp, E. L., Rieger, E., & Cooper, J. 1986, Advances in Space Research, 6, 115
Forrest, D. J., Vestrand, W. T., Chupp, E. L., Rieger, E., Cooper, J. F., & Share, G. H. 1985, in International Cosmic Ray Conference, Vol. 4, International Cosmic Ray Conference, ed. M. Garcia-Munoz, K. R. Pyle, & J. A. Simpson, 146–149
Frost, K. J. & Dennis, B. R. 1971, ApJ, 165, 655
Gary, D. E., Chen, B., Dennis, B. R., Fleishman, G. D., Hurford, G. J., Krucker, S., McTiernan, J. M., Nita, G. M., Shih, A. Y., White, S. M., & Yu, S. 2018, ApJ, 863, 83
Gary, D. E., Dulk, G. A., House, L., Illing, R., Sawyer, C., Wagner, W. J., McLean, D. J., & Hildner, E. 1984, A&A, 134, 222
Glesener, L., Krucker, S., Bain, H. M., & Lin, R. P. 2013, ApJL, 779, L29
Gopalswamy, N., Lara, A., Kaiser, M. L., & Bougeret, J.-L. 2001, J. Geophys. Res., 106, 25261
Gopalswamy, N., Xie, H., Mäkelä, P., Yashiro, S., Akiyama, S., Uddin, W., Srivastava, A. K., Joshi, N. C., Chandra, R., Manoharan, P. K., Mahalakshmi, K., Dwivedi, V. C., Jain, R., Awasthi, A. K., Nitta, N. V., Aschwanden, M. J., & Choudhary, D. P. 2013, Advances in Space Research, 51, 1981
Gopalswamy, N., Yashiro, S., Krucker, S., Stenborg, G., & Howard, R. A. 2004, Journal of Geophysical Research (Space Physics), 109, 12105
Hartman, R. C., Bertsch, D. L., Fichtel, C. E., Hunter, S. D., Kanbach, G., Kniffen, D. A., Kwok, P. W., Lin, Y. C., Mattox, J. R., Mayer-Hasselwander, H. A., Michelson, P. F., von Montigny, C., Nolan, P. L., Pinkau, K., Rothermel, H., Schneid, E., Sommer, M., Sreekumar, P., & Thompson, D. J. 1992, in NASA Conference Publication, Vol. 3137, NASA Conference Publication, ed. C. R. Shrader, N. Gehrels, & B. Dennis
Hua, X., Kozlovsky, B., Lingenfelter, R. E., Ramaty, R., & Stupp, A. 2002, ApJS, 140, 563
Hua, X.-M., Ramaty, R., & Lingenfelter, R. E. 1989, ApJ, 341, 516
Hudson, H. S. 2018, in IAU Symposium, Vol. 335, Space Weather of the Heliosphere: Processes and Forecasts, ed. C. Foullon & O. E. Malandraki, 49–53
Hurford, G. J., Schmahl, E. J., Schwartz, R. A., Conway, A. J., Aschwanden, M. J., Csillaghy, A., Dennis, B. R., Johns-Krull, C., Krucker, S., Lin, R. P., McTiernan, J., Metcalf, T. R., Sato, J., & Smith, D. M. 2002, SoPh, 210, 61
Ji, H., Wang, H., Schmahl, E. J., Moon, Y.-J., & Jiang, Y. 2003, ApJL, 595, L135
Jin, M., Petrosian, V., Liu, W., Nitta, N. V., Omodei, N., Rubio da Costa, F., Effenberger, F., Li, G., Pesce-Rollins, M., Allafort, A., & Manchester, IV, W. 2018, ArXiv e-prints
Kahler, S. W. 1982, J. Geophys. Res., 87, 3439
Kanbach, G., Bertsch, D. L., Fichtel, C. E., Hartman, R. C., Hunter, S. D., Kniffen, D. A., Kwok, P. W., Lin, Y. C., Mattox, J. R., & Mayer-Hasselwander, H. A. 1993, A&AS, 97, 349
Kaufmann, P., White, S. M., Freeland, S. L., Marcon, R., Fernandes, L. O. T., Kudaka, A. S., de Souza, R. V., Aballay, J. L., Fernandez, G., Godoy, R., Marun, A., Valio, A., Raulin, J.-P., & Giménez de Castro, C. G. 2013, ApJ, 768, 134
Kocharov, L., Debrunner, H., Kovaltsov, G., Lockwood, J., McConnell, M., Nieminen, P., Rank, G., Ryan, J., & Schoenfelder, V. 1998, A&A, 340, 257
Kocharov, L., Laitinen, T., Vainio, R., Afanasiev, A., Mursula, K., & Ryan, J. M. 2015, ApJ, 806, 80

Lario, D., Aran, A., Gómez-Herrero, R., Dresing, N., Heber, B., Ho, G. C., Decker, R. B., & Roelof, E. C. 2013, ApJ, 767, 41
Leibacher, J., Sakurai, T., Schrijver, C. J., & van Driel-Gesztelyi, L. 2010, SoPh, 263, 1
Lin, R. P. 1985, SoPh, 100, 537
Luhmann, J. G., Curtis, D. W., Schroeder, P., McCauley, J., Lin, R. P., Larson, D. E., Bale, S. D., Sauvaud, J.-A., Aoustin, C., Mewaldt, R. A., Cummings, A. C., Stone, E. C., Davis, A. J., Cook, W. R., Kecman, B., Wiedenbeck, M. E., von Rosenvinge, T., Acuna, M. H., Reichenthal, L. S., Shuman, S., Wortman, K. A., Reames, D. V., Mueller-Mellin, R., Kunow, H., Mason, G. M., Walpole, P., Korth, A., Sanderson, T. R., Russell, C. T., & Gosling, J. T. 2008, SSRv, 136, 117
Magdalenić, J., Marqué, C., Zhukov, A. N., Vršnak, B., & Veronig, A. 2012, ApJ, 746, 152
Mäkelä, P., Gopalswamy, N., Akiyama, S., Xie, H., & Yashiro, S. 2015, ApJ, 806, 13
Mandzhavidze, N. & Ramaty, R. 1992, ApJ, 389, 739
McLean, D. J. & Labrum, N. R. 1985, Solar radiophysics: Studies of emission from the sun at metre wavelengths
Meegan, C., Lichti, G., Bhat, P. N., Bissaldi, E., Briggs, M. S., Connaughton, V., Diehl, R., Fishman, G., Greiner, J., Hoover, A. S., van der Horst, A. J., von Kienlin, A., Kippen, R. M., Kouveliotou, C., McBreen, S., Paciesas, W. S., Preece, R., Steinle, H., Wallace, M. S., Wilson, R. B., & Wilson-Hodge, C. 2009, ApJ, 702, 791
Mewaldt, R. A., Cohen, C. M. S., Mason, G. M., Haggerty, D. K., Looper, M. D., Vourlidas, A., Desai, M. I., Giacalone, J., Labrador, A. W., Leske, R. A., & Mazur, J. E. 2005, in ESA Special Publication, Vol. 592, Solar Wind 11/SOHO 16, Connecting Sun and Heliosphere, ed. B. Fleck, T. H. Zurbuchen, & H. Lacoste, 67
Miller, J. A. & Ramaty, R. 1989, ApJ, 344, 973
Murphy, R. J., Dermer, C. D., & Ramaty, R. 1987, ApJS, 63, 721
Murphy, R. J., Kozlovsky, B., & Share, G. H. 2016, ApJ, 833, 196
Murphy, R. J., Kozlovsky, B., Share, G. H., Hua, X., & Lingenfelter, R. E. 2007, ApJS, 168, 167
Murphy, R. J., Share, G. H., DelSignore, K. W., & Hua, X.-M. 1999, ApJ, 510, 1011
Murphy, R. J., Share, G. H., Grove, J. E., Johnson, W. N., Kinzer, R. L., Kroeger, R. A., Kurfess, J. D., Strickman, M. S., Matz, S. M., Grabelsky, D. A., Purcell, W. R., Ulmer, M. P., Cameron, R. A., Jung, G. V., Jensen, C. M., Vestrand, W. T., & Forrest, D. J. 1993, in American Institute of Physics Conference Series, Vol. 280, American Institute of Physics Conference Series, ed. M. Friedlander, N. Gehrels, & D. J. Macomb, 619–630
Murphy, R. J., Share, G. H., Grove, J. E., Johnson, W. N., Kinzer, R. L., Kurfess, J. D., Strickman, M. S., & Jung, G. V. 1997, ApJ, 490, 883
Nitta, N. V., Aschwanden, M. J., Boerner, P. F., Freeland, S. L., Lemen, J. R., & Wuelser, J.-P. 2013, SoPh, 288, 241
Pesce-Rollins, M., Omodei, N., Petrosian, V., Liu, W., Rubio da Costa, F., Allafort, A., & Chen, Q. 2015a, ApJL, 805, L15
Pesce-Rollins, M., Omodei, N., Petrosian, V., Liu, W., Rubio da Costa, F., Allafort, A., & for the Fermi-LAT Collaboration. 2015b, ArXiv e-prints
Petrosian, V. 2016, ApJ, 830, 28
Plainaki, C., Mavromichalaki, H., Laurenza, M., Gerontidou, M., Kanellakopoulos, A., & Storini, M. 2014, ApJ, 785, 160
Plotnikov, I., Rouillard, A. P., & Share, G. H. 2017, A&A, 608, A43
Prince, T. A., Forrest, D. J., Chupp, E. L., Kanbach, G., & Share, G. H. 1983, International Cosmic Ray Conference, 4, 79
Ramaty, R., Kozlovsky, B., & Lingenfelter, R. E. 1979, ApJS, 40, 487
Ramaty, R., Mandzhavidze, N., & Kozlovsky, B. 1996, in American Institute of Physics Conference Series, Vol. 374, American Institute of Physics Conference Series, ed. R. Ramaty, N. Mandzhavidze, & X.-M. Hua, 172–183
Rank, G., Ryan, J., Debrunner, H., McConnell, M., & Schönfelder, V. 2001, A&A, 378, 1046
Reames, D. V. 1995, Advances in Space Research, 15, 41
—. 2013, SSRv, 175, 53
Richardson, I. G., von Rosenvinge, T. T., & Cane, H. V. 2015, SoPh, 290, 1741
Rouillard, A. P., Sheeley, N. R., Tylka, A., Vourlidas, A., Ng, C. K., Rakowski, C., Cohen, C. M. S., Mewaldt, R. A., Mason, G. M., Reames, D., Savani, N. P., StCyr, O. C., & Szabo, A. 2012, ApJ, 752, 44
Ryan, D. F., Chamberlin, P. C., Milligan, R. O., & Gallagher, P. T. 2013, ApJ, 778, 68
Ryan, J. M. 1986, SoPh, 105, 365
—. 2000, SSRv, 93, 581
Ryan, J. M. & Lee, M. A. 1991, ApJ, 368, 316
Ryan, J. M., Lee, M. A., de Nolfo, G., Anderson, E., & Nair, A. 2015, in AAS/AGU Triennial Earth-Sun Summit, Vol. 1, AAS/AGU Triennial Earth-Sun Summit, 205.04
Sauer, H. H. 1993, International Cosmic Ray Conference, 3, 250
Schlemm, C. E., Starr, R. D., Ho, G. C., Bechtold, K. E., Hamilton, S. A., Boldt, J. D., Boynton, W. V., Bradley, W., Fraeman, M. E., Gold, R. E., Goldsten, J. O., Hayes, J. R., Jaskulek, S. E., Rossano, E., Rumpf, R. A., Schaefer, E. D., Strohbehn, K., Shelton, R. G., Thompson, R. E., Trombka, J. I., & Williams, B. D. 2007, SSRv, 131, 393
Schneid, E. J., Bertsch, D. L., Dingus, B. L., Esposito, J. A., Fichtel, C. E., Hartman, R. C., Hunter, S. D., Kanbach, G., Kniffen, D. A., Lin, Y. C., Mayer-Hasselwander, H. A., Michelson, P. F., von Montigny, C., Mukherjee, R., Nolan, P. L., Sreekumar, P., & Thompson, D. J. 1996, A&AS, 120, C299
Share, G. H., Chupp, E. L., Forrest, D. J., & Rieger, E. 1983, in American Institute of Physics Conference Series, Vol. 101, Positron-Electron Pairs in Astrophysics, ed. M. L. Burns, A. K. Harding, & R. Ramaty, 15–20
Share, G. H. & Murphy, R. J. 1995, ApJ, 452, 933
Share, G. H. & Murphy, R. J. 2000, in American Institute of Physics Conference Series, Vol. 528, Acceleration and Transport of Energetic Particles Observed in the Heliosphere, ed. R. A. Mewaldt, J. R. Jokipii, M. A. Lee, E. Möbius, & T. H. Zurbuchen, 181–184
Share, G. H., Murphy, R. J., Kiener, J., & de Séréville, N. 2002, ApJ, 573, 464
Sharykin, I. N., Kosovichev, A. G., Sadykov, V. M., Zimovets, I. V., & Myshyakov, I. I. 2017, ArXiv e-prints
Sheeley, Jr., N. R., Howard, R. A., Koomen, M. J., & Michels, D. J. 1983, ApJ, 272, 349
Shih, A. Y., Lin, R. P., & Smith, D. M. 2009, ApJL, 698, L152
Talon, R., Trottet, G., Vilmer, N., Barat, C., Dezalay, J.-P., Sunyaev, R., Terekhov, O., & Kuznetsov, A. 1993, SoPh, 147, 137
Tanaka, Y. T., Omodei, N., Giglietto, N., & et al. 2012, The Astronomer's Telegram, 3886, 1
Tanaka, Y. T., Omodei, N., Takahashi, H., Grove, E., & et al. 2011, The Astronomer's Telegram, 3417, 1
Trottet, G. 1994, in American Institute of Physics Conference Series, Vol. 294, High-Energy Solar Phenomena - a New Era of Spacecraft Measurements, ed. J. Ryan & W. T. Vestrand, 3–14
Trottet, G., Raulin, J.-P., Mackinnon, A., Giménez de Castro, G., Simões, P. J. A., Cabezas, D., de La Luz, V., Luoni, M., & Kaufmann, P. 2015, SoPh, 290, 2809

Tylka, A. J. & Dietrich, W. F. 2009, in International Cosmic Ray Conference, Vol. 31, Proceedings of the 31st International Cosmic Ray Conference, Lod'z, Poland, 1

Tylka, A. J., Share, G. H., Dietrich, W. F., Murphy, R. J., Keong Ng, C., Shea, M. A., & Smart, D. F. 2014, in EGU General Assembly Conference Abstracts, Vol. 16, EGU General Assembly Conference Abstracts, 16847

Verma, V. K. 1993, ApJ, 403, 797

Vestrand, W. T. & Forrest, D. J. 1993, ApJL, 409, L69

Vestrand, W. T., Share, G. H., Murphy, R. J., Forrest, D. J., Rieger, E., Chupp, E. L., & Kanbach, G. 1999, ApJS, 120, 409

Vilmer, N., MacKinnon, A. L., Trottet, G., & Barat, C. 2003, A&A, 412, 865

Wild, J. P., Smerd, S. F., & Weiss, A. A. 1963, ARA&A, 1, 291

Zhang, J., Dere, K. P., Howard, R. A., Kundu, M. R., & White, S. M. 2001, ApJ, 559, 452

Zhang, X. L., Gruber, D., Kiener, J., & von Kienlin, A. 2012, in Proceedings of "An INTEGRAL view of the high-energy sky (the first 10 years)" - 9th INTEGRAL Workshop and celebration of the 10th anniversary of the launch (INTEGRAL 2012). 15-19 October 2012. Bibliotheque Nationale de France, Paris, France., 139

Zimovets, I., Vilmer, N., Chian, A. C.-L., Sharykin, I., & Struminsky, A. 2012, A&A, 547, A6